geodiversitas

2023 • 45 • 18

A sabre-tooth predator from the Neotropics: Cranial morphology of *Anachlysictis gracilis* Goin, 1997 (Metatheria, Thylacosmilidae), based on new specimens from La Venta (Middle Miocene, Colombia)

Catalina SUAREZ, Analia M. FORASIEPI, María Judith BABOT, Tatsuya SHINMURA, Javier LUQUE, Ruben D. VANEGAS, Edwin A. CADENA & Francisco J. GOIN

in Juan D. CARRILLO (ed.),
Neotropical palaeontology: the Miocene La Venta biome

art. 45 (18) — Published on 12 October 2023
www.geodiversitas.com

PUBLICATIONS SCIENTIFIQUES

MUSÉUM NAL HIST NATURELLE

Geodiversitas est indexé dans / Geodiversitas *is indexed in:*
– Science Citation Index Expanded (SciSearch®)
– ISI Alerting Services®
– Current Contents® / Physical, Chemical, and Earth Sciences®
– Scopus®

Geodiversitas est distribué en version électronique par / Geodiversitas *is distributed electronically by:*
– BioOne® (http://www.bioone.org)

Les articles ainsi que les nouveautés nomenclaturales publiés dans *Geodiversitas* sont référencés par / *Articles and nomenclatural novelties published in* Geodiversitas *are referenced by:*
– ZooBank® (http://zoobank.org)

Geodiversitas est une revue en flux continu publiée par les Publications scientifiques du Muséum, Paris
Geodiversitas *is a fast track journal published by the Museum Science Press, Paris*

Les Publications scientifiques du Muséum publient aussi / *The Museum Science Press also publish:* ***Adansonia***, ***Zoosystema***, ***Anthropozoologica***, ***European Journal of Taxonomy***, ***Naturae***, ***Cryptogamie*** **sous-sections** ***Algologie***, ***Bryologie***, ***Mycologie, Comptes Rendus Palevol***

Diffusion – Publications scientifiques Muséum national d'Histoire naturelle
CP 41 – 57 rue Cuvier F-75231 Paris cedex 05 (France)
Tél. : 33 (0)1 40 79 48 05 / Fax : 33 (0)1 40 79 38 40
diff.pub@mnhn.fr / http://sciencepress.mnhn.fr

ISSN (imprimé / *print*) : 1280-9659/ ISSN (électronique / *electronic*) : 1638-9395

A sabre-tooth predator from the Neotropics: Cranial morphology of *Anachlysictis gracilis* Goin, 1997 (Metatheria, Thylacosmilidae), based on new specimens from La Venta (Middle Miocene, Colombia)

Catalina SUAREZ
Current affilition: Instituto Argentino de Nivología, Glaciología y Ciencias Ambientales (IANIGLA), CCT-CONICET Mendoza, Av. Ruiz Leal s/n, Parque General San Martín, Mendoza, 5500 (Argentina)
and Grupo de Paleontología Neotropical Tradicional y Molecular (PaleoNeo), Facultad de Ciencias Naturales, Universidad del Rosario, Bogotá (Colombia)
and Smithsonian Tropical Research Institute, Box 0843-03092, Balboa-Ancón (Panama)
catasuarezg@gmail.com (corresponding author)

Analia M. FORASIEPI
Instituto Argentino de Nivología, Glaciología y Ciencias Ambientales (IANIGLA), CCT-CONICET Mendoza, Av. Ruiz Leal s/n, Parque General San Martín, Mendoza, 5500 (Argentina)
and Consejo Nacional de Investigaciones Científicas y Técnicas (CONICET) (Argentina)

María Judith BABOT
Unidad Ejecutora Lillo-CONICET, Fundación Miguel Lillo, Miguel Lillo 251, San Miguel de Tucumán, Tucumán, 4000 (Argentina)

Tatsuya SHINMURA
Ashoro Museum of Paleontology, 29-1 Konan, Ashoro, Ashoro District, Hokkaido 089-3727 (Japan)

Javier LUQUE
Museum of Zoology, Department of Zoology, University of Cambridge, Downing Street, Cambridge CB2 3EJ (United Kingdom)
and Smithsonian Tropical Research Institute, Box 0843-03092, Balboa-Ancón (Panama)

Rubén D. VANEGAS
Museo de Historia Natural La Tatacoa, Centro Poblado La Victoria, Villavieja, Huila Department (Colombia)

Edwin A. CADENA
Grupo de Paleontología Neotropical Tradicional y Molecular (PaleoNeo), Facultad de Ciencias Naturales, Universidad del Rosario, Bogotá (Colombia)
and Smithsonian Tropical Research Institute, Box 0843-03092, Balboa-Ancón (Panama)
and Field Museum of Natural History, Chicago, IL 60605 (United States)

Francisco J. GOIN
Consejo Nacional de Investigaciones Científicas y Técnicas (CONICET) (Argentina)
and División Paleontología de Vertebrados, Museo de La Plata, Facultad de Ciencias Naturales y Museo, Universidad Nacional de La Plata, Paseo del Bosque s/n, La Plata, Buenos Aires, B1900FWA (Argentina)

Submitted on 18 October 2022 | accepted on 11 May 2023 | published on 12 October 2023

urn:lsid:zoobank.org:pub:BB77B691-635A-4B92-9820-DBE74776B7E2

Suarez C., Forasiepi A. M., Babot M. J., Shinmura T., Luque J., Vanegas R. D., Cadena E. A. & Goin F. J. 2023. — A sabre-tooth predator from the Neotropics: Cranial morphology of *Anachlysictis gracilis* Goin, 1997 (Metatheria, Thylacosmilidae), based on new specimens from La Venta (Middle Miocene, Colombia), *in* Carrillo J. D. (ed.), Neotropical palaeontology: the Miocene La Venta biome. *Geodiversitas* 45 (18): 497-572. https://doi.org/10.5252/geodiversitas2023v45a18. http://geodiversitas.com/45/18

ABSTRACT

The fossil metatherian assemblage from La Venta (Middle Miocene, Colombia) is one of the most diverse in South America, and it is critical to understand the Neogene radiation of this group in this continent. La Venta contains the northernmost record of Thylacosmilidae Riggs, 1933 (Metatheria, Sparassodonta): *Anachlysictis gracilis* Goin, 1997, the first thylacosmilid species named for the Neotropics. This taxon was described mostly based on mandibular remains. Recent fieldwork and work in collections led to the discovery of new materials for this species, including the most complete skeleton ever found for this Sparassodonta Ameghino, 1894. Here, we present a detailed description of the cranial osteology and dentition of *A. gracilis*, which elucidates anatomical aspects previously inferred but hitherto unconfirmed. We investigate the phylogeny, and ecomorphological parameters of this taxon (diet and body mass) to set the evolutionary context of the species, understand its paleobiology, and evaluate palaeoecological implications. Additionally, we revise the phylogeny of the thylacosmilids, recovering the traditional classification of the group, differentiated from the proborhyaenids and borhyaenids. This work also proposes a new reconstruction of the external morphology of the head of *A. gracilis* based on 3D scans of the new referred materials.

KEY WORDS
South America,
La Victoria Formation,
Neogene,
Sparassodonta,
paleobiology.

RÉSUMÉ

*Un prédateur à dents de sabre des Néotropiques : morphologie crânienne d'*Anachlysictis gracilis *Goin, 1997 (Metatheria, Thylacosmilidae), d'après de nouveaux spécimens de La Venta (Miocène Moyen, Colombie).*

L'assemblage des métathériens fossiles de La Venta (Miocène Moyen, Colombie), qui est l'un des plus diversifiés d'Amérique du Sud, est crucial pour la connaissance des radiations néogènes de ce groupe sur ce continent. Il présente le registre le plus septentrional de Thylacosmilidae Riggs, 1933 (Metatheria, Sparassodonta) : *Anachlysictis gracilis* Goin, 1997, la première espèce décrite pour cette famille sous les néotropiques. Ce taxon a été décrit principalement sur la base de restes mandibulaires. De nouvelles missions de terrain ainsi que la révision de matériel connu, ont permis la découverte de nouveaux restes pour cette espèce. Parmi ces spécimens nous pouvons mentionner l'existence d'un squelette, le plus complet découvert pour cette espèce de Sparassodonta Ameghino, 1894. Cette étude, qui consiste en une description détaillée de l'ostéologie crânienne et de la dentition d'*A. gracilis*, a permis de confirmer certaines hypothèses quant à l'anatomie, encore jamais démontrées. La phylogénie et les paramètres écomorphologiques de ce taxon (régime alimentaire et masse corporelle) ont été analysés afin d'établir le contexte évolutif de l'espèce, comprendre sa paléobiologie et évaluer les implications paléoécologiques. De plus, une reconsidération de la phylogénie des thylacosmilidés a permis d'obtenir une classification plus traditionnelle du groupe, où ils se différencient des proborhyaenidés et des borhyaenidés. Cette étude propose également une nouvelle reconstruction de la morphologie externe de la tête d'*A. gracilis*, sur la base de scans 3D des nouveaux spécimens étudiés.

MOTS CLÉS
Amérique du Sud,
Formation La Victoria,
Néogène,
Sparassodonta,
paléobiologie.

RESUMEN

Un depredador dientes de sable del Neotrópico: morfología craneal de Anachlysictis gracilis *Goin, 1997 (Metatheria, Thylacosmilidae), basada en nuevos especímenes de La Venta (Mioceno medio, Colombia).*

La asociación fósil de metaterios de La Venta (Mioceno Medio, Colombia) es una de las más diversas de América del Sur y es fundamental para entender la radiación neógena del grupo en este continente. La Venta contiene el registro más septentrional de Thylacosmilidae Riggs, 1933 (Metatheria, Sparassodonta): *Anachlysictis gracilis* Goin, 1997, la primera especie de tilacosmílido nombrada para el Neotrópico. Este taxón se describió principalmente con base en restos mandibulares. Reciente trabajo en campo y colecciones llevaron al descubrimiento de nuevos materiales para esta especie, incluido el esqueleto más completo jamás encontrado para este Sparassodonta Ameghino, 1894. Aquí presentamos una descripción detallada de la osteología craneana y la dentición de *A. gracilis*, que aclara aspectos anatómicos previamente inferidos, pero hasta ahora no confirmados. Se analizó la filogenia y los parámetros ecomorfológicos de este taxón (dieta y masa corporal), con el fin de establecer el contexto evolutivo de la especie, comprender su paleobiología y evaluar implicaciones paleoecológicas. Adicionalmente, se revisó la filogenia de los tilacosmílidos, recuperando la clasificación tradicional del grupo, diferenciados de los proboriénidos y boriénidos. Este trabajo también propone una nueva reconstrucción de la morfología externa de la cabeza de *A. gracilis* basada en escaneos 3D de los nuevos materiales referidos.

PALABRAS CLAVE
América del Sur,
Formación La Victoria,
Neógeno,
Sparassodonta,
paleobiología.

INTRODUCTION

The South American metatherian sabre-tooth predators (Sparassodonta, Thylacosmilidae) stand among the most noticeable carnivorous metatherians (living or extinct) known up to date. In the words of Elmer Riggs, who first described the skull of *Thylacosmilus* Riggs, 1933, it is "the most highly specialized, the strongest and no doubt the most destructive of all the long line of South American marsupial carnivores" (Riggs 1934: 3). Their most distinctive feature is the presence of hypertrophied upper canines, seemingly similar to those of sabre-toothed felids. However, this character is associated with a set of cranial and mandibular characteristics that, besides superficial similarities, differ substantially from those of eutherian counterparts, both structurally and functionally (see Riggs 1933; Prevosti *et al.* 2010; Wroe *et al.* 2013; Janis *et al.* 2020; Gaillard *et al.* 2023).

The family Thylacosmilidae Riggs, 1933 (ranked as subfamily; posteriorly raised to family rank by Marshall 1976; see also Riggs 1929) originally included the single genus *Thylacosmilus*. Some authors included different species to this genus (e.g., Riggs 1933, 1934; Riggs & Patterson 1939) or nominated related genera (e.g., Reig 1958; Kraglievich 1960; Ringuelet 1966; Marshall 1976). However, Goin & Pascual (1987) have shown that the numerous thylacosmilid species from the Miocene-Pliocene of Argentina named in the 20th century cannot be meaningfully distinguished from one another and should be regarded as synonyms of *Thylacosmilus atrox* Riggs, 1933, the earliest valid name apart from an unused senior synonym, *Achlysictis lelongi* Ameghino, 1891, now suppressed (see Goin & Pascual 1987). Up to date, there is a consensus on this genus being represented by a single species: *T. atrox* (Goin & Pascual 1987; Marshall *et al.* 1990; Goin 1995, 1997; MacKenna & Bell 1997; Argot 2004a; Forasiepi 2009; Forasiepi & Carlini 2010; Forasiepi *et al.* 2019; Janis *et al.* 2020; Gaillard *et al.* 2023).

Thylacosmilus atrox is represented by several specimens (most of them being fragmentary material and isolated teeth) from several localities in Argentina, spanning from Huayquerian to Chapadmalan SALMAs (*c.* 9-3.3 Ma; Riggs 1933, 1934; Kraglievich 1960; Marshall 1976; Goin & Pascual 1987; Cione *et al.* 2000; Goin *et al.* 2000; Álvarez & Tauber 2004; Forasiepi *et al.* 2007); in addition to material from the Huayquerian SALMA of Uruguay (Mones & Rinderknecht 2004; Forasiepi & Carlini 2010). The best-preserved remains of *T. atrox* are those from Catamarca Province, originally described by Riggs (1933, 1934) and a more recently described specimen from the Atlantic coast of Buenos Aires Province (Goin & Pascual 1987). Additional material originally identified as an indeterminate Thylacosmilidae comes from the Colhuehuapian SALMA of Argentina (Goin *et al.* 2007), but still pending of inclusion in phylogenetic analysis.

More recently, two other species were included in the family Thylacosmilidae: *Anachlysictis gracilis* Goin, 1997 (Middle Miocene, Lavenentan SALMA 13.5-11.8 Ma, Colombia) and *Patagosmilus goini* Forasiepi & Carlini, 2010 (Middle Miocene, Colloncuran SALMA, 15.5-14 Ma, Argentina; and Laventan SALMA, Bolivia [see Appendix 1, Material examined, *Patagosmilus goini*]). In this context, Thylacosmilidae was considered as the group that includes the common ancestor of *Thylacosmilus atrox*, *Patagosmilus goini*, and *Anachlysictis gracilis* plus all its descendants (e.g., Prevosti & Forasiepi 2018; Forasiepi *et al.* 2019; Gaillard *et al.* 2023).

Anachlysictis gracilis is by now represented by its holotype (an almost complete right dentary, fragment of the left, a very fragmentary frontal part of the skull, and a few postcranial elements) and UCMP 39705 specimen (posterior fragment of right mandibular ramus, as mentioned by Suarez 2019). To these specimens, we add here VPPLT-1612, an almost complete specimen consisting of a nicely preserved skull and postcranial material. All the fossil specimens of *A. gracilis* are from the Middle Miocene Honda Group, La Victoria Formation, cropping out in the La Venta area (Tatacoa desert in the Upper Magdalena Valley, Huila Department, Colombia). Additionally, another still-unnamed species from La Venta was mentioned by Goin (1997) as probably belonging to this group (see Material and methods). As such, the family Thylacosmilidae spans from the Middle Miocene to the mid-Pliocene. However, their origins could be earlier, at least Early Miocene (see Goin *et al.* 2007) or even older and related to an important mammalian turnover that occurred in South America by the Eocene-Oligocene boundary (Goin *et al.* 2010, 2016; see also Engelman *et al.* 2020). In this context, a recently described sparassodont species, *Eomakhaira molossus* Engelman, Flynn, Wyss & Croft, 2020, from the lower Oligocene of Cachapoal locality, central Chile was claimed as belonging to Thylacosmilidae (= Thylacosmilinae in Engelman *et al.* 2020; but see below); it was regarded as stem taxon to the group formed by *T. atrox* and *P. goini* (*A. gracilis* was not included in their analysis). As such, Thylacosmilidae was redefined using a stem-based definition. However, considering this proposed definition, not only *Eomakhaira molossus* (see Engelman *et al.* 2020) but other sparassodonts (e.g., *Callistoe vincei* Babot, Powell & Muizon, 2022 and *Paraborhyaena boliviana* Hoffstetter & Petter, 1983, traditionally considered Proborhyaenidae Ameghino, 1897) should be included in the group because, according to some phylogenetic hypotheses (e.g., Babot *et al.* 2002; Forasiepi *et al.* 2015: fig. 7; Suarez *et al.* 2016: fig. 3; Muizon *et al.* 2018: fig. 29; Muizon & Ladevèze 2020: fig. 49), they are closer to *Thylacosmilus* than to any other sparassodont.

The goal of this contribution is to re-describe the skull of *Anachlysictis gracilis* based on previous observations from the unpublished Ph.D. thesis of Suarez (2019) and new data from recently collected materials. We also perform new cladistic analyses to test the affinities of *Anachlysictis gracilis* and re-evaluate the phylogenetic definition of the Thylacosmilidae. We reconstruct some paleobiological aspects (body mass and diet) with the aim of better understanding the autecological role of this species. The description of the postcranium and other related analyses will be engaged separately in a study in progress.

GEOLOGICAL SETTING

The Honda Group is a Middle Miocene sedimentary continental unit cropping out across several localities along the Upper and Middle Magdalena valley, located between the Central and Eastern cordilleras of the Colombian Andes (Guerrero 1997). The Honda Group spans 5.5 million years, from *c.* 16 Ma to *c.* 10.5 Ma, with most the accumulation occurring between 13.8 and 11.8 Ma (Mora-Rojas *et al.* 2023; see also Flynn *et al.* 1997; Guerrero 1997; Anderson *et al.* 2016 and Montes *et al.* 2021). The Honda Group is divided into two main units: the lower La Victoria Formation, and the upper Villavieja Formation (see detailed stratigraphy in Mora-Rojas *et al.* 2023). The shift in accumulation regimes in the Villavieja Formation could have been forced by tectonics and/or climate changes (Mora-Rojas *et al.* 2023).

The most complete and productive fossiliferous sections from the Honda Group crop out along the Upper Magdalena Valley, between *c.* 2°N and *c.* 5°N, in an area locally known as La Tatacoa Desert (Fig. 1) but commonly known in the scientific literature as the "La Venta area" (Kay *et al.* 1997). The La Venta fossil assemblage allowed Madden *et al.* (1997) to propose a new chronostratigraphic/biostratigraphic unit: the Laventan Stage/Age. Its age spans between 13.5 and 11.8 Ma.

The Villavieja Formation has traditionally been known for containing the richest fossiliferous levels, especially at its lower part (Guerrero 1997). Nevertheless, it should be recognized that collecting efforts have been historically concentrated in this upper unit. Recent fieldwork has focused on the exploration of the older La Victoria Formation, considerably increasing the number of fossils collected from this unit, including the new materials described in this work.

The La Victoria Formation, dominated by a gravel-sand meandering fluvial system, is composed of alterations of fining-upward sequences of grey "salt and pepper" pebbly volcanic litharenite and variegated mudstone (Guerrero 1997), standing out three sandstone marker beds along the unit, and a clast-supported bed, the Cerbatana Conglomerate, which is the uppermost level (Guerrero 1997).

MATERIAL AND METHODS

Abbreviations

Institutional abbreviations

IGM	Servicio Geológico Colombiano, Colombia (former "INGEOMINAS"; fieldworks in cooperation with Duke University), Bogotá, Colombia;
MACN	Museo Argentino de Ciencias Naturales "Bernardino Rivadavia", Buenos Aires, Argentina;
MLP	Museo de La Plata, La Plata, Argentina;
MNHN-Bol	Museo Nacional de Historia Natural, La Paz, Bolivia;
PRI	Primate Research Institute, Kyoto University, Inuyama, Aichi, Japan;
UF	Florida Museum of Natural History, Gainesville, Florida, United States;
UCMP	University of California Museum of Paleontology, Berkeley, California, United States;
VPPLT	Vigías del Patrimonio Paleontológico de La Tatacoa, Museo de Historia Natural La Tatacoa, La Victoria, Huila, Colombia;
DU	Duke University, Durham, North Carolina, United States.

Anatomical abbreviations

Capital and lower-case letters refer to upper and lower teeth, respectively:

C/c	canine;
I/i	incisor;
M/m	molar;
P/p	premolar.

Other abbreviations

A	area;
CI	consistency index;
L	length;
Log	common logarithm (with base 10);
ln	natural logarithm (with base *e*);
Ma	*Megannum* (one million years in the radioisotopic time scale);
%PE	percent prediction error;
R^2	ratio estimate;
RGA	relative grinding area;
RI	retention index;
SE	smearing estimate correction factor;
W	width.

Description and measurements

The comparative work comprised the study of the published species included in Thylacosmilidae, as well as unpublished specimens such as a thylacosmilid of generalized morphology from the Middle Miocene of La Venta (IGM 251108), preliminarily described by Goin (1997), treated in Suarez (2019) and currently being analyzed in a work in progress; and an undescribed specimen here referred to *P. goini* (see also Goin & Carlini 1993), which comes from Quebrada Honda, Bolivia (field number B:p2-154 [MNHN-Bol]: see Appendix 1, Material examined). Since the holotype consists of a partial skull with upper dentition lacking the basicranium (Forasiepi & Carlini 2010), all the comparisons here with *P. goini* regarding the posterior portion of the skull, dentary, and lower dentition are based on observations on the last specimen.

Dental and mandibular measurements were taken with a digital caliper and with the software 'Image J' (Schneider *et al.* 2012); this software was also used to measure angles. The nomenclature and positional terms for the skull descriptions follow Wible (2003). Additionally, the *Nomina Anatomica Veterinaria* (Schaller 2007) and other specific references (e.g., Forasiepi 2009; Forasiepi *et al.* 2019) were taken as references for certain details and discussions. The nomenclature and positional terms for the dentition follow Goin *et al.* (2016), with the modifications proposed by Suarez (2019) based on Cifelli (1993a) and Luo *et al.* (2003).

Positional terms

Skull. Anterior, posterior, lateral, medial, dorsal, and ventral;
Dentary. Anterior, posterior, lateral, medial, occlusal, and ventral.
Teeth. Anterior, posterior, labial, lingual, occlusal, proximal (to the base of the canine), distal (to the tip or the canine).

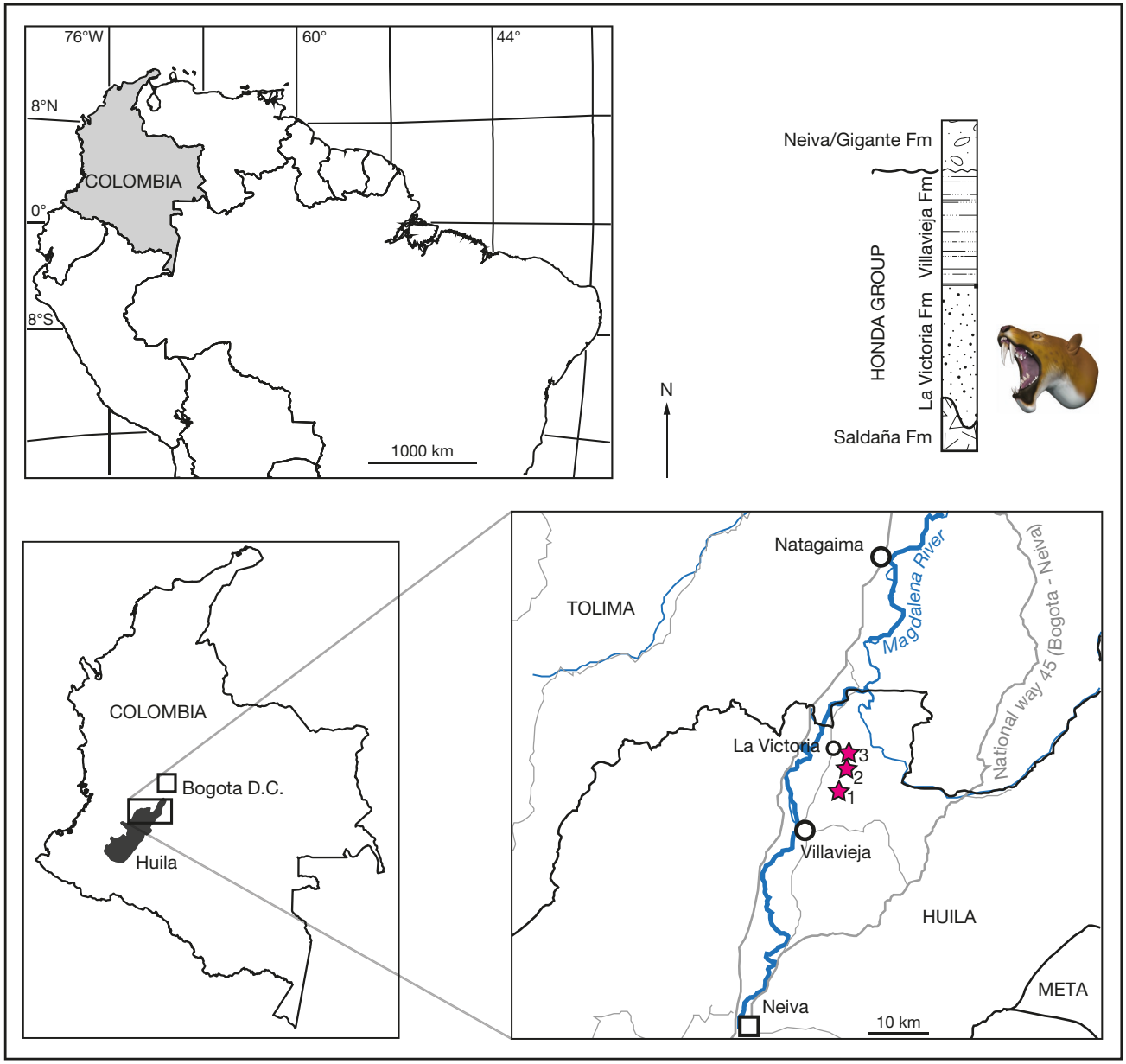

Fig. 1. — Geographical setting of the study area, indicating the collection points of specimens referred to *Anachlysictis gracilis* Goin, 1997 and generalized stratigraphic position. **1**, IGM locality 75 (specimen IGM 184247, holotype); **2**, UCMP locality V4531 ("Cerro Gordo 2": specimen UCMP 39705); **3**, VPPLT locality "Finca Tres Pasos" (specimen VPPLT-1612).

Cladistic analysis

In order to test the phylogenetic affinities of *A. gracilis* within Thylacosmilidae and the relationships of this group with other sparassodonts (see Appendix 1), we performed a set of analyses based on the comprehensive matrix of Engelman *et al.* (2020), which is the most taxon-rich analysis of relationships within Sparassodonta Ameghino, 1894 to date, and is based on Forasiepi (2009) and posterior contributions (Engelman & Croft 2014; Forasiepi *et al.* 2015; Suarez *et al.* 2016), with additions of character and character-state data from Muizon *et al.* (2018). The resulting data matrix (see Appendix 2), containing 52 taxa and 403 morphological characters, was edited using the Mesquite software for Linux (version 3.70; Maddison & Maddison 2021). We made some modifications to the version of Engelman *et al.* (2020), including the return to previous versions of some characters by redundancy or ambiguity and the addition of some characters proposed by Suarez (2019), which aim to elucidate some remarkable features present in thylacosmilids (see Modifications in Data Matrix in Appendix 1). Scoring for new characters and changes in coding were made using original specimens, casts or photographs, and additional information from the literature (see Material examined in Appendix 1).

The matrix is composed of 403 characters, including 158 cranial (1-158), 119 dental (159-277), and 126 postcranial characters (278-403). Of these characters, 75 (those showing

a logical sequence of transformation) were treated as ordered (see List of Characters in Appendix 1). The matrix includes 52 taxa: 27 sparassodont metatherians and 25 non-sparassodont taxa, including metatherians and eutherians (see Material examined in Appendix 1 for the taxa list and correspondent specimens studied). We used this set of taxa following Engelman *et al.* (2020) due to the importance of their results and conclusions regarding the Thylacosmilidae, which is the group of interest in the present work. We modified the taxa list adding two taxa (*Anachlysictis gracilis* and the species represented by the specimen IGM 251108; see list of Material examined in Appendix 1) and excluding *Vincelestes neuquenianus* Bonaparte, 1986, used by Engelman *et al.* (2020) as the outgroup taxon. This last change was made considering that this species, a stem Theria Parker & Haswell, 1897 (see Rougier *et al.* 2021) is in a phylogenetic position too distant from Metatheria Huxley, 1880. In our analysis, *Prokennalestes* Kielan-Jaworowska & Dashzeveg, 1989 was selected as the outgroup taxon.

The extant taxa in the crown-group Marsupialia include the didelphids *Monodelphis* spp., *Didelphis albiventris* Lund, 1840 and *Metachirus nudicaudatus* Geoffroy, 1803; and the australidelphians *Dromiciops gliroides* Thomas, 1894, *Sminthopsis crassicaudata* Gould, 1844, *Thylacinus cynocephalus* Harris, 1808 and *Dasyurus* spp.

The dataset was analyzed with equal weights and implied weights parsimony, and Bayesian Inference. Following Engelman *et al.* (2020), for all the parsimony analyses, the Dasyuromorphia Gill, 1872 taxa (i.e., *Dasyurus* Geoffroy, 1796, *Sminthopsis crassicaudata* and *Thylacinus cynocephalus*) were constrained to form a monophyletic group, as it has been recovered in molecular analyses (e.g., Krajewski *et al.* 1997; Westerman *et al.* 2016; Kealy & Beck 2017) to avoid the potential recovery of Sparassodonta within Dasyuromorphia. This is a problem also found in previous studies due to their strong convergent similarities, especially in the dentition (Forasiepi 2009; Engelman & Croft 2014; Forasiepi *et al.* 2015; Suarez *et al.* 2016; Suarez 2019). These previous studies addressed the problem by excluding *T. cynocephalus* from the analyses. We tested that option in an additional analysis and obtained the same topology as with Dasyuromorpha constrained to form a clade (Appendix 1, Fig. A1).

The parsimony analyses were performed in TNT 1.1 for Linux (version 1.6; Goloboff *et al.* 2008), using traditional search. The initial trees were obtained through 1000 random replications. The resulting Wagner trees were treated as dichotomic, and the branch-swapping method was applied with tree bisection and reconnection (TBR). The consensus tree for the equal weights analysis was calculated as a Strict (= Nelsen) consensus tree. The Bremer supports in the equal weights analysis were calculated as absolute supports, with TBR from existing trees, retaining trees suboptimal by nine steps, and collapsing nodes below 0. The implied-weighted parsimony analyses were performed with default concavity constants of k = 3 and k = 12, following Engelman *et al.* (2020), and also an analysis with k = 6 that resulted in a similar topology to that with k = 12 (see Results). A bootstrap resampling was made in both equal and implied weight analyses, with the following parameters: bootstrap standard (sample with replacement), traditional search, output results as absolute frequencies, and 10000 replicates.

The Bayesian Inference analysis was performed in MrBayes v. 3.2.6. (Ronquist *et al.* 2012), using a dataset with 51 taxa (*T. cynocephalus* was excluded in this analysis). The aim is to better detect the inconsistencies in the topology of the tree, product of the analysis of our matrix with maximum parsimony. The data set was analyzed under the traditional Mk model with an ascertainment bias correction to account for scoring only variable morphological characters. Each analysis was performed with two independent runs of 3×10^7 generations each. We used four chains (one cold and three heated) per each independent run. The relative burn-in fraction was set to 25% and the chains were sampled every 200 generations. We used Tracer v.1.7 (Rambaut *et al.* 2018) to determine whether the runs reached stationary phase, and to ensure that the effective sample size for each parameter was greater than 200. The results of the Bayesian Inference runs were summarized as a majority-rule consensus tree of the post-burn-in sample, with a node support threshold of 75%.

Ecomorphological analysis

An ecomorphological analysis was performed in order to estimate the body mass and dietary habits of *A. gracilis*, using the methodology explained below:

Body mass

Estimations were made based on dental variables, using the equations constructed by Myers (2001) from the 'all species' and dasyuromorphian data sets and Zimicz (2012; based on Gordon 2003). The equations from Zimicz (2012) are expressed in natural logarithm (ln), while Myers (2001) used common logarithm (with base 10: log).

Each independent variable was included in the equation, and the resulting logarithmic value was exponentiated. The exponentiated value was multiplied by its corresponding correction factor, the Smearing Estimate (SE). This factor is expressed as a percentage for the equations from Myers (2001). "A typical value for a correction factor, for example, 1.085, would indicate that body mass estimates derived from the equation underestimate the arithmetic mean mass for any value of the independent variable by 8.5%" (Smith 1993). This statement was followed when using the equations from Myers (2001): e.g., for an SE expressed as 3.5 %, the value used as a correction factor in the estimations was 1.035. If this transformation is not made, the estimations will be overestimated.

The lowest % PE and a good adjusted R^2 (closest to 1) indicate the best predictor variable for each case. In the case of the equations by Zimicz (2012), the best predictor variables for her sample set are the length of the second upper molar and the length of the third lower molar. The M2 length presents the lowest value of % PE (7.03) for upper dentition variables and a good adjusted R^2 (0.95). The m3 length presents the lowest value of % PE (12.82) for lower dentition variables

and a good adjusted R^2 (0.95). In the case of the equations from Myers (2001), the best predictor dental variables are the lower molar row length (LMRL) for the dasyuromorphians data-set equations and the upper molar occlusal row length (UMORL) for the 'all species' data-set equations. However, for this analysis, we avoided those variables involving measurements of a complete dental series, as we consider there could be errors due to the sigmoid (or bowed) morphology of the thylacosmilids dental row (see Description and Discussion). For this reason, the independent variables used in this analysis were only those based on individual dental elements.

The size classification used in this work follows the size categories proposed by Prevosti *et al.* (2013) for South American carnivorous mammals (both metatherian and eutherian): small size, below 7 kg; medium size, between 7 and 15 kg; and large size, above 15 kg.

Diet inferences

The dietary habits of *A. gracilis* were inferred from the molar morphology using the carnivory indexes based on the carnassial molar, which in metatherians corresponds to the m4 (Prevosti *et al.* 2013; modified from Van Valkenburgh 1991). This tooth has pronounced carnivorous features, being analogous to the m1 in Carnivora (Werdelin 1987; Prevosti *et al.* 2013). One of these indexes was the RGA, based on the relative grinding area of the carnassial molar (i.e., talonid basin area/trigonid length; Van Valkenburgh 1991; Prevosti *et al.* 2013). A taxon is considered hypercarnivorous when the RGA is 0-0.48; mesocarnivorous, with 0.48-0.54; and omnivorous, with more than 0.54 (Prevosti *et al.* 2013). Other index evaluated was the relative length of the trigonid of the m4 (i.e., trigonid length/total molar length; Zimicz 2012), which is interpreted using four categories: omnivorous, with values below 0.7; mesocarnivorous, between 0.7 and 0.8; bone-breaker hypercarnivorous, between 0.8 and 0.9; and meat-eater hypercarnivorous, with relative length over 0.9 (Zimicz 2012).

The inferences about the possible mammal prey for *A. gracilis* were made through a comparative analysis using the body mass estimation resulted in this study and previous body mass estimations for the La Venta fossil mammalian assemblage (e.g., Kay & Madden 1997). These data were plotted in the results of the analysis of Ercoli *et al.* (2014), to see the range of prey body mass that would correspond to a predator of the size of *A. gracilis*. With this information, we selected the species from La Venta that fall within that body mass range.

DIGITAL RECONSTRUCTION OF *A. GRACILIS* HEAD

The reconstruction of *A. gracilis* was performed based on the specimen VPPLT-1612, using the 3D-CG software ZBrush 2022. The 3D digital models used in this reconstruction (Appendices 3-5) were acquired using a handheld 3D surface scanner model Go!Scan Spark (Creaform, Lévis, Québec, Canada) and software VXElements (Creaform, Lévis, Québec, Canada). A retrodeformation was performed, raising the right side of the skull and lowering the left, based on the less deformed mandible and anatomical structures (e.g., orbits, teeth row, external acoustic meatus), and replacing the missing left upper canine and incomplete right mandible with the opposite side (via mirroring). The mastication muscles were referenced in extant opossums, and the eyeballs and tongue were built to fit in the orbits and the oral cavity. As there is no evidence of extant closer relatives, the external appearance (including color pattern) was based on opossums and complemented with lions and leopards (see Discussion). Whiskers and fur were added with Photoshop elements (Adobe inc.) to the rendered 2D life appearance. Five whiskers' lines were represented, following O'Leary *et al.* (2013).

SYSTEMATIC PALEONTOLOGY

Class MAMMALIA Linnaeus, 1758
Infraclass METATHERIA Huxley, 1880
Order SPARASSODONTA Ameghino, 1894
Superfamily BORHYAENOIDEA Simpson, 1930
Family THYLACOSMILIDAE Riggs, 1933

Genus *Anachlysictis* Goin, 1997

TYPE SPECIES. — *Anachlysictis gracilis* Goin, 1997 by original designation.

INCLUDED SPECIES. — Type species only.

OCCURRENCE. — La Venta area (La Tatacoa Desert, Upper Magdalena Valley, Huila Department, Colombia; Fig. 1); Laventan SALMA (13.5-11.8 Ma.), Middle Miocene.

DIAGNOSIS. — The same as the type species (Goin 1997: 202).

Anachlysictis gracilis Goin, 1997
(Figs 2-11; 12C)

HOLOTYPE. — IGM 184247 (Fig. 2), a small portion of skull roof with the left postorbital process, and fragments of frontal, lacrimal and nasal; nearly complete right mandible with almost complete m2-4 and roots of p2-m1; left horizontal ramus fragment with m2-3; fragment of left symphyseal flange; almost complete atlas; fragment of the third cervical vertebra; fragments of neural arc, pre and post-zygapophyses of undetermined vertebral elements; ribs fragments; proximal portion of right scapula; right magnum; pyramidal?; two distal fragments of metapodials; proximal phalanx; and indeterminate postcranial fragments.

REFERRED SPECIMENS. — UCMP 39705 (Fig. 3), a posterior fragment of the right mandibular ramus, preserving the condyle and angular process; VPPLT-1612 (Figs 4-11; see also Appendices 3-5), a partial skeleton, including its nearly complete skull.

LOCALITIES AND STRATIGRAPHY. — IGM 184247 (holotype), IGM locality 75, level between the Chunchullo Sandstone Beds and the Tatacoa Sandstone Beds; UCMP 39705, UCMP locality V4531 ("Cerro Gordo 2"), level between the Chunchullo Sandstone Beds and the Tatacoa Sandstone Beds; VPPLT-1612, locality "Finca Tres Pasos", La Victoria, Chunchullo Sandstone Beds (StL4 in Mora-Rojas *et al.* 2023). These localities are part of the La Venta area, La Tatacoa Desert, Huila Department, Colombia; La Victoria Formation, Honda Group, Middle Miocene, Laventan SALMA.

TABLE 1. — Dental measurements of the specimens of *Anachlysictis gracilis* Goin, 1997. Abbreviations: **C/c**, upper/lower canines; **P/p**, premolars; **L**, length; **M/m**, molars; **Tal.**, talonid; **Trg**, trigonid; **W**, width. Measurements expressed in millimeters.

Specimen		C	P2	P3		M1	M2	M3	M4
VPPLT 1612 (right)	L	20.63	3.47	6.46		12.3	13.22	12.99	3.99
	W	6.74	1.88	4.42		6.97	8.83	10.2	10.8
VPPLT 1612 (left)	L	?	?	6.41		12.5	*c.* 12.60	*c.* 13.18	4
	W	?	*c.* 2.60	2.56		6.45	8.67	10.3	*c.* 10.70
		c	**p2**	**p3**		**m1**	**m2**	**m3**	**m4**
IGM 184247 (right)	L	?	*c.* 6.00	*c.* 7.20		*c.* 9.50	11.45	13.6	13.4
	W	?	*c.* 3.00	*c.* 3.30	Trg	*c.* 4.45	5.25	6	6
					Tal.	*c.* 4.00	4.75	5.05	1.75
IGM 184247 (left)	L	?	?	?		?	11.3	13.6	?
	W	?	?	?	Trg	?	5	5.8	?
					Tal.	?	4.45	5.1	?
VPPLT 1612 (right)	L	?	*c.* 4.25	*c.* 6.70		9.38	11.81	13.38	13.6
	W		*c.* 2.26	*c.* 3.91	Trg	4.25	5.6	6.59	6.73
					Tal.	3.6	4.85	5.41	2.5
VPPLT 1612 (left)	L	8.94	3.39	6.7		9.24	*c.* 12.05	*c.* 13.35	*c.* 14.00
	W	5.32	1.76	2.5	Trg	3.88	5.29	*c.* 6.46	6.23
					Tal.	*c.* 3.20	4.55	*c.* 5.62	2.5

EMENDED DIAGNOSIS. — Differs from other thylacosmilids in having a proportionally lower and longer skull (longer than twice its width at the level of the zygomatic arch); facial and dorsal portion of the skull flatter; posterior end of palate concave, single arched; mandible much slender and with the symphyseal flange less developed; upper canine not triangular in cross-section and with much shorter root whose implantation is less dorsalized; postcanine teeth rows (upper and lower) less bowed; and protocones and talonids more developed (modified from Goin 1997: 202). Differing from *P. goini* in a less developed postorbital process; less developed *juga alveolaria*; upper canine proportionally wider (less laterally compressed); P2 single-rooted.

MEASUREMENTS. — See Table 1.

COMMENT

Several characters from the diagnosis proposed by Goin (1997) were excluded from the emended diagnosis, as they are now known to be also present in *P. goini*.

DESCRIPTION

The description here proposed is based on the holotype and the new referred specimens reported in this work.

Skull

The skull of *A. gracilis* is relatively gracile compared with that of *T. atrox.* It is relatively lower and longer than the skull of *T. atrox* and *P. goini* (Fig. 12). The snout is longer than wide (Fig. 4) and lower than in *T. atrox* and *P. goini* (Fig. 12). The rostrum of *A. gracilis* (measured from the anterior margin of the orbit and the anterior end of the snout (approximately) is longer than *T. atrox* and *P. goini* or even longer than in borhyaenids.

The maximum width of the skull is at the level of the cranial vault (between the roots of the zygomatic arches), being *c.* 30% wider than the postorbital widest point, differing from *T. atrox*, in which the maximum width is at the level of the postorbital bars. The postorbital constriction is well-marked. The braincase is *c.* 30% longer than wide. In lateral view (Figs 6; 7), the dorsal outline of the skull is roughly straight, slightly curving upwards at the level of the nasofrontal suture and descending forward in a convex outline. This shape is notably different from the skull of *T. atrox*, where the dorsal outline is curved, being dorsally convex in almost all its extension (except at the level of the cranial vault). The occipital condyles project posteriorly approximately until the level of the nuchal crest, differing from the condition in *T. atrox*, where they protrude posteriorly markedly beyond. Breakage and deformation preclude many comparisons with the skull shape of *P. goini*.

The palate is at the same level as the basicranium floor (Appendix 3). In ventral view (Fig. 5), the palate is roughly triangular, diverging backwards and reaching the maximum width at the level of M3. The lateral edge of the palate, corresponding to part of the maxilla, is markedly high, as in *P. goini* (Forasiepi & Carlini 2010) and *T. atrox* (Riggs 1933, 1934; Goin & Pascual 1987), and the postcanine teeth are set in concave (bowed) arcades, less marked than in *P. goini* and much less than in *T. atrox*. In more generalized sparassodonts, the postcanine upper tooth row is generally laterally straight or nearly straight (Sinclair 1906; Babot *et al.* 2002; Forasiepi 2009).

The premaxilla is poorly preserved, cracked, and partially broken. In palatal view, the sutures with the maxilla are obscured by breakage, and it is not possible to see the posterior extension of the lateral palatal process of the premaxilla (Fig. 5). The bone around the incisive foramina was poorly preserved, so their posterior limits are unclear. However, we assume that the bone around the foramen corresponds to the premaxilla anteriorly and laterally, and the maxilla posteriorly, as in other sparassodonts and marsupials (e.g., Sinclair 1906; Wible 2003; Babot *et al.* 2002; Forasiepi 2009; Forasiepi *et al.*

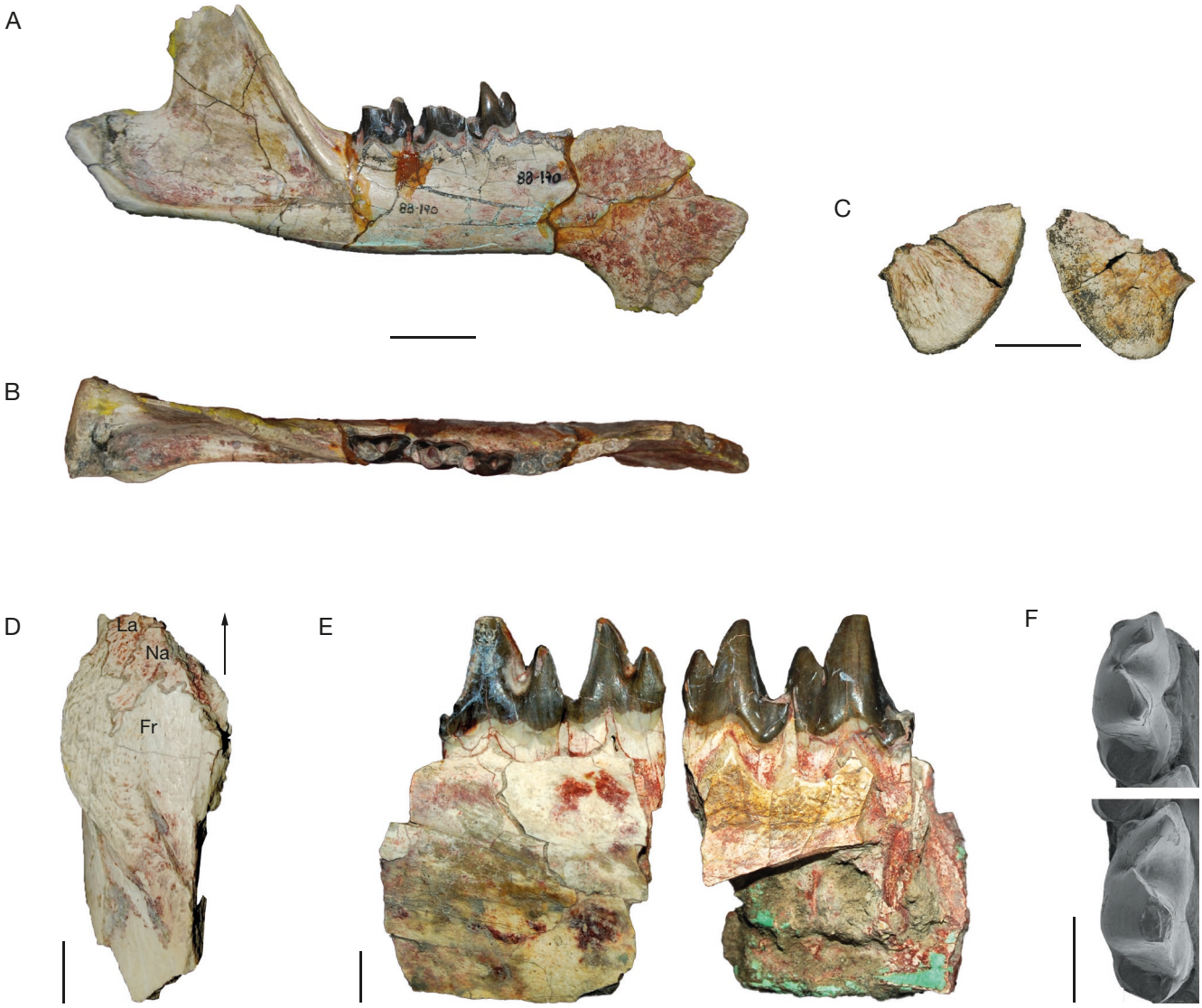

FIG. 2. — *Anachlysictis gracilis* Goin, 1997; IGM 184247 (holotype). Right mandibular ramus in lateral (**A**) and occlusal (**B**) views; **C**, left symphyseal flange fragment in medial and lateral views; **D**, left cranial fragment (postorbital portion; **arrow** indicates anterior direction); **E**, left mandibular ramus fragment with m2-3 in labial and lingual views; **G**, left m2-3 in occlusal view. Abbreviations: **Fr**, frontal; **La**, lacrimal; **Na**, nasal. Scale bars: 5 mm (vertical); 20 mm (horizontal).

2015). There is a thin medial bridge of bone between the incisive foramina, which is part of the medial palatal process of the premaxilla. As suggested by the preserved portion, this structure would be placed in a horizontal position. The foramen occupied a position mostly anterior to the canine with a small extension between the canines (the posterior margin of the incisive foramina is posterior to the anterior edge of the canines). In dorsal view, the posterior end of the facial process of the premaxilla (the posteriormost point of the premaxilla-nasal contact) projected backwards, reaching the level of the upper canine (posterior to its anterior edge; Figs 4; 7). The paracanine fossa is deep and delimited by a crest (it is better visible in ventral view: Fig. 5) and there is not an evident precanine notch. However, the lateral wall of this fossa is crushed, and it is not possible to identify if it is formed only by the premaxilla, as seen in all the sparassodonts with this portion preserved (e.g., *Acyon myctoderos* Forasiepi, Sánchez-Villagra, Goin, Takai, Shigehara & Kay, 2006, *Cladosictis patagonica* Ameghino, 1887, *Lycopsis longirostrus* Marshall, 1976, *Prothylacynus patagonicus* Ameghino, 1891, *Thylacosmilus atrox*, borhyaenids, etc.), or if there is participation of the maxilla.

The maxilla is exposed in dorsal, lateral, and palatal views, and on the orbit floor (in dorsal and dorsolateral views; Figs 4; 6B, C). This bone contributes significantly to the lateral aspect of the skull (though less than in *T. atrox*). It is separated from the frontal by the nasal and lacrimal, which are in contact, as in other sparassodonts (Figs 6; 7), including *P. goini* (e.g., Sinclair 1906; Petter & Hoffstetter 1983; Marshall 1976; Babot *et al.* 2002; Forasiepi & Carlini 2010; Forasiepi *et al.* 2015). However, it differs from the condition of *T. atrox*, in which the maxilla projects dorsally over the dorsal surface of the skull and posteriorly beyond the level of the orbit (forming an ascendant dorsally convex surface), in company of the

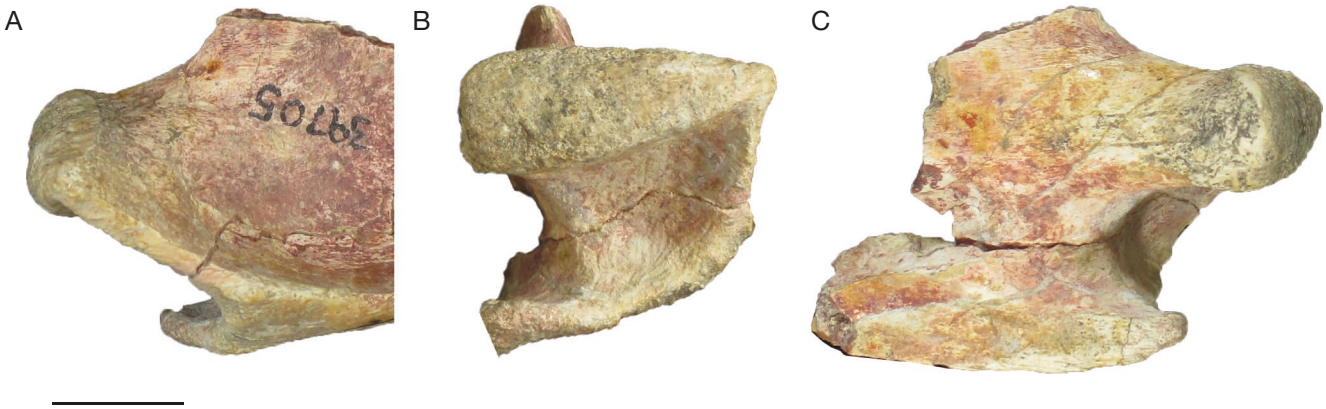

FIG. 3. — *Anachlysictis gracilis* Goin, 1997; UCMP 39705, posterior fragment of right mandibular ramus, in lateral (**A**), posterior (**B**) and medial (**C**) views. Scale bar: 10 mm.

hypertrophied root of the ever-growing canine (Gaillard *et al.* 2023); its posterior border has an extended contact with the frontal bones.

In lateral view (Figs 6; 7), the canine root defines a well-developed swelling (corresponding to the *juga alveolaria*), which projects dorsally, reaching the suture with the nasal. However, this swelling seems to be less prominent than in *P. goini* (but the skull is distorted and this feature seem to be artificially stressed; Fig. 12). In *T. atrox*, this is much more stressed; see the Discussion), however it looks different because this swelling follows all the long dorsal projection of the bone extending posteriorly to the orbit. The infraorbital foramen is relatively small compared to that of other sparassodonts (e.g., *Borhyaena* Ameghino, 1887; see Sinclair 1906), it is placed located dorsal to the posterior root of the P3, as in *P. goini* and *T. atrox*. There is neither an anteorbital fossa nor a small foramen on the facial aspect of the maxillary below the infraorbital foramen (near the alveolar border), like in *T. atrox* (Riggs 1934: 10, pl. I; Goin & Pascual 1987). Below the zygomatic arch, the maxilla bears a small shallow depression at the level of the M3 (more clearly observable on the right side; Fig. 7) that probably corresponds to the depression for the masseter muscle (Turnbull 1970).

In ventral view, the maxilla is not expanded behind the infraorbital foramen as in several sparassodonts (e.g., *Cladosictis* Ameghino, 1887, *Arminiheringia* Ameghino, 1902, *Callistoe* Babot, Powell & Muizon, 2022, *Borhyaena*, *Arctodictis* Mercerat, 1891) where the maxilla is markedly flares forming "cheeks" (Marshall 1981; Babot *et al.* 2002; Forasiepi 2009). The condition in *A. gracilis* is closer to that of *P. goini* and *T. atrox*, with almost flat maxilla (flatter than in *A. gracilis*).

On the palatal process of the maxilla, there are palatal pits between all upper molars. These circular depressions (for the reception of the protoconids when the jaws are closed) are deeper between the M2-3 and M3-4 (Fig. 5). The palatal surface of the maxilla shows several minute foramina (to transmit the major palatine nerve and accompanying vasculature: Forasiepi 2009, characters 22 and 23), as in other sparassodonts (e.g., Sinclair 1906; Marshall 1976; Babot *et al.* 2002; Forasiepi & Carlini 2010; Forasiepi *et al.* 2015), instead of having large fenestrae (vacuities) as seen in living marsupials, or individual major palatine foramina as in placentals. A pair of small minor palatine foramina, nearly circular, is present lateral to both sides of the choanae edges at the level of the posterior-most palatal pit (between the M3 and M4; Fig. 5). They are placed on the maxillo-palatine suture and are largely formed by the palatine and, in less proportion, by the maxilla (contributing to the lateral margin). This position is similar to that of *T. atrox* (Riggs 1934: 19, pl. II-2) and the condition inferred by Forasiepi & Carlini (2010) for *P. goini*. However, in at least one specimen of *T. atrox* (MLP 35-X-41-1), the minor palatine foramen opens entirely in the palatine bone (Forasiepi & Carlini 2010).

A pair of well-defined semicircular notches is present posterior to the minor palatine foramina (at the level of the posterior margin of the M4), medially to each tooth row (see "n" in Fig. 5B). Similar notches (in shape and location) have been identified in some non-thylacosmilid sparassodonts (e.g., *Arctodictis sinclairi* Marshall, 1978; see Forasiepi 2009). They have been interpreted as corresponding to the anterior margin of the minor palatine foramina, which would be opened posteriorly, lacking its posterior bridge (see Forasiepi 2009: character 24). However, in the specimen VPPLT-1612, it is possible to see this structure, while a minor palatine foramen (well-defined, with closed margins) is also clearly identifiable (see "mpf" in Fig. 5).

The zygomatic arch is formed by the jugal and squamosal. It is longer and slenderer than in *T. atrox* (Riggs 1933, 1934) but similar to other sparassodonts, such as the borhyaenoids (e.g., Sinclair 1906; Forasiepi 2009; Forasiepi *et al.* 2015). The maxilla-jugal suture is irregular and forms a roughly zigzag line, as in *T. atrox* (Fig. 7). The suture between the jugal and squamosal is almost straight. In lateral view (Fig. 4), the anteriormost edge of the jugal reaches the level of the M2 (approximately posterior to the metacone). The external surface of the zygomatic arch (including both jugal and squamosal) has long, narrow parallel striae. The anterodorsal margin of the jugal is concave, forming the ventral border of the orbit and ending posteriorly in a frontal process of the jugal, which is tall. The jugal usually ends posteriorly bifurcated in two branches, one dorsal and

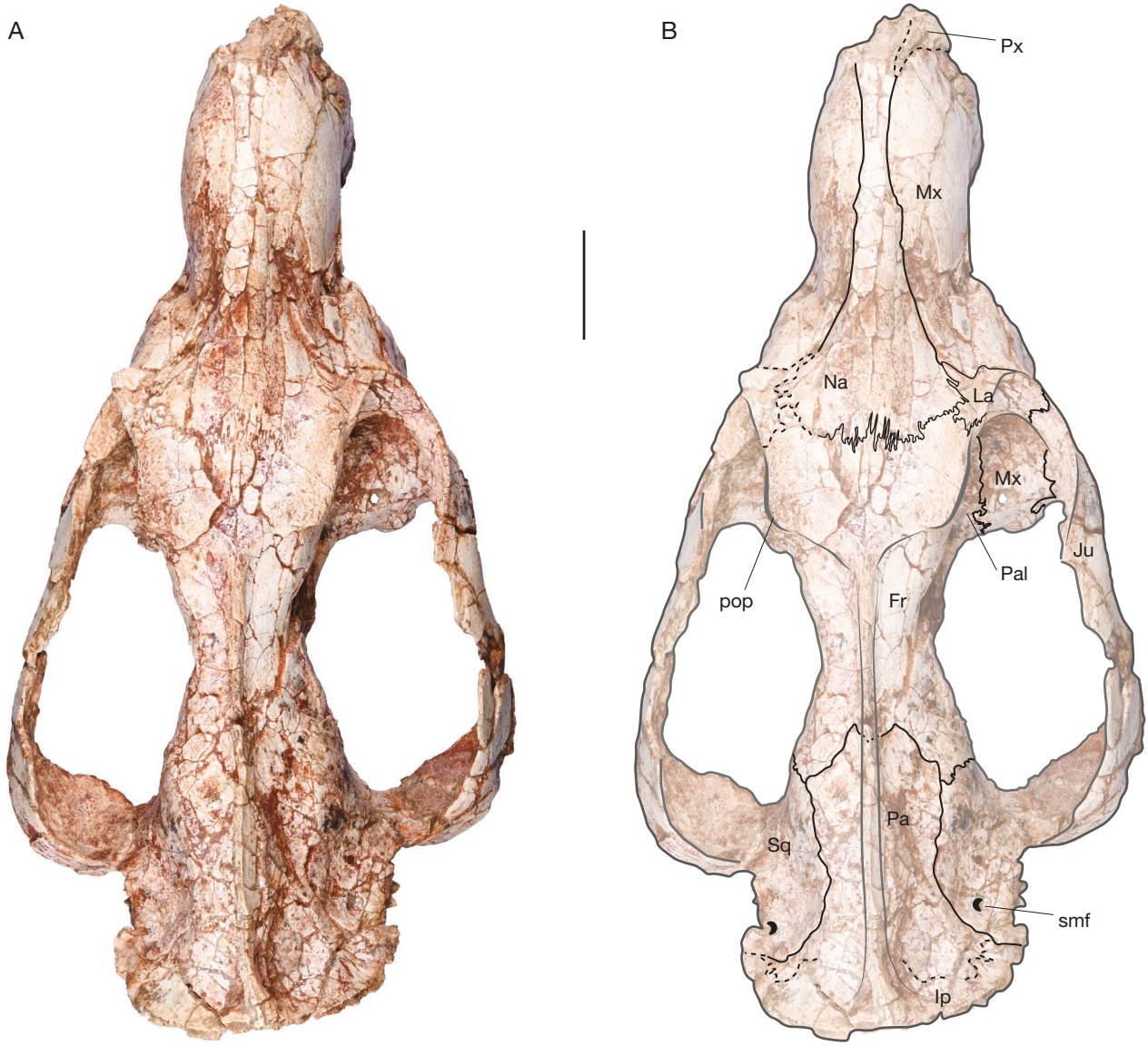

FIG. 4. — *Anachlysictis gracilis* Goin, 1997; VPPLT 1612, skull in dorsal view (**A**) and lineal draw (**B**). Abbreviations: **Ip**, interparietal; **Ju**, jugal; **La**, lacrimal; **Mx**, maxilla; **Na**, nasal; **Pa**, parietal; **Pal**, palatine; **pop**, postorbital process; **Px**, premaxilla; **smf**, suprameatal foramen; **Sq**, squamosal. Scale bar: 20 mm.

one ventral. Only the ventral branch is completely preserved in the specimen VPPLT-1612 (Fig. 7). It is ventrally curved and extends posteriorly to form the preglenoid process.

The palatine (paired) contributes to the posterior hard palate, the nasopharyngeal passage, and the medial wall and floor of the orbit. In ventral view, the palatine contacts the maxilla anteriorly and the presphenoid and pterygoid posteriorly in the nasopharyngeal passage (Fig. 5). In this view, the palatines extend anteriorly until the level of the M2, forming an irregular parabolic suture with the maxilla; and posteriorly to the level of the last molar, as in *P. goini* and *Borhyaena tuberata* Ameghino, 1887. The posterior end of the palatines on the palate is slightly thicker than the rest of the horizontal plate, forming the border of the choanae. This border is posteriorly concave, single-arched, differing from *T. atrox*, with a double-arched margin. The choanae open at the level of the contact between M3-4. The portion of the palatines exposed into the nasopharyngeal passage (immediately behind the choanae border) is strongly cracked. However, it is possible to see that they are well developed and expanded on the medial side but without midline contact, as the presphenoid is visible between them (Fig. 5).

In dorsal and dorsolateral views, the palatine is exposed on the orbit floor and separated from the maxilla by an irregular suture. It contributes to the infraorbital canal. In lateral view, the sutures delimiting the palatine are interrupted by bone fractures. However, it is possible to see the contact with the maxilla and lacrimal anteriorly and the frontal dorsally. The palatine also contacts the orbitosphenoid, alisphenoid, and pterygoid posteriorly, but these sutures are difficult to differentiate due to the specimen's poor preservation (see Fig. 6). At the junction of the floor and lateral wall of the orbit, the sphenopalatine foramen is observed, though poorly preserved. This aperture is close to the anterior border of the orbit, as

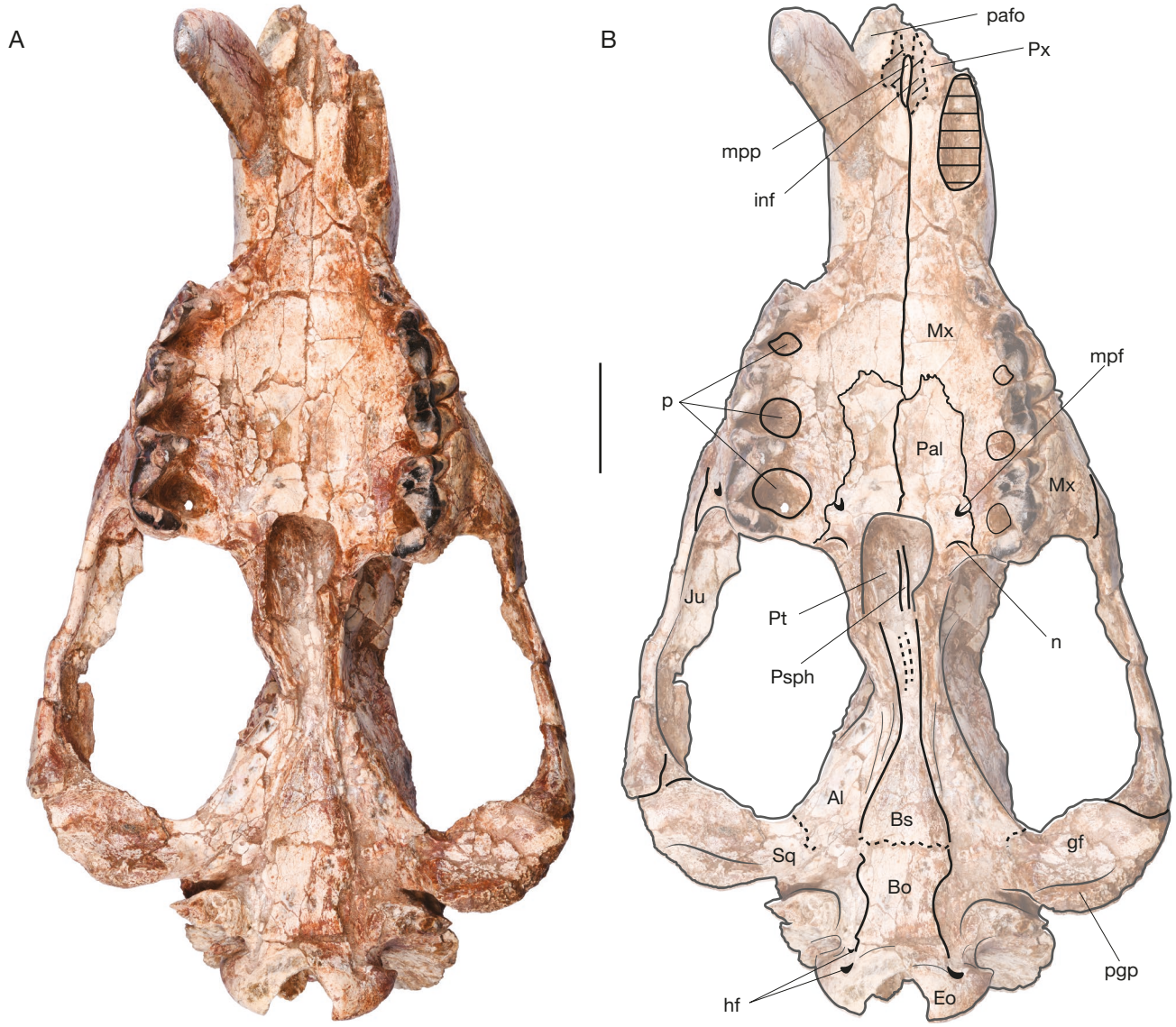

Fig. 5. — *Anachlysictis gracilis* Goin, 1997; VPPLT 1612, skull in ventral view (**A**) and lineal draw (**B**). Abbreviations: **Al**, alisphenoid; **Bo**, basioccipital; **Bs**, basisphenoid; **Eo**, exoccipital; **gf**, glenoid fossa; **hf**, hypoglossal foramina; **inf**, incisive foramen; **Ju**, jugal; **mpf**, minor palatine foramen; **mpp**, medial palatine process of premaxilla; **Mx**, maxilla; **n**, notch; **p**, pits; **pafo**, paracanine fossa; **Pal**, palatine; **pgp**, postglenoid process; **Psph**, presphenoid; **Pt**, pterygoid; **Px**, premaxilla; **Sq**, squamosal. Scale bar: 20 mm.

in *P. goini* (Forasiepi & Carlini 2010), while in other sparassodonts, including *T. atrox*, this aperture is more posterior (Riggs 1934; Forasiepi 2009; Forasiepi & Carlini 2010).

The pterygoid is a paired bone exposed in the mesocranium in ventral and lateral views. In ventral view, the pterygoids are well developed and expanded on the medial side but without middle contact, exposing the presphenoid. Posteriorly, the pterygoids project posterolaterally (at each side) on the ventral surface of the alisphenoid, forming thin ribbons (i.e., probably part of the pterygoid hamulus or hamular processes), better preserved on the right side (Figs 5; 8AB).

The nasals are well exposed in dorsal view (Fig. 4), they are very narrow anteriorly and broad posteriorly, widening abruptly at the level of the orbit, as in *P. goini* (Forasiepi & Carlini 2010). This difference in width is even more conspicuous than in other sparassodonts (Sinclair 1906; Babot *et al.* 2002; Forasiepi 2009). This morphology differs from *T. atrox*, where the nasals narrow backwards in dorsal view, although they are long (Riggs 1934; Turnbull & Segall 1984), compressed between the maxilla and reaching the level of the orbit. The nasofrontal suture is posteriorly convex, forming an open "U", as in *P. goini* (Forasiepi & Carlini 2010), similar to other sparassodonts (Sinclair 1906; Forasiepi 2009) and differing from *T. atrox*, where the frontal is not in contact with the nasal, because of the enlargement of the maxilla as described before (e.g., Riggs 1934; Marshall 1976; Goin & Pascual 1987; Muizon 1999).

In lateral view (Figs 6; 7), the lacrimal of *A. gracilis* extends anteriorly beyond the orbit and orbital rim, with a relatively wide exposition on the rostrum (the width of

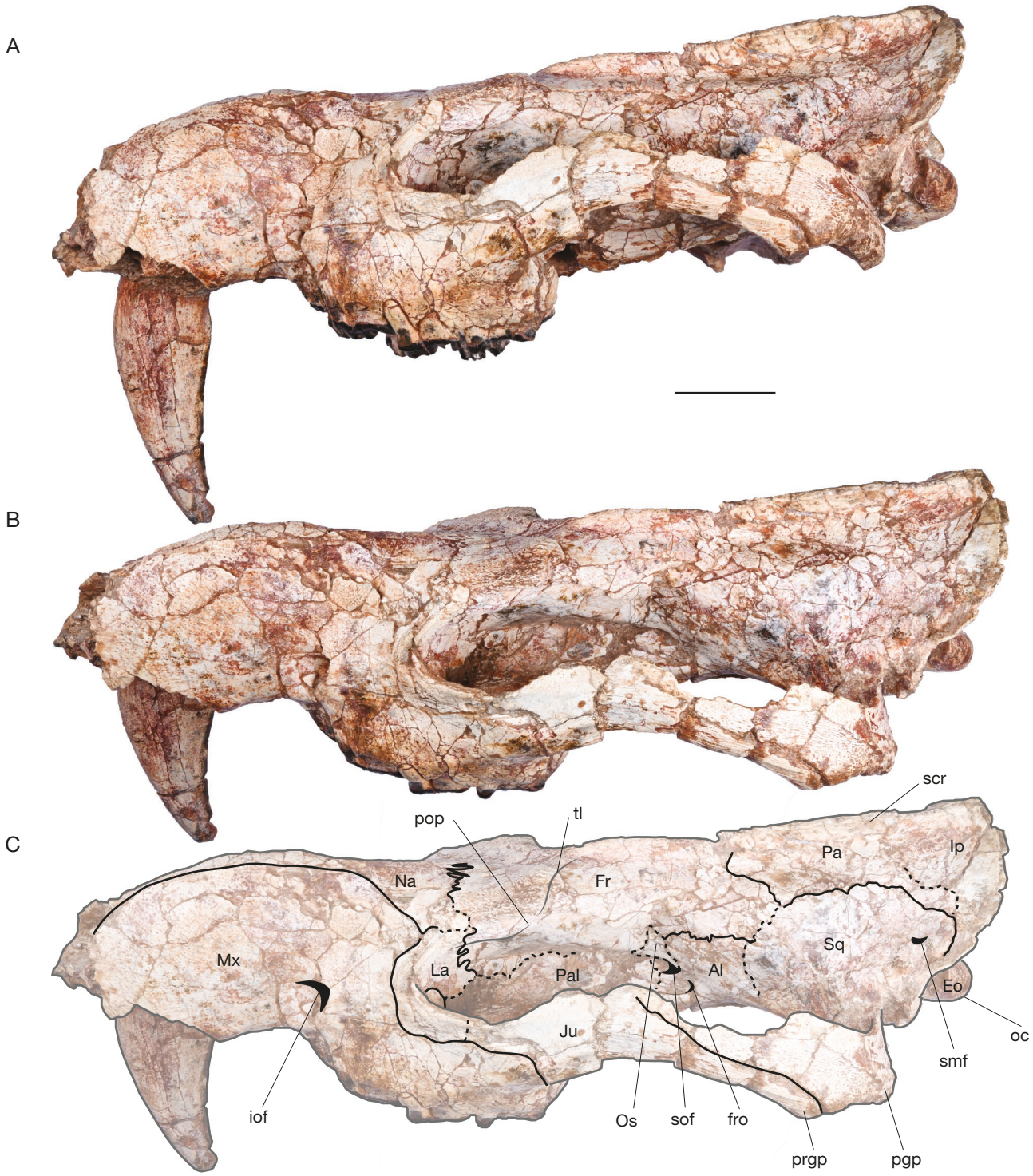

Fig. 6. — *Anachlysictis gracilis* Goin, 1997; VPPLT 1612, left side of the skull: **A**, lateral view; **B**, dorsolateral view; **C**, lineal draw in dorsolateral view. Abbreviations: **Al**, alisphenoid; **Eo**, exoccipital; **Fr**, frontal; **fro**, foramen rotundum; **iof**, infraorbital foramen; **Ip**, interparietal; **Ju**, jugal; **La**, lacrimal; **Mx**, maxilla; **Na**, nasal; **oc**, occipital condyle; **Os**, orbitosphenoid; **Pa**, parietal; **Pal**, palatine; **pgp**, postglenoid process; **pop**, postorbital process; **prgp**, preglenoid process of jugal; **sof**, sphenorbital fissure; **smf**, suprameatal foramen; **Sq**, squamosal; **scr**, sagittal crest; **tl**, temporal line. Scale bar: 20 mm.

the facial process of the lacrimal is more than half of its height; Fig. 4), similar to the condition seen in *T. atrox* and some non-thylacosmilid sparassodonts with the lacrimal extended onto rostrum (e.g., *Callistoe vincei*, *Arctodictis sinclairi*, *Borhyaena tuberata*, *Prothylacynus patagonicus*). There is one lacrimal foramen on each lacrimal bone, inside the orbit, a generalized condition among sparassodonts (Sinclair 1906; Riggs 1934). The lacrimal tubercle in *A. gracilis* is less developed than in *P. goini* and *T. atrox* (relatively more developed in the latter).

The frontals contact the nasals and lacrimals anteriorly, the palatine and alisphenoid ventrally, and the parietals and squamosal posteriorly, all by irregular sutures. The suture with the nasals is posteriorly convex (seen in dorsal view: Fig. 4); the one with the lacrimal and palatine is roughly anteriorly convex (visible in orbital view; Fig. 6B, C). The suture with the parietals is transverse (visible in dorsal view: Fig. 4); while the one with the squamosal is slightly anteriorly convex (visible in lateral view: Fig. 7). The point of contact between the nasal, lacrimal, and frontal is located approximately at the level of the postorbital process in the holotype of *A. gracilis* (Fig. 2D), as in *P. goini* (the appearance of this portion of the skull is almost identical). However, the condition in the specimen VPPLT-1612 is different, with the contact anterior to the postorbital process (Fig. 7), similar to other sparassodonts (e.g., *Hondadelphys* Marshall, 1976, *Sallacyon* Villarroel & Marshall, 1982, *Acyon* Ameghino, 1887, *Cladosictis*, *Prothylacynus* Ameghino, 1891, *Arctodictis*, *Pharsophorus* Ameghino, 1897, *Callistoe*). In *T. atrox*, the relationship between these bones is different because the posterodorsal projection of the maxilla interposes between the nasal and lacrimal. However, the posteriormost point of the lacrimal-frontal suture extends beyond the level of the postorbital bar, being even more posterior than in *A. gracilis* and *P. goini*. Besides these three thylacosmilid taxa (excepting the specimen VPPLT-1612), none of the other metatherian taxa observed for the present work (see Material examined in Appendix 1) shows the lacrimal reaching the level of the postorbital process (or bar).

The postorbital processes are well developed (Figs 4; 6), similar to *P. goini,* and differing from *T. atrox*, where there is a bony postorbital bar, being the only sparassodont with the orbit completely separated from the temporal fossa (Riggs 1933, 1934), and one of the few metatherians with a complete osseous postorbital bar (Gaillard *et al.* 2023). A small foramen is present anteroventrally to the postorbital process, probably corresponding to the foramen for the frontal diploic vein (Fig. 7), following a similar structure recognized in *Monodelphis domestica* Wagner, 1842 (see Wible 2003). The temporal lines are weak and contact at the mid-line of the skull, forming the anterior base of the sagittal crest (Figs 4; 6). This condition is similar to *P. goini* (Forasiepi & Carlini 2010), resembling other sparassodonts and differing from *T. atrox,* with temporal lines strongly developed, converging more posteriorly in the skull and describing a sigmoid line (Riggs 1933, 1934; Forasiepi & Carlini 2010).

The parietal is paired and both elements form most of the roof of the skull (Fig. 4). It contacts the frontals anteroventrally, the squamosal posteroventrally, and the interparietal posteriorly, by irregular sutures. The suture between the parietals and frontals shows a posterior wedge of frontals entering between the parietals. The contact with the interparietal is partially visible in VPPLT-1612; in *P. goini* (see referred specimen: Material and methods, and Appendix 1, Material examined) the suture is incomplete due to partial fusion with the parietal. In *T. atrox*, the interparietal is also distinguishable from the parietal, as in several metatherians (e.g., *Didelphis* Linnaeus, 1758, *Monodelphis* Burnett, 1830, *Macropus* Shaw, 1790*, Sipalocyon* Ameghino, 1887*,* and *Cladosictis*; Clark & Smith 1993; Forasiepi 2009), in contrast with other borhyaenoids, where it is not (e.g., *Arctodictis, Lycopsis* Cabrera, 1927*, Borhyaena*; see Forasiepi 2009). Fusion with parietals is inferred in those cases in which suture is not observed, since presence of interparietal seems to be primitive common pattern of mammals (Koyabu *et al.* 2012). The interparietal contacts the squamosal anteroventrally by an irregular suture and forms most of the nuchal crest.

The sagittal crest is formed at the midline of the skull by frontals, parietals and interparietals and becomes taller posteriorly (Figs 4; 6; 7; see also Appendix 3). It is well developed and long, extending from the anterior area of the temporal fossa to the nuchal crest, similar to *P. goini* (Forasiepi & Carlini 2010); in *T. atrox,* the sagittal crest is considerably shorter and much more taller and robust (likely to enlarge the area of attachment of the temporal muscle by considering the shorter length of the temporal fossa; Gaillard *et al.* 2023). The nuchal crest is located at the posterodorsal border of the skull (Figs 6; 7; Appendix 3). It is formed by the interparietal and supraoccipital medially and the squamosal lateroventrally. It is well developed, flaring posterolaterally and posterodorsally, and extends back to the level of the occipital condyles (see Appendix 3), as in *P. goini*, but differing from *T. atrox*, where the nuchal crest is located more anteriorly, thus the condyle is fully visible in a dorsal view of the skull.

The squamosal forms the posterior portion of the zygomatic arch and the posteroventral portion of the temporal region; it also contributes to the walls of the middle ear cavity as seen in ventral view. It contacts the frontal anteriorly, the alisphenoid anteroventrally, the jugal anteriorly and ventrally (in the zygomatic arch), the frontal anterodorsally, the parietal dorsally, and the interparietal posteriorly (Figs 4-8). In ventral view, the squamosal contacts the jugal at the anterolateral margin of the glenoid cavity and the alisphenoid medially in the ear region (Fig. 5). The zygomatic process of the squamosal, in lateral view, has a roughly elongated shape with well-defined borders. In lateral view, the temporal portion of the squamosal is well developed, roughly semicircular, and its surface is convex, defined by an irregular suture (Figs 4; 6; 7). The suprameatal foramen opens on the posterolateral region of the squamosal (Figs 6; 7; Appendix 3), at the level of the external acoustic meatus and above the suprameatal crest. This foramen is oval-shaped and opens posterodorsally.

The glenoid cavity is formed only by the squamosal, because the preglenoid process of the jugal contacts it but does not contribute to the cavity, lacking an articular facet (as in *P. goini* and *T. atrox*). The alisphenoid does not either contribute to the glenoid cavity (Fig. 5) and there is no alisphenoid glenoid process, as in marsupials (see Wible 2003). The glenoid cavity is concave and ellipsoidal, with the transverse length less than twice the anteroposterior width and faces ventrally (Fig. 5). In lateral view, the preglenoid process of jugal and the postglenoid process of the

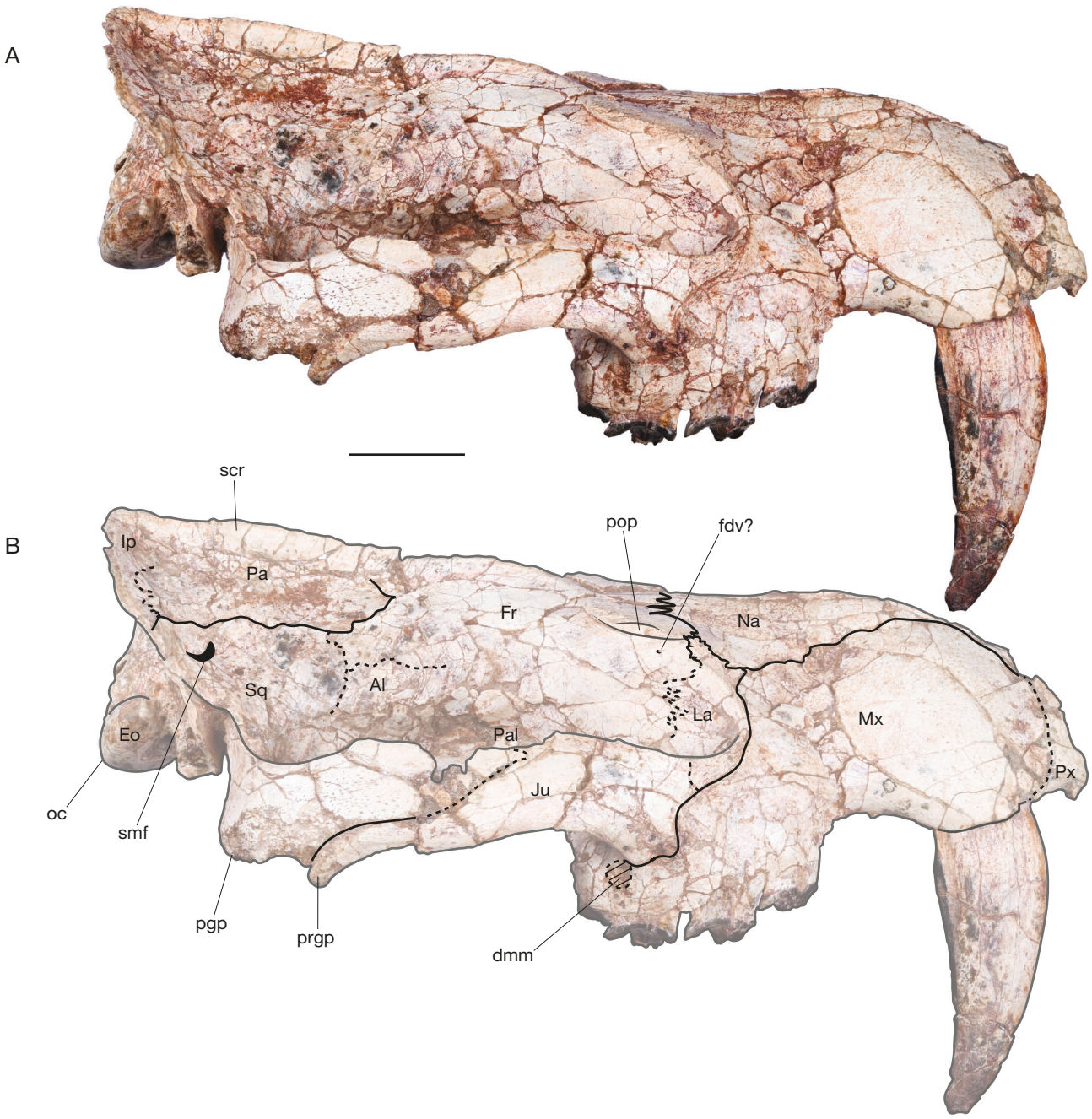

FIG. 7. — *Anachlysictis gracilis* Goin, 1997; VPPLT 1612, right side of the skull: **A**, lateral view; **B**, dorsolateral view; **C**, lineal draw in dorsolateral view. Abbreviations: **Al**, alisphenoid; **dmm**, depression for the masseter muscle; **Eo**, exoccipital; **fdv**, foramen for diploic vein; **Fr**, frontal; **Ip**, interparietal; **Ju**, jugal; **La**, lacrimal; **Mx**, maxilla; **Na**, nasal; **oc**, occipital condyle; **Pa**, parietal; **Pal**, palatine; **pgp**, postglenoid process; **pop**, postorbital process; **prgp**, preglenoid process of jugal; **Px**, premaxilla; **smf**, suprameatal foramen; **Sq**, squamosal; **scr**, sagittal crest. Scale bar: 20 mm.

squamosal have a similar ventral extension (better seen on the right side, with less deformation), though the postglenoid process is wider (lateromedially) and relatively more robust anteroposteriorly than the preglenoid process. The postglenoid foramen is placed on the anterior wall of the external acoustic meatus, medial to the postglenoid process.

Regarding the sphenoid complex, the orbitosphenoid and alisphenoid are exposed in the lateral wall, while the presphenoid and basisphenoid are on the skull floor. However, the synchondrosis between the components of the sphenoid complex are only partly seen. In lateral view, the orbitosphenoid is small, in contact with the alisphenoid, palatine, and frontal. The sphenorbital fissure is the largest aperture on the lateral wall of the skull. It is limited by the orbitosphenoid anteriorly and the alisphenoid posteriorly (Figs 6B, C; Appendix 3) as in other metatherians (e.g., Wible 2003).

The alisphenoid mainly contributes to the lateral wall of the braincase and the anterior wall of the tympanic cavity. In lateral view, the alisphenoid contacts the pterygoid,

palatine, and orbitosphenoid anteriorly, the frontal dorsally, and the squamosal posteriorly (Fig. 6B, C). On the alisphenoid, the foramen rotundum is located posterior to the sphenorbital fissure, opening at the angle between the lateral wall and the floor of the infratemporal fossa. The foramen rotundum is small compared to the sphenorbital fissure, round, and anteriorly directed. There is a relatively wide and shallow sulcus running forward from the foramen rotundum (Fig. 6B, C), which was likely occupied in life by the maxillary division of the trigeminal nerve V_2 and accompanying vessels (Sisson 1965; Hiatt 2020).

In ventral view, there is no contribution of the alisphenoid to the tympanic floor (it lacks an alisphenoid tympanic process similar to *T. atrox*; Forasiepi *et al.* 2019). The foramen ovale is bounded by the alisphenoid only (without any contribution of the petrosal). Similar to *T. atrox* and the specimen from Quebrada Honda referred to *P. goini* (see Material and methods, and Appendix 1, Material examined), there is a posterior rod of alisphenoid bone that posteriorly limits the foramen ovale as seen in the right side of the skull. This piece of bone does not qualify as a component of the alisphenoid tympanic process because it does not participate in bounding the middle ear cavity and for that reason, we interpret that there is not a secondary foramen ovale, like in other sparassodonts (see Forasiepi 2009).

The middle ear cavity is so poorly preserved and fragile that its preparation could not be completed. In consequence, neither the petrosal (which we do not discard it could be preserved internally, as in *Thylacosmilus*; Forasiepi *et al.* 2019) nor the suture with this bone is observable by surface examination; similarly, its suture with the exoccipital is not clearly visible.

In ventral view, the presphenoid, basisphenoid and basioccipital forms the floor of the caudal cranium. The synchondroses between sphenoid elements are not clear. The presphenoid exposes on the nasopharyngeal passage. The basisphenoid is roughly triangular and anteroposteriorly elongated (Fig. 5). It contacts the basioccipital posteriorly, through an almost transverse synchondrosis, and the alisphenoid laterally. There are two thick, robust, and parallel crests, the sphenoidal tubercles or basilar tubercles (Riggs 1934; Forasiepi *et al.* 2019), which decrease in height anteriorly (Fig. 8A, B; more details in Appendix 3). These structures are much weaker than those of *T. atrox*, where they are hyperdeveloped. In *P. goini*, they are intermediate in size. Lateral to the basilar tubercles, there is a very narrow and shallow groove that becomes shallower anteriorly (Figs 5; 8A, B; Appendix 3). The carotid foramen opens posterolaterally anterior to the basisphenoid-basioccipital synchondrosis is (Fig. 8A, B).

The posterior floor of the caudal cranium is formed by the basioccipital. It contacts the basisphenoid anteriorly and the exoccipitals posterolaterally. It would also contact the petrosal laterally as in other marsupials and sparassodonts (e.g., Babot *et al.* 2002; Wible 2003; Forasiepi 2009; Forasiepi *et al.* 2019), but matrix prevents further confirmation. In ventral view, the basioccipital is roughly rectangular (with the lateral borders laterally convex; Figs 5; 8A, B). In ventral view, and at the anterolateral limit with the condyle, there is a large foramen; posterior to it, there is another one, similar in size but placed on the condyle surface (Fig. 8A, B). Both foramina open anteriorly and correspond to two hypoglossal foramina (rostral and caudal). At each side of the basioccipital, there is a deep basijugular sulcus (Forasiepi *et al.* 2019) running with a constant width in direction to the rostral hypoglossal foramen (Fig. 8). This sulcus ends anteriorly in a concavity that could correspond to the foramen for the inferior petrosal sinus but its margins are broken (Fig. 8). For the same reason, the morphology of the jugular foramen (or fossa) and its convergence with the inferior petrosal sinus could not be evaluated for this specimen.

In posterior view (Fig. 8C), synchondroses between the occipital bones (or their absence due to fusion) are not seen due to the bad preservation condition of the occiput. Similarly, it is also unclear if the mastoid portion of the petrosal contributes to the occipital shield, and the extension of the contribution of the squamosal. The dorsal portion of the occipital shield is slightly concave in posterior view. It contacts the interparietal dorsally at the level of the nuchal crest. Numerous minor grooves and rugosities are mainly distributed on the lateral sides of the occipital surface (Fig. 8C). All these scars would correspond to the attachment area of the nuchal musculature (Turnbull 1970). There are also several small foramina, likely related to the feed of the occipital musculature. The occipital condyle protrudes posteriorly and is ellipsoidal in posterior view, with the longer axis in a horizontal position. The articular facets of the condyle continue at the sagittal plane, connecting ventrally.

Dentary

The dentary is intermediate in height (depth below m3/m4 embrasure/total length of dentary = 0.17), and the horizontal ramus represents approximately 60% of the total length. The ventral border of the dentary is nearly horizontal behind the level of the p2 (Figs 2A; 9; Appendices 4, 5). Anterior to the p2, the dentary increases in height and its ventral border curves, expanding ventrally, forming a symphyseal flange (Figs 2A, C; 9; Appendices 4, 5), less developed than in *T. atrox* and *P. goini* (inferred from a portion present in the specimen from Quebrada Honda; see Material and methods, and Appendix 1, Material examined). The dentary is laterally concave at the level of the canine-premolar series and laterally convex at the level of the molar series, resulting in a sigmoid morphology, better seen in dorsal and ventral views (Figs 2B; 9C; Appendices 4, 5), less marked than in *P. goini* and much less than in *T. atrox*. This morphology is accompanied by a bowed lower postcanine tooth row, slightly less marked than in the upper arcade and less than in the other thylacosmilids.

The height of the coronoid process is at least twice that of the horizontal ramus (behind the p2), being taller than in *T. atrox*, where it is also strongly reduced. The angle between the anterior coronoid crest and the alveolar border is *c.* 116º,

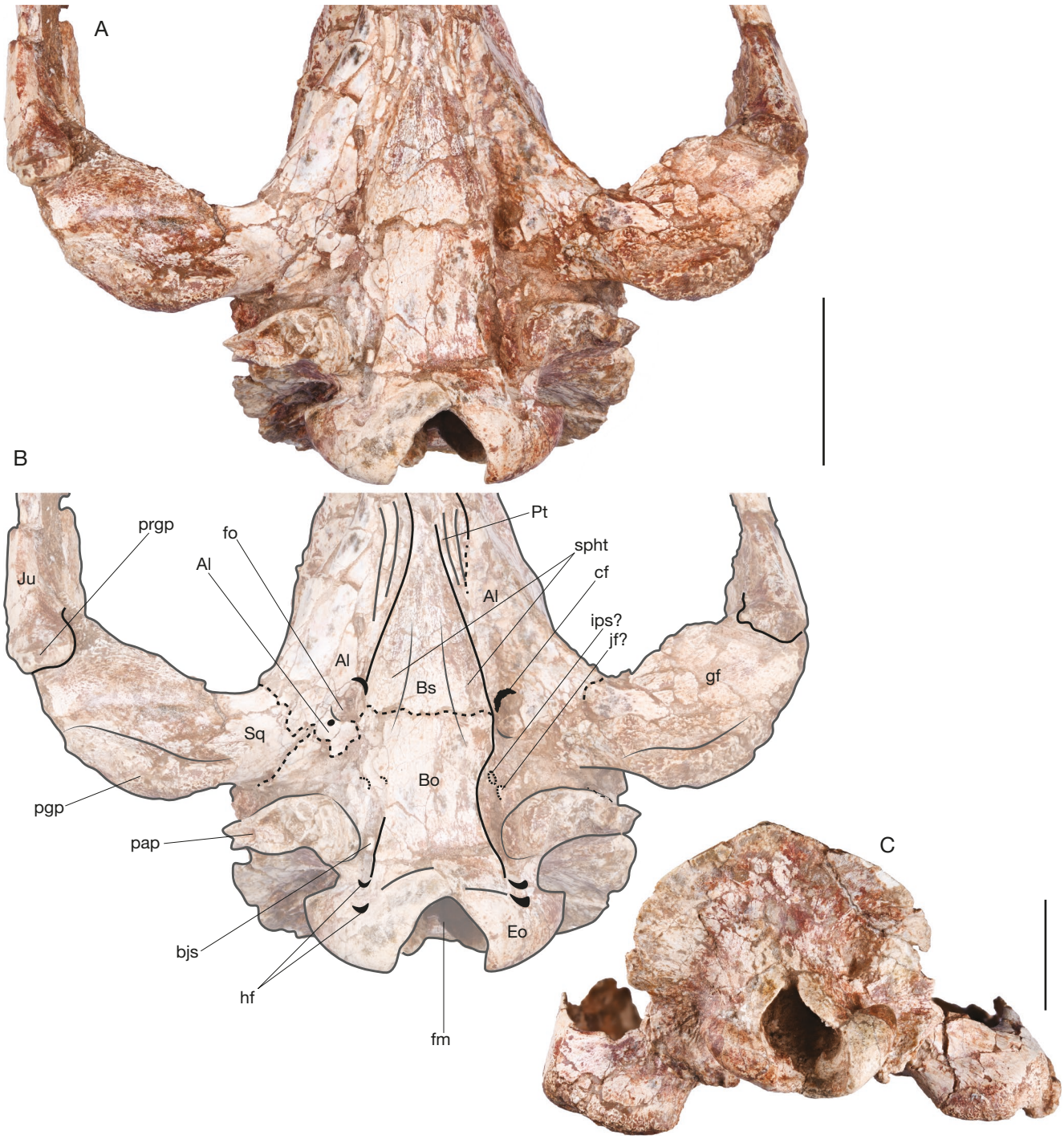

Fig. 8. — *Anachlysictis gracilis* Goin, 1997; VPPLT 1612, posterior portion of the skull: **A**, detail of basicranium in ventral view; **B**, lineal draw of the basicranium in ventral view; **C**, occipital view of the skull. Abbreviations: **Al**, alisphenoid; **Bo**, basioccipital; **Bs**, basisphenoid; **bjs**, basijugular sulcus; **cf**, carotid foramen; **Eo**, exoccipital; **fm**, foramen magnum; **fo**, foramen ovale; **gf**, glenoid fossa; **hf**, hypoglossal foramina; **ips**, foramen for the inferior petrosal sinus; **jf**, jugular fossa; **Ju**, jugal; **pap**, paracondylar process of exoccipital; **pgp**, postglenoid process; **prgp**, preglenoid process of jugal; **Pt**, pterygoid; **spht**, sphenoidal tubercles (basilar tubercles); **Sq**, squamosal. Scale bar: 20 mm.

greater than in *T. atrox* (*c.* 90°). The masseteric crest is horizontal at the three quarters anterior while its posteriormost portion bends upwards, forming an obtuse angle, and projects along the coronoid process as a continuous, flat shelf. The masseteric fossa is wide and well developed, differing from the strongly reduced fossa in *T. atrox*. The mandibular condyle is cylindrical, oval in posterior view, with a well-defined mandibular neck, and located at the level of the tooth row as in *T. atrox* (Figs 3; 9; Appendix 5). The shape of the angular process is shelf-like (following Sánchez-Villagra & Smith 1997) and extends medially slightly beyond the level of the medial end of the mandibular condyle (Appendix 5).

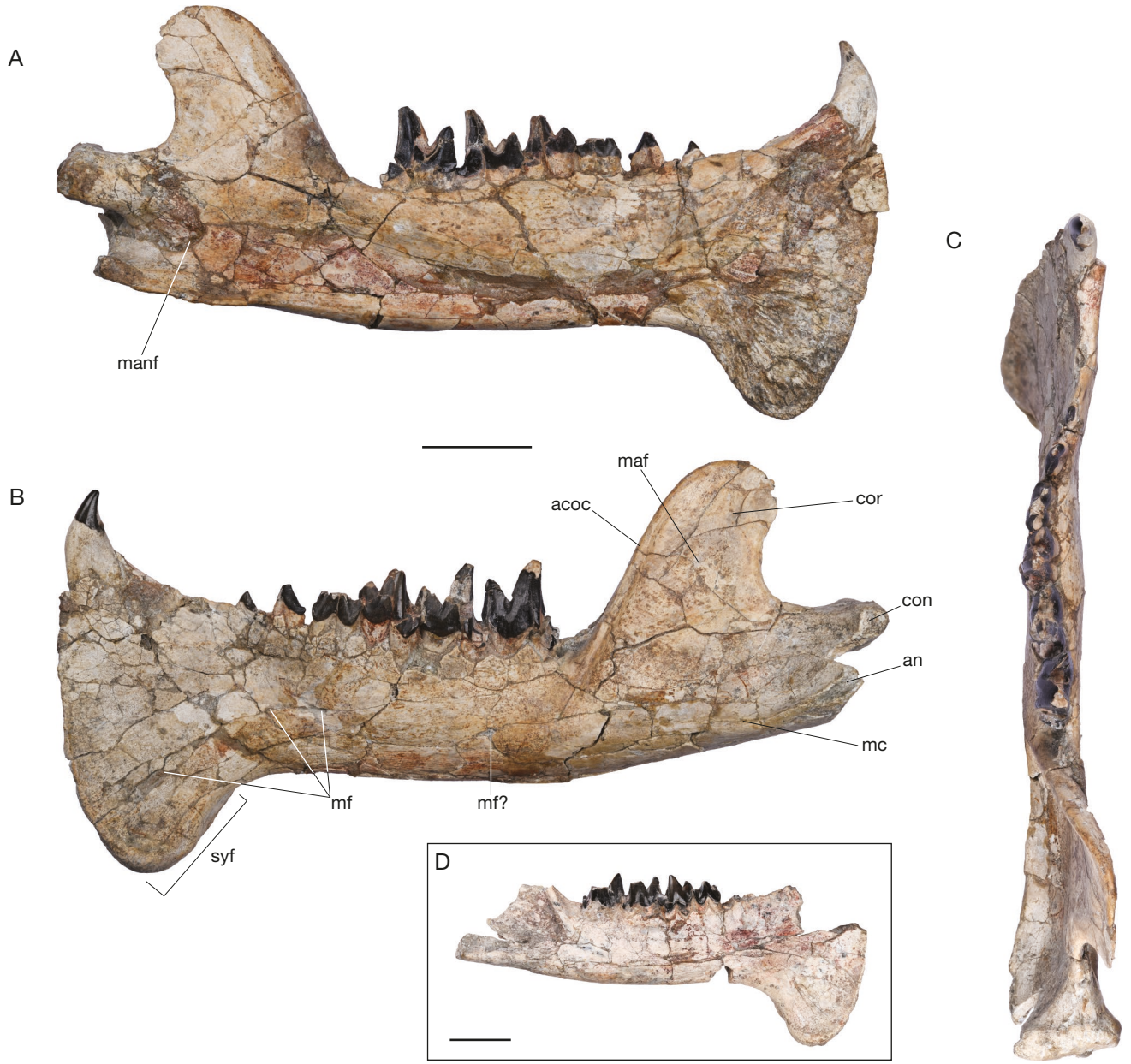

FIG. 9. — *Anachlysictis gracilis* Goin, 1997; VPPLT 1612, left dentary in lingual (**A**), labial (**B**) and occlusal (**C**) views; and right dentary in labial view (**D**). Abbreviations: **acoc**, anterior coronoid crest; **an**, angular process; **con**, mandibular condyle; **cor**, coronoid process; **maf**, masseteric fossa; **manf**, mandibular foramen; **mc**, masseteric crest (= inferior coronoid crest); **mf**, mental foramen; **syf**, symphyseal flange. Scale bars: 20 mm.

In lateral view, three mental foramina are present: the anteriormost and largest is located on the symphyseal flange slightly posterior to the level of the canine; the second is located below the p2-3 contact level; and the third, below the anterior root of the m1 (Figs 2A, C; 9B). The specimen VPPLT-1612 shows what apparently could be a broken fourth mental foramen below the anterior root of the m4. However, it is not clear if it is, in fact, a foramen or just an artificial aperture, because the bone is broken at this exact point in both the left and right dentaries. The anteriormost mental foramen in *A. gracilis* is located on the lower portion of the symphyseal flange, being topographically not aligned with the other foramina but markedly lower, surpassing ventrally the level of the ventral margin of the horizontal ramus (the portion behind the flange), similar to *T. atrox* (in this species the foramen is below the lower canine). This condition differs from that in other compared sparassodonts in which the first mental foramen is aligned or nearly aligned to the other foramina. In medial view, the mandibular foramen of *A. gracilis* is large, located at the midpoint of the coronoid process in the holotype, similar to *T. atrox*, and posterior to this point in the specimen VPPLT-1612 (Fig. 9A).

Dentition

The dental formula of *A. gracilis* is: I4?/i?, C1/c1, P2/p2, M4/m4. The premolars are uninflated and reduced in number (see

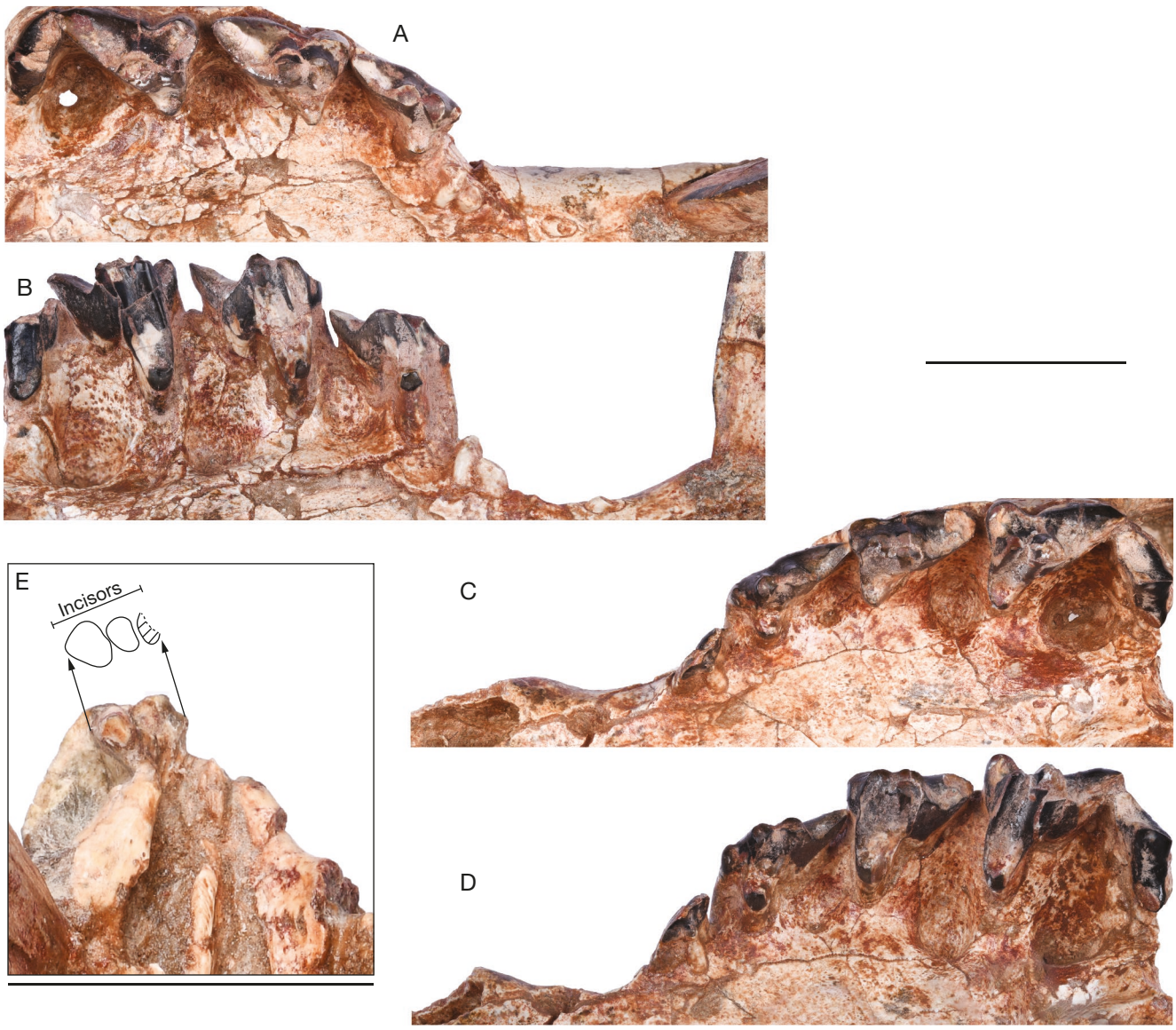

FIG. 10. — *Anachlysictis gracilis* Goin, 1997; VPPLT 1612, upper dentition. Right row in occlusal (**A**) and lingual (**B**) views; left side in occlusal (**C**) and lingual (**D**) views; and detail of the incisors area in occlusal view (**E**). Scale bars: 20 mm.

below). The dentition shows a marked carnassial morphology: a moderate reduction of the protocone, talonid basin (participants in the crushing mechanism), and stylar shelf; and a strong development of cutting blades (preparacrista, postmetacrista, and paracristid). However, these carnivorous adaptations are slightly less developed than in *P. goini* and much less than in *T. atrox* (and other sparassodonts such as borhyaenids). Although some cusps are secondarily broken, it is possible to see a moderate wear (in both specimens with dentition preserved: the holotype and VPPLT-1612). Additionally, the molars are completely erupted (Figs 10-11; Appendix 3), indicative of an adult or young adult ontogenetic stage.

Upper dentition. The premaxilla is broken anteriorly in the specimen VPPLT-1612 (not preserved in the holotype), but there is evidence of at least three incisors at the right side: an incomplete alveolus with a fragment of root, followed by a second alveolus preserving the root, and a posterior incisor with almost complete crown (only the tip is broken; Fig. 10E). However, although the bone is broken at the anterior margin of the palate, there is enough space between the first preserved alveolus and the midline to allocate an additional incisor, suggesting the presence of four incisors in this specimen. Following the position of the incisors on the right side, the arcade would be slightly parabolic in shape. The upper incisors, if present, are unknown in *P. goini* and *T. atrox* but based on wear surfaces on the lower incisors and the transverse breadth between the upper canines, *T. atrox* could have possessed upper incisors (Churcher 1985; Goin & Pascual 1987). However, no specimen has yet been collected preserving upper incisors.

Such as *T. atrox* and *P. goini*, the most outstanding feature of the upper dentition of *A. gracilis* is the hyperdeveloped

canine. This tooth is long, narrow, and sabre-like. It is proportionally less developed than in *P. goini*, being vertically and anteroposteriorly shorter, though relatively slightly wider (laterally less compressed), and markedly less developed than in *Thylacosmilus*. In lateral view, the anterior border is convex and more curved, while the posterior is also convex at the proximal portion but concave at the distal (Appendix 3). The anterior border is blunt and slightly thicker, whereas the posterior one is sharp (Fig. 7), forming a crest which is covered by enamel. This enamel is slightly more extended on the labial side than on the lingual and is mostly restricted to the posterior crest, but it widens distally, extending on the entire tip surface. This condition is partially similar to that in *P. goini*, but in that species the enamel is more extended on the labial surface; and differs from *T. atrox*, with the enamel extended along the entire tooth. The surface of the canine root has wide and shallow longitudinal sulci: three shallower (almost vestigial) on the labial face and one, wider and deeper, on the lingual. Additionally, there are small and shallow ridges (wrinkles) restricted to the base of the canine. The labial surface of the canine is slightly convex, differing from *P. goini* and *T. atrox*, where this surface is divided into two facets, forming a triangular shape in transverse section (being more marked in the last).

Only two premolars are present in the upper dental series. The first (serially homologous to the P2, as interpreted for the thylacosmilids; see Forasiepi 2009; Forasiepi & Carlini 2010; Suarez 2019) is represented only by a root fragment at the right side and an alveolus at the left (Fig. 10A-D). The preserved portion shows a strongly reduced tooth, apparently single-rooted, preceded and followed by long diastemata and set nearly equidistantly separated from the canine and the following premolar (Fig. 10A, B), similar to *P. goini* (Forasiepi & Carlini 2010). In *T. atrox*, the P2 is also single-rooted but set closer to other cheek teeth than the canine (Riggs 1933, 1934; Marshall 1978a; Goin & Pascual 1987; Forasiepi & Carlini 2010). On the other hand, in *P. goini*, this tooth was apparently double-rooted and nearly equidistantly separated from the canine and the following premolar (Forasiepi & Carlini 2010). The last premolar of the specimen VPPLT-1612 (P3) is almost complete on the left side of the skull, and it preserves only the roots on the right side (Fig. 10A-D). It is a small molariform tooth, as in the P3 of *P. goini*, resembling the deciduous premolar of other sparassodonts (Sinclair 1906; Marshall 1978a; Forasiepi & Carlini 2010; Forasiepi & Sánchez-Villagra 2014), and has three roots (one lingual and two labial). A third upper molariform premolar with three roots has been previously described for *T. atrox* (Riggs 1933; Goin & Pascual 1987; Mones & Rinderknecht 2004; Forasiepi & Carlini 2010) and interpreted as a retained deciduous tooth DP3 in the adult dentition (Goin & Pascual 1987; Forasiepi & Carlini 2010; Forasiepi & Sánchez-Villagra 2014). Due to the wear degree in the specimens studied here (indicating adult individuals), we extend this interpretation to *A. gracilis*.

The upper molars increase in width posteriorly, and the length increases from the M1 to the M3, while the M4 is anteroposteriorly short (because it lacks the metastylar region; Fig. 10A-D). The paracone and metacone are aligned, with their bases adjoined. The paracone is present in all molars, while the metacone is only present in the M1-3 (it is completely absent in the M4, not even a vestigial cusp is present). The metacone is markedly larger than the paracone in the M3, but the size difference decreases anteriorly, so they are subequal in the M1. Both cusps are conical, circular in section in the M1, becoming subtriangular towards the last molar. The protocone is reduced and markedly lower than the para- and metacone, though more developed than in *P. goini* and *T. atrox*. Despite the difference in size, it is similar in shape to the protocone of *P. goini*, being anteroposteriorly compressed and lingually elongated. The state of preservation does not allow observation of the trigon basin, but it is apparently strongly reduced, similar to *P. goini* (with a vestigial trigon basin). The preservation condition does not allow the observation of either the paraconule and/or the metaconule.

The preparacrista is absent in the M1 and well developed, oblique to the labial edge in the M4. Its condition is obscured by wear in the M2-3. The portion corresponding to the centrocrista (postparacrista plus premetacrista) is strongly worn in the M1-3, in such a way that it is impossible to observe the crests. Due to the marked proximity between the paracone and metacone, these crests were likely very short. The postparacrista in the M4 is well-defined, short but more developed than in the precedent molars, and descends vertically through the posterior face of the paracone. The postmetacrista is strongly developed in the M1-3, long and oblique, similar to *P. goini* and less developed than in *T. atrox*. The wear degree does not allow determining the presence of a deep carnassial notch in this crest, as in *P. goini* and *T. atrox*.

The parastylar shelf is absent labial to the paracone in the M1 of *A. gracilis*, with the labial face of the tooth nearly vertical. It is present in the other molars, more developed in the M3 similar to *P. goini* (Forasiepi & Carlini 2010), but strongly reduced compared with non-thylacosmilid sparassodonts. In *T. atrox*, the parastylar shelf is absent in all molars (Goin & Pascual 1987). On the M1, there is a tiny, blunt cusp located almost at the same height as the protocone, nearly aligned with the paracone and metacone (as in *P. goini*), corresponding to the parastyle (Forasiepi & Carlini 2010). As in *P. goini*, the parastyle on the M2 connects with a very short cingulum that descends towards the labial side of the tooth, forming a small ectocingulum (sensu Marshall 1978a), being better defined in the M3 (Forasiepi & Carlini 2010). The metastylar shelf is present in the M1-3, increasing in size from the M1 to the M3, as in *T. atrox* and *P. goini*.

Lower dentition. There is no clear evidence of the number of lower incisors because the dentaries are broken at that portion in both the holotype and in specimen VPPLT-1612 (Figs 2A; 9; 11A, B). The anterior margin of the left dentary of the specimen VPPLT-1612 is very cracked and poorly preserved (Fig. 9A). So, it is not clear if there was an alveolus is present immediately anterior to the canine. However, the possible space for incisors is strongly restricted, so they should be strongly reduced in size or set very tightly, and close to

FIG. 11. — *Anachlysictis gracilis* Goin, 1997; VPPLT 1612, lower dentition. Left lower dentition in occlusal (**A**), labial (**E**) and lingual (**F**) views; and right lower dentition in occlusal (**B**), labial (**C**) and lingual (**D**) views. Scale bar: 20 mm.

the canine, as in *T. atrox*. The presence of at least two lower incisors (in each hemimandible) is inferred for *T. atrox*, based on the position and size of those preserved (i.e., one at each side, with different position and size; Churcher 1985; Goin & Pascual 1987).

The lower canine is laterally compressed (Fig. 9A; Appendix 5) but less than in *T. atrox*. Its orientation is oblique to the dental row in occlusal views, as in *T. atrox*; and its implantation is sub-vertical (in lateral and lingual views; Figs 9A, B; 11A; char. 179), similar to other sparassodonts as *Arctodictis*, *Australohyaena* Forasiepi, Babot & Zimicz, 2015, and *Callistoe*, but less than in *T. atrox*, which shows completely vertical implantation. The extra-alveolar portion of the lower canine shows a main, wide, and very shallow groove at its lingual face, with small lineal ridges on and near the main groove. Only the tip of the lower canine (*c.* ¼ of the extra-alveolar portion) is covered by enamel.

At least two lower premolars are identified, corresponding to p2-3, as interpreted for *T. atrox* (Forasiepi 2009; Forasiepi & Carlini 2010; Suarez 2019). The dorsal portion of the dentary of the holotype of *A. gracilis* is broken anterior to the p2, and it is not possible to confirm the presence of an alveolus for the p1 (Fig. 2A, B). On the other hand, the left dentary of the specimen VPPLT-1612 shows a small opening (width = 1.58; length unknown) anterior to the p2, separated by a bone space (diastema?). It is roughly ellipsoidal, but its limits are broken, and the bone is poorly preserved, being unclear if it corresponds to an alveolus for a p1 or breakage. However, this small opening is not present in the right dentary, so we interpret that it is unlikely to be an alveolus. If that was the case, the p1 would be smaller than the p2, which is *c.* 49% shorter than the p3, showing a marked reduction. In the dentary of *T. atrox*, the p2-3 are similar in size and located closer to the molars than to the canine. In the specimen IGM 251108 from La Venta (Goin 1997; Suarez 2019), there are three lower premolars: the p1 strongly reduced, almost vestigial, and the p2-3 much larger, being the p2 smaller than the p3. The p2-3 of *A. gracilis* are triangular in lateral view and asymmetrical, with the anterior edge of the cusp convex and shorter than the posterior (Fig. 11E, F), which is slightly

FIG. 12. — Skulls of three species of Thylacosmilidae: **A**, *Thylacosmilus atrox* Riggs, 1933; **B**, *Patagosmilus goini* Forasiepi & Carlini, 2010; **C**, *Anachlysictis gracilis* Goin, 1997. Scale bar: 20 mm.

concave. Both teeth are uninflated, with flat roots and placed obliquely to the main axis of the molars row, but aligned with the dentary, following its sigmoid geometry.

The lower molars show a marked posterior increase in size, common in sparassodonts (Fig. 11). The posterior lobe of the crown is lower than the anterior one in m1-3 (seen in labial view), being strongly marked in the m2-4 (more in the m2) and less evident in the m1 (Figs 2A, E; 11C, E). The main cusps in m1 are aligned in a single longitudinal row. The trigonid configuration in the m2-4 is open, with the paraconid in an antero-lingual position. The protoconid is the main cusp of the trigonid in all molars. The paraconid and protoconid increase in size posteriorly. A tiny structure is present in the m1, on the posterolingual face of the protoconid, which looks like a vestigial metaconid. However, this would differ from the two conditions seen in other borhyaenoids: 1) the metaconid present only in the m2-4; or 2) absent (or vestigial) in all molars. However, a recently described specimen of *Callistoe vincei* (Babot *et al.* 2022) shows another unusual condition, with a strongly reduced metaconid in the m3, probably also present in the m1 (inferred from a wear facet located on the mesiolingual corner of the trigonid); but "given the absence of a metaconid in the m2, that option is possible but unlikely" (Babot *et al.* 2022: 475). The antero-lingual vertical crest of the paraconid (preparacristid interlocking mechanism) forms a keel. The precingulid is reduced, extended only on the base of the paraconid. There is a clear notch between these last two structures (hypoconulid notch) for contact with the preceding molar. The postparacristid and preprotocristid are well developed, at least in the m2-4, forming a carnassial notch between them. The postprotocristid is long, well defined and oriented to the antero-lingual corner of the talonid.

TABLE 2. — Body mass estimations. Abbreviations: **Log**, common logarithm (with base 10); **ln**, natural logarithm (with base e); **M2A**, second upper molar area; **M2L**, second upper molar length; **m2A**, second lower molar area; **m3L**, third lower molar length; **%PE**, percent prediction error; **R2**, ratio estimate; **SE**, smearing estimate correction factor; **X**, selected variable. Body mass expressed in kilograms. Equation source references: **1**, Myers 2001, 'All species' data-set; **2**, Myers 2001, Dasyuromorphian data set; **3**, Zimicz 2012.

Species	Equation	X	%PE	R2	SE	Body mass	Ref.
"*A. gracilis* (IGM 184247)"	log(y) = 1.005 + 1.857 log(x)	m2A	7.00	0.951	1.119	22.77	1
	log(y) = 0.567 + 3.400 log(x)	m3L	12.00	0.945	1.035	27.29	2
	ln(y) = 1.76 + 3.17 ln(x)	m3L	12.08	0.950	1.110	25.29	3
"*A. gracilis* (VPPLT 1612)"	log(y) = 0.426 + 1.890 log(x)	M2A	7.00	0.989	1.029	22.15	2
	log(y) = 1.005 + 1.857 log(x)	m2A	7.00	0.951	1.119	27.19	1
	ln(y) = 1.89 + 3.14 ln(x)	M2L	7.03	0.950	1.160	25.47	3
	log(y) = 0.567 + 3.400 log(x)	m3L	12.00	0.945	1.035	25.82	2
	ln(y) = 1.76 + 3.17 ln(x)	m3L	12.08	0.950	1.110	24.02	3
"*P. goini* (MLP 07-VII-1-1)"	log(y) = 0.426 + 1.890 log(x)	M2A	7.00	0.989	1.029	25.93	2
	ln(y) = 1.89 + 3.14 ln(x)	M2L	7.03	0.950	1.160	19.79	3
"*T. atrox* (P14531)"	log(y) = 0.426 + 1.890 log(x)	M2A	7.00	0.989	1.029	42.50	2
	ln(y) = 1.89 + 3.14 ln(x)	M2L	7.03	0.950	1.160	41.12	3

The trigonid is longer than the talonid in all molars (more than three to four times the length of the talonid), especially in the m2. The talonid is narrower than the trigonid in all molars and is reduced in relative size (compared to the trigonid) posteriorly, being almost vestigial in the m4, showing only a minuscule cuspid (Fig. 11; Table 1). The talonid basin is slightly longer than wide in the m1, slightly wider than long in the m2 and markedly wider than long in the m3. The basin is divided into two portions: a labial one, with a concave and sub-horizontal surface, and a lingual one, markedly more vertical and flatter. The hypoconid is reduced in the m1-3, located approximately at the middle of the labial margin of the talonid. The entoconid is located in a posterolingual position. A vestigial hypoconulid is apparently present posterior to the entoconid and twinned with it. The bases of these two cuspids are merged, forming one block, although their tips are still differentiated. This lingual block of the talonid is laterally compressed and higher than the hypoconid, forming a verticalized lingual portion of the talonid basin. The preentocristid is well-developed and runs lingually to the trigonid. A labial postcingulid is present in the talonid of the m1-3, descending from the hypoconulid to the base of the labial face of the hypoconid. The overall talonid morphology (general morphology, basin morphology and cuspids distribution and morphology) is similar to that observed in the specimen from Quebrada Honda, referable to *P. goini* (see Material and methods, and Appendix 1, Material examined).

RESULTS

CLADISTIC ANALYSIS

The equal weights parsimony analysis produced six most-parsimonious trees, whose strict consensus is shown in Fig. 13 (Appendix 1, Figs A2; A3). The consensus tree had a length of 1626 steps; CI = 0.306; and RI = 0.663; each of the most parsimonious tree with a length of 1617 steps, a consistency index (CI) of 0.307 and a retention index (RI) of 0.666. The implied weights analyses produced single trees for each case, obtaining the best score of 177.10957 with k = 3, 118.35478 with k = 6 and 71.89551 with k = 12 (Appendix 1, Figs A4, A5). The analysis using the k = 6 constant resulted in a similar topology to that where k = 3, with a few changes in the arrangement within Hathliacynidae Ameghino, 1894 and *Lycopsis*.

The results of the Bayesian Inference analysis are presented in the Fig. 14, showing the high posterior probability support values over 75%.

ECOMORPHOLOGICAL ANALYSIS

The body mass of 22.15 kg, obtained from the M2 area of the specimen VPPLT-1612, was selected as the best estimation because it presents the lowest value of %PE and best-adjusted R^2 (Table 2; see Material and methods). Additional estimations were made using other dentition variables with the next lowest %PE values, obtaining estimations between 22.29 kg and 27.29 kg (Table 2). These estimations fall within the 'large size' category for South American carnivorous mammals (Prevosti *et al.* 2013; see Material and methods).

Regarding to the diet inferences, a value of 0 was obtained for the RGA carnivory index, because the griding area is 0 (the talonid basin in the m4 is absent; see Material and methods), falling within the range of the hypercarnivorous mammals (i.e., those with diets including 70% or more of vertebrate flesh; see Van Valkenburgh & Koepfli 1993). The same value was obtained for *T. atrox* and *P. goini*. These results are congruent with those obtained for the relative length of the trigonid index calculated for the carnassial molar (m4) of *A. gracilis* (following Zimicz 2012; see Material and methods), between 0.92 (in the specimen VPPLT-1612) and 0.95 (in the holotype), falling within the category of meat-eater hypercarnivorous.

DIGITAL RECONSTRUCTION OF THE SKULL

The specimen VPPLT-1612 is deformed, with the right side of the skull shifted lower and the left side relatively raised due to taphonomic processes (more evident in anterior view;

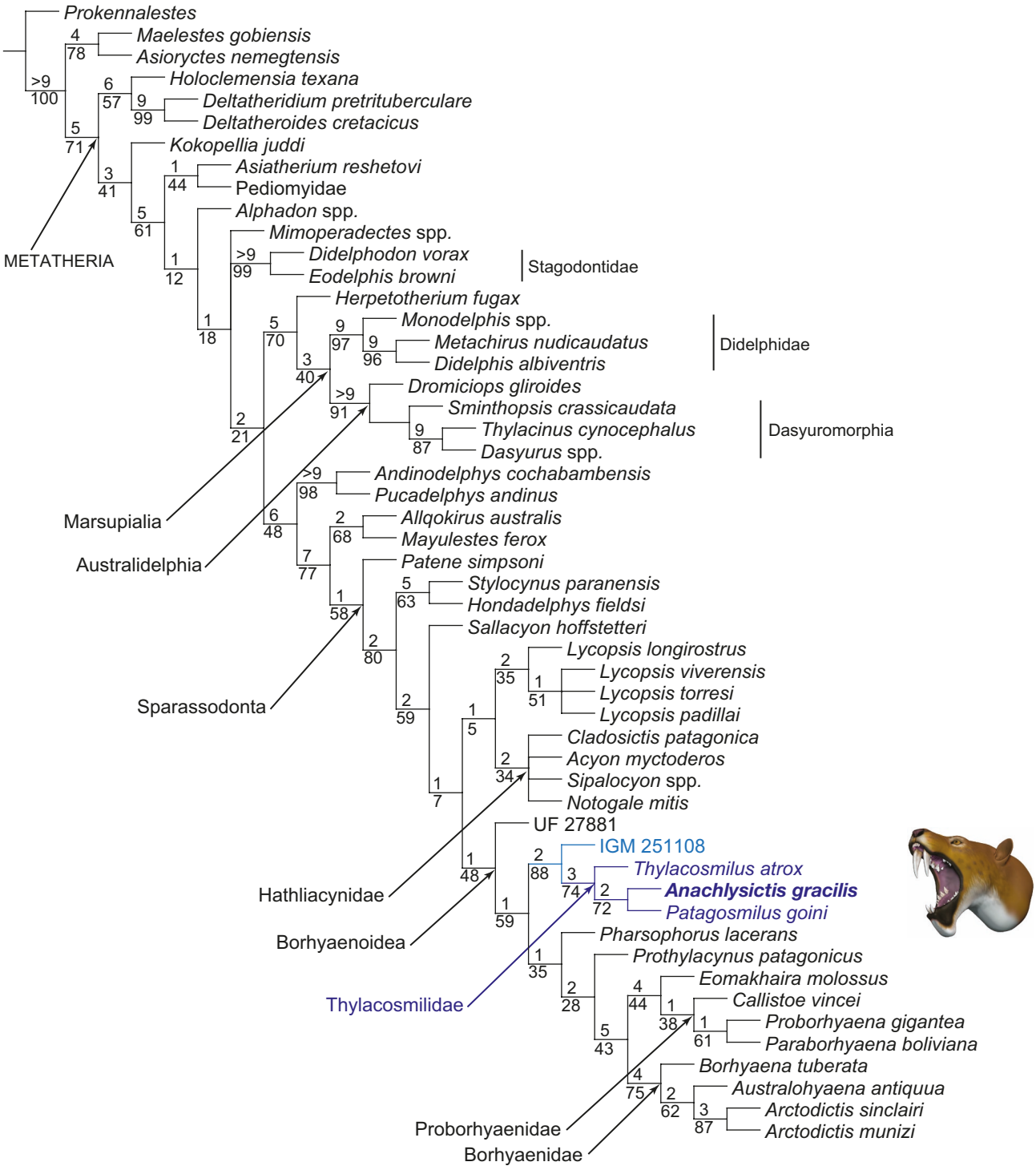

FIG. 13. — Consensus tree obtained from parsimony cladistic analysis under equal weights. Bremer supports (from 6411 trees, cut 0) indicated over branches; Bootstrap support values indicated below branches. Supports not given for Dasyuromorphia, as this node was constrained a priori (see text).

Fig. 15A, B). Although the right dentary has missing regions, the left is completely preserved, and there is no evidence of significant deformation in any of them (Fig. 15B). Based on the minor deformation in mandibles, it is inferred that the compression in anteroposterior and lateromedial directions of the skull was not strong. However, the compression degree in the dorsoventral direction could not be determined, so it was assumed that the dorsoventral deformation was not significant.

For the reconstruction presented here, the first step was a retrodeformation, raising the right side of the skull and lowering the left (see Material and methods), based on the less deformed hemimandible and particular anatomical structures (e.g., orbits, teeth row, external acoustic meatus; Fig. 15C,

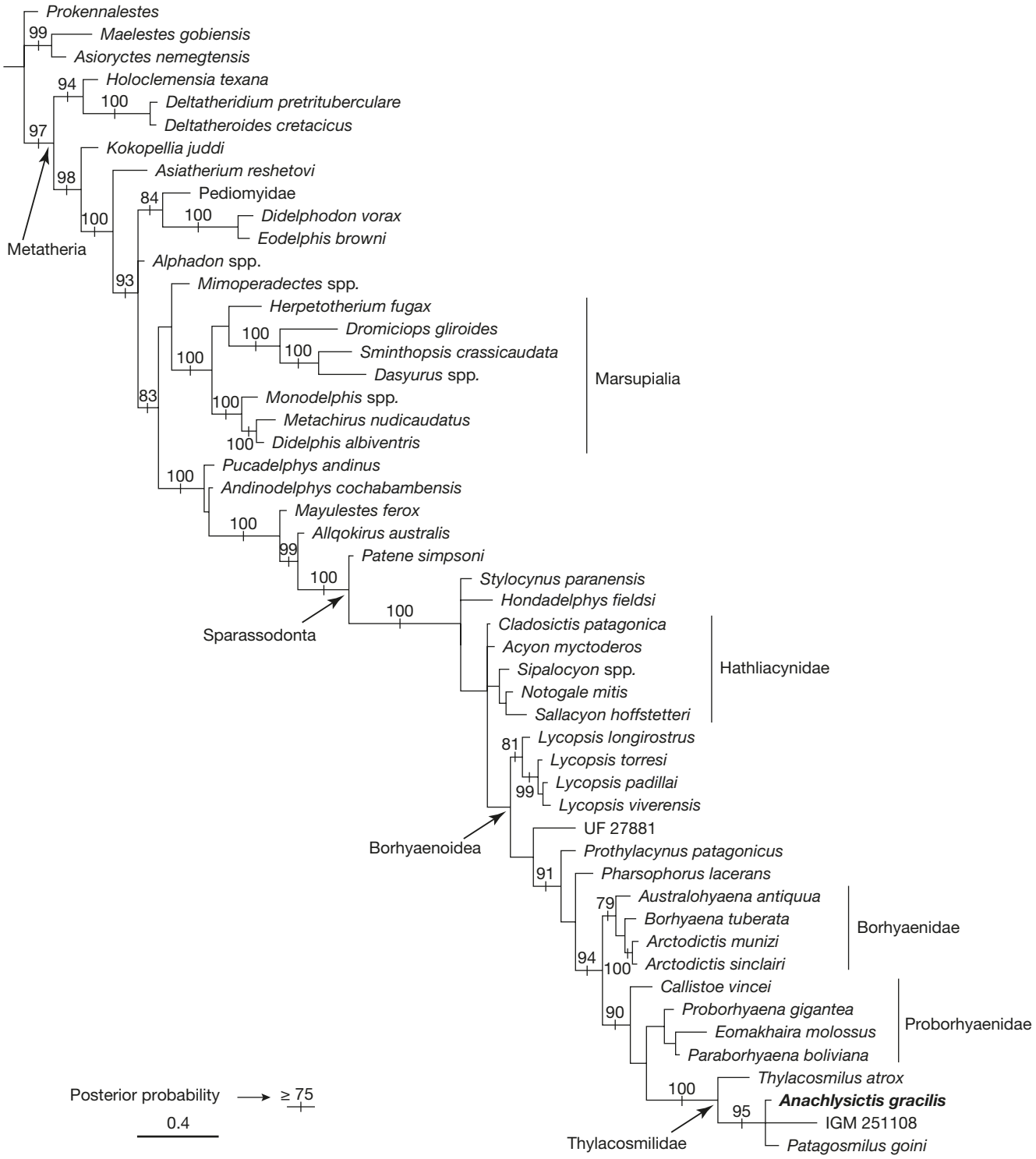

FIG. 14. — Bayesian majority-rule consensus topology of the post-burnin sample of trees for selected taxa (eutherian outgroup and metatherian ingroup), including the thylacosmilid sparassodont *Anachlysictis gracilis* Goin, 1997, focus of this study. Posterior probability support values > 75% indicated in branches.

D). This retrodeformation did not pretend to restore with precision the original morphology of the skull, but instead the general shape of the skull with the aim to perform a life reconstruction of the head. After the retrodeformation, the mouth was opened to create a more informative appearance (Fig. 16A). The missing left upper canine and the right jaw were reconstructed from the corresponding structures on the opposite side (via mirroring; Fig. 16B). The skull surface was smoothed (Fig. 16B) and the missing upper incisors and incomplete molars were reconstructed. Posteriorly, the masticatory muscles, eyeballs, and tongue were constructed on the skull (Fig. 16B, C). The masticatory muscles were based

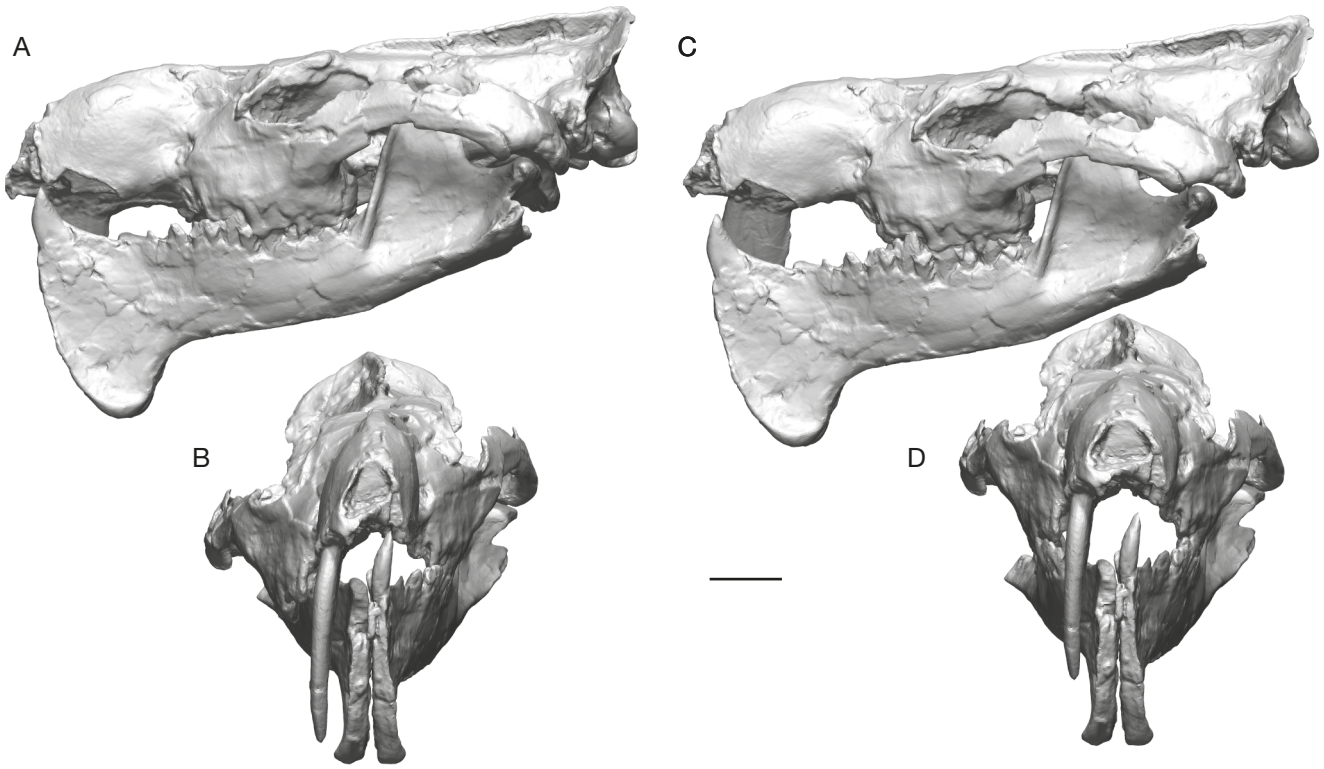

FIG. 15. — 3D digital models of the skull of *Anachlysictis gracilis* Goin, 1997, based on the specimen VPPLT 1612. Original 3D scans of the skull in lateral (**A**) and anterior (**B**) views; modified retrodeformed skull with original unmodified mandible, in lateral (**C**) and anterior (**D**) views. Scale bar: 20 mm.

on modern opossums, and the eyeballs and tongue were built to fit in the orbits and the oral cavity. As there is no fossil evidence of the external appearance of *A. gracilis* (e.g., exterior details and fur color pattern), we used several mammalian taxa for reference: opossum, lion and leopard (Fig. 16D). In the first case, due to its closer phylogenetic affinities; in the remaining ones, because its ecological role falls closer to that of large modern felines (though not completely analogous; see discussion above). The reconstructed life appearance of the head of *A. gracilis* is shown in Fig. 17.

DISCUSSION

PHYLOGENY

Sparassodonta is defined as the group that includes the most recent common ancestor of *Patene* Simpson, 1935, *Borhyaena* (Borhyaenoidea) and *Cladosictis* (Hathliacynidae), and all its descendants (e.g., see Forasiepi *et al.* 2019 and Gaillard *et al.* 2023 for discussion). This cladistic definition adjusts to the classical concept of Sparassodonta by considering species of *Patene* (from Eocene deposits of Argentina, Brazil, and Peru) as possessing the most primitive morphology of the group (e.g., Simpson 1948; Couto 1952; Marshall 1981; Goin *et al.* 1986; Goin & Candela 2004) and it is represented in the cladistic analyses (e.g., Forasiepi 2009; Engelman & Croft 2014; Forasiepi *et al.* 2015; Suarez *et al.* 2016; Muizon *et al.* 2018, Muizon & Ladevèze 2020). Muizon *et al.* (2018) and Muizon & Ladevèze (2020) recovered the early Paleocene Tiupampan *Mayulestes* Muizon, 1994 and *Allkoqirus* Marshall & Muizon, 1988 to form a monophyletic clade with *Patene* and consequently were treated as Sparassodonta.

Comparing our different results, in most of the trees obtained, Sparassodonta does not include *Mayulestes* and *Allkoqirus* in the ingroup. In the parsimony analyses with equal weights and implied weights with k = 12 (Fig. 13; Appendix 1, Figs A2, A3, A5), *Mayulestes* and *Allkoqirus* are consistently shown to form a monophyletic group stem to Sparassodonta. Similarly, the Bayesian Inference analysis recovered both Tiupampan species as successive stem taxa to Sparassodonta, with a clade formed by *Allkoqirus* as the sister taxon of Sparassodonta supported with a high posterior probability of 99 (Fig. 14). A position of the Tiupampan taxa (or at least of *Mayulestes*, which has been included in high levels phylogenetic analyses since the nineties) stem to the monophyletic group that includes sparassodonts (as defined above) agrees with the topologies obtained by Rougier *et al.* (1998), Babot (2005), Forasiepi (2009), Engelman & Croft (2014), Forasiepi *et al.* (2015), Suarez *et al.* (2016), Wilson *et al.* (2016), Carneiro (2018), Rangel *et al.* (2019), Engelman *et al.* (2020), Oliveira *et al.* (2021), among others.

In our analyses, we recovered *Mayulestes* and *Allkoqirus* within Sparassodonta only under implied-weighted parsimony analyses with k = 3 (Appendix 1, Fig. A4) and k = 6. These inconsistencies claim for the necessity to review other early taxa to test the position of the Tiupampan species inside or outside Sparassodonta to better understand the taxonomic con-

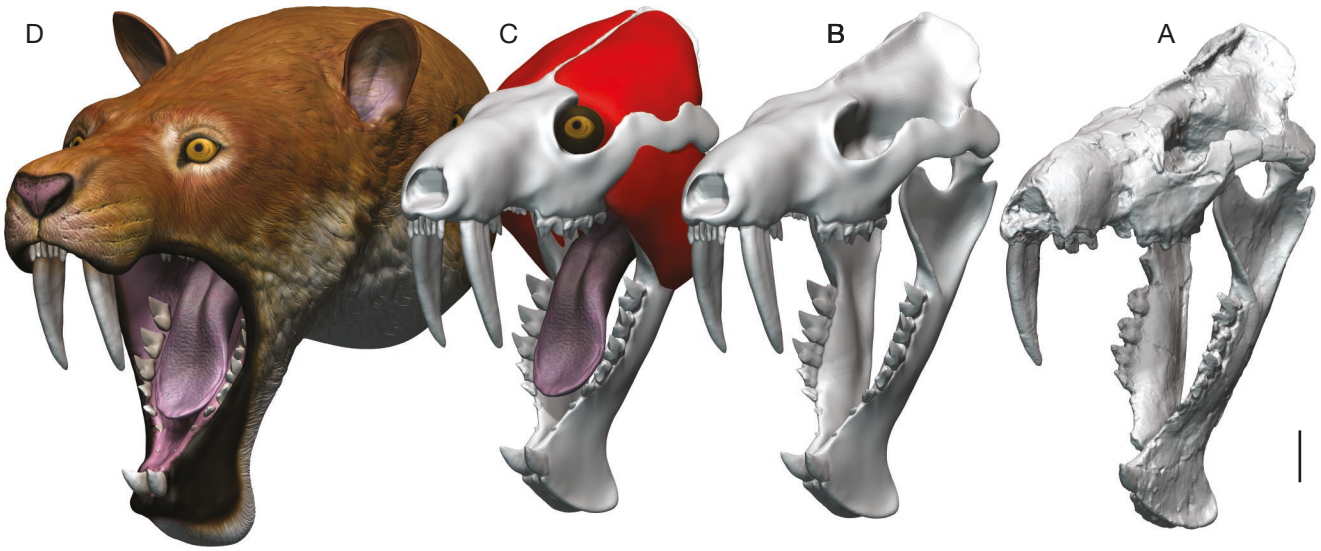

FIG. 16. — Sequential reconstruction of the skull of *Anachlysictis gracilis* Goin, 1997: **A**, modified skull with original mandible; **B**, smoothed skull after mirroring; **C**, skull with reconstructed eyes, masticatory muscles and a tongue; **D**, 3D model of a reconstructed head. Artist: Tatsuya Shinmura. Scale bar: 20 mm.

tent and character evolutionary history of the group. In both the equal weights consensus tree and the Bayesian Inference analysis, Hathliacynidae is not recovered as a monophyletic group (Figs 13; 14). In the Bayesian Inference analysis, among the hathliacynids, *Sipalocyon* spp., *Notogale mitis* Ameghino, 1897, and *Sallacyon hoffstetteri* Villarroel & Marshall, 1982, are recovered in a clade with low posterior probability, and this clade is recovered in a polytomy with the two other hathliacynids in the analysis, ie., *Cladosictis patagonica* and *Acyon myctoderos*, plus the superfamily Borhyaenoidea (Fig. 14). It is important to note that *Cladosictis patagonica* and *Acyon myctoderos* have a great number of polymorphic characters, compared to *Sipalocyon* spp., *Notogale mitis,* and *Sallacyon hoffstetteri*. This issue could be generating less confidence in the phylogenetic position of these taxa and, consequently, being pulled into a polytomy as result of the uncertainty. However, this does not mean that the clade Hathliacynidae is not a natural group (as it is shown in the analyses under implied-weighted parsimony; Figs A3, A4), but only not currently consistently recovered with the morphological data available to date.

Regarding the Borhyaenoidea, in the consensus tree of the equal weight analysis *Lycopsis* is shown as the sister taxon of Hathliacynidae (Fig. 13), but this node has a very low support (Bremmer support 1 and bootstrap 5). However, in all the other analyses, *Lycopsis* is recovered as a the basal-most borhyaenoid, being consistent with previous analyses (e.g., Forasiepi 2009; Engelman & Croft 2014; Forasiepi *et al.* 2015; Suarez *et al.* 2016; Engelman *et al.* 2020). The Borhyaenidae Ameghino, 1894 (formed by the species of *Borhyaena*, *Australohyaena*, and *Arctodictis*, their common ancestor and all descendants) remain grouped together as a monophyletic group in all the analyses, with *Borhyaena tuberata* as the least inclusive taxon in most of the analyses (except in implied weights with k = 3, where it is *Australohyaena antiquua* Forasiepi, Babot & Zimicz, 2015).

Thylacosmilidae, which is the family focus of our study, is defined as the group that includes the most recent common ancestor of *Thylacosmilus atrox*, *Patagosmilus goini* and *Anachlysictis gracilis* (see Fig. 12) and all its descendants (e.g., Prevosti & Forasiepi 2018; see also Gaillard *et al.* 2023). This clade is consistently recovered in all our parsimony analyses, with *P. goini* and *A. gracilis* as sister taxa (Fig. 13; Appendix 1, Figs A2-A5). Contrary to Engelman *et al.* (2020), we did not find support in any of our results (maximum parsimony or Bayesian Inference) to the hypothesis of considering *Eomakhaira molossus* from the early Oligocene of Cachapoal locality, central Chile, to be included within Thylacosmilidae. This species only appears related to thylacosmilids in the implied-weighted parsimony analyses (Appendix 1, Figs A4, A5), as the sister taxon of the clade conformed by Thylacosmilidae + the species represented by the specimen IGM 251108 (which is being described and named in a study in progress). However, in the equal weights analysis, *E. molossus* is recovered as the sister taxon of Proborhyaenidae. On the other hand, in the Bayesian Inference analysis, *E. molossus* is conforming a paraphyletic group with Proborhyaenidae, which is stem to Thylacosmilidae. It is important to note that many characters cannot be evaluated for *E. molossus* due to its fragmentary preservation; future findings will help testing better its phylogenetic affinities. However, thylacosmilid synapomorphies (present in all the thylacosmilid species included in this work; see below) are unambiguously absent in *E. molossus*, which supports its exclusion from the group.

The thylacosmilids *T. atrox*, *P. goini,* and *A. gracilis* are recovered as a monophyletic group in all the maximum parsimony analyses, being supported by the following synapomorphies in the equal weights analysis: 1) presence of a well-developed symphyseal flange (Char. 144, state 2); 2) large canines, with the upper hyper-developed and sabre-like (Char. 171, state 2); 3) marked asymmetry in the anteroposterior length

of the canines (taken at the alveolar level; Char. 172, state 2); and 4) reduction in number of premolars, having only two (Char. 180, state 2). Regarding to the last character, it is important to highlight that, although the specimen IGM 251108 did not lose the first premolar as in thylacosmilids, it is extremely reduced (almost vestigial), much more than in the other taxa with a marked difference in size between P/p1 and P/p2-3. In the equal weights analysis, the clade conformed by *T. atrox*, *P. goini,* and *A. gracilis* has a moderate bootstrap support value (74) and a Bremer support of 3. In the implied weights analyses, it has a also moderate bootstrap support value (74 in the analysis with k = 3, and 72 with k = 6 and 12).

In all our parsimony analyses, we consistently recovered the specimen IGM 251108 as sister taxon to Thylacosmilidae (Fig. 13; Appendix 1, Figs A2-A5). As such, several characteristics present in thylacosmilids, including some related to hypercarnivorous traits, are also present in IGM 251108 but in a more generalized state. (see discussion below: Insights into the Cranial Thylacosmilid Morphology). However, in the Bayesian Inference analysis, the taxon represented by IGM 251108 is recovered within the family Thylacosmilidae, in a trichotomy with *A. gracilis* and *P. goini* with a posterior probability of 95, and such clade as the sister taxon of *Thylacosmilus atrox*, all together forming the monophyletic Thylacosmilidae with a posterior probability of 100 (Fig. 14). This hypothesis will be further explored in a work in progress.

The clade conformed by the Thylacosmilidae plus the species represented by IGM 251108 has a high bootstrap support value (88) and a Bremer support of 2 in the equal weights analysis. In the implied weights analyses, it has also high bootstrap support value (80 in the analysis with k = 3, 83 with k = 6 and 85 with k = 12). This clade is supported by the following synapomorphies in the equal weights analysis: 1) sigmoid shape of dentary (laterally concave at the canine-premolar series and laterally convex at the molar series) in occlusal view (Char. 140, state 1); 2) shape of the anterior portion of dentary increasing in height forward, with ventral border bending upwards in an angle > or = 40º and forming an antero-labial crest (Char. 142, state 2); 3) presence of a symphyseal flange (Char. 144, states 1 and 2); 4) anterior-most mental foramen located clearly ventral to the level of the other mental foramina (Char. 147, state 1); 5) reduction in the number of lower incisors, having two or less (Char. 168, state 2); 6) asymmetry in the antero-posterior length of the canines (taken at the alveolar level; Char. 172, states 1 and 2); 7) strong lateral compression of the lower canine (Char. 173, state 1); 8) subvertical to vertical implantation of the lower canine (Char. 179, states 1 and 2); and 9) distinct paraconid in m1 (Char. 260, state 0).

The Proborhyaenidae (i.e., *Callistoe vincei*, *Proborhyaena gigantea* Ameghino, 1897, and *Paraborhyaena boliviana* (Bond & Pascual 1983; Petter & Hoffstetter 1983; Babot *et al.* 2002) is recovered as monophyletic only in the equal weight parsimony analysis (Fig. 13; Appendix 1, Figs A2, A3), being paraphyletic in the rest of them (Fig. 14; Appendix 1, Figs A4, A5) and including *E. molossus* in the Bayesian Inference analysis (Fig. 14). In that analysis, *P. gigantea*, *E. molossus,* and *P. boliviana* form a monophyletic group, while *C. vincei* is the sister taxon of a group conformed by that monophyletic clade plus Thylacosmilidae. However, all the branches supporting these relationships are supported by low posterior probabilities (i.e., below 75; e.g, *E. molossus* + *P. boliviana* with 51, and *P. gigantea* + *E. molossus* + *P. boliviana* with 71). We consider that the high number of unscored characters in *P. gigantea* and *E. molossus* could be contributing to the proborhyaenids being recovered as a paraphyletic (or polyphyletic) group.

In the Bayesian Inference analysis, the clade conformed by *P. gigantea*, *E. molossus*, *P. boliviana* + Thylacosmilidae is supported by a low posterior probability. However, the clade conformed by these taxa + *C. vincei* is supported by a high posterior probability (90) (Fig. 14). The monophyly of proborhyanids has been questioned in recent years by inconsistent results obtained by different authors (e.g., Babot *et al.* 2002; Babot 2005; Forasiepi *et al.* 2015; Suarez *et al.* 2016; Suarez 2019; Muizon *et al.* 2018; Engelman *et al.* 2020; Muizon & Ladevèze 2020; for discussion see also Argot & Babot 2011; Babot & Forasiepi 2016; Prevosti & Forasiepi 2018). These inconsistencies are probably a consequence of the incompleteness of the available data.

Insights into the cranial thylacosmilid morphology

Goin (1997: 203) made some inferences on the cranial morphology of *A. gracilis* based on the postorbital fragment preserved in the holotype: "(1) the skull roof is flat; (2) there is no postorbital bar; (3) there is no ascending process of the maxillary following the canine implantation; and (4) the frontal crests (= temporal lines in this work) converge posteriorly from the postorbital processes to the sagittal crest". Additionally, he mentioned that conditions 1 and 3 suggested that the intra-alveolar extension of the upper canine was much less than in *T. atrox*, resulting in a differently facial skull shape. These interpretations received more support after the finding of skull of *P. goini* with a morphology similar to *A. gracilis* (Forasiepi & Carlini 2010). In *P. goini* most of those characters inferred by Goin (1997) for *A. gracilis,* that are primitive for *Thylacosmilus*, are also present.

Goin & Carlini (1993) noticed similarities between the specimen IGM 184247 which would later be the holotype of *A. gracilis* (Goin 1997), and an undescribed specimen from Quebrada Honda, Bolivia, (field number B:p2-154 [MNHN-Bol]; see Material examined in Appendix 1). In the present study this specimen is referred to *P. goini*, based on the morphology of the upper dentition, similar curvature of the upper teeth row, and similar morphology of the upper canine.

Forasiepi & Carlini (2010) inferred some differences between *A. gracilis* and *P. goini* that allowed them to define a new taxon, which corresponded to derived features shared between *P. goini* and *T. atrox*, apparently absent in *A. gracilis* (i.e., the upper arcade somewhat more bowed, the shorter distance between the glenoid cavity and the end of the postmetacrista of M3, and a smaller and thinner upper canine).

The recently collected skull VPPLT-1612, referred to *A. gracilis,* allows to confirm all the inferences made by Goin (1997) and Forasiepi & Carlini (2010). It also shows several other

FIG. 17. — Reconstructed head of *Anachlysictis gracilis* Goin, 1997. Artist: Tatsuya Shinmura.

features worth mentioning (see Description and discussion below). The main differences are mainly related to the development degree of certain structures, more conspicuous in *P. goini* (e.g., the *juga alveolaria*, the bowed upper and lower postcanine row, the size of the canine, etc.; see Fig. 12), while the dentition only shows little differences. The similitude observed in cranial and dental characters suggested these taxa were closely related. This relationship is supported in the results of the cladistic analysis, which recover *A. gracilis* and *P. goini* as sister taxa. The morphology of *A. gracilis* and *P. goini* is more generalized than in *Thylacosmilus*, although it is framed in the general thylacosmilid evolutionary trend, with a hypertrophied upper canine and strong rostral modification of the skull and mandible. On the other hand, the specimen IGM 251108 exhibits more plesiomorphic traits than *A. gracilis* and *P. goini*.

One of the modifications observed in the rostral portion of the skull of thylacosmilids and IGM 251108 is the development of the *juga alveolaria* (a protuberance on the facial portion of the maxilla, at the level of the upper canine), the implantation of the upper canine, and its disproportionately larger size in relation to the lower one (at least in *T. atrox*, *A. gracilis,* and also IGM 251108; the lower canine is unknown in *P. goini*). The *juga alveolaria* in *A. gracilis* is much more developed (extended and salient) than in non-thylacosmilid sparassodonts (e.g., Sinclair 1906; Marshall 1976; Babot *et al.* 2002; Forasiepi *et al.* 2015), but less salient than in *P. goini* and, particularly, *T. atrox.* However, the morphology of this structure could be exaggerated in the holotype of *P. goini* due to deformation. The development of this structure is related to the intra-alveolar extension of the canine. In other words, the *juga alveolaria* enlarges as the evergrowing root of the canine inserts deeper into the skull. Although more laterally compressed, the canine in *P. goini* has a more robust intra-alveolar portion that ascends deeper inside the skull than in *A. gracilis*. In *T. atrox*, the canine reaches the dorsal portion of the skull, overpassing the level of the orbits, on the cranial roof. This cranial portion of *T. atrox* suggest an evolutionary process where, as the root of the canine grows, it displaces dorsally inside the skull, and the maxilla accompanies in the process, increasing in size and ascending over the skull roof. *Thylacosmilus* and *Patagosmilus* Forasiepi & Carlini, 2010 have open-rooted, ever-growing (hypselodont) upper canines, similar to those present in proborhyaenids (Riggs 1934; Simpson 1948; Marshall 1978a; Babot *et al.* 2002; Forasiepi & Carlini 2010). The hypertrophied ever-growing upper canine of *Thylacosmilus* associates with a reorganization of the cranium seen in the facial area (as described), in the telescoping of the neurocranium, and in the development of the postorbital bar (see Gaillard *et al.* 2023).

As in all thylacosmilids, the horizontal mandibular ramus has a similar height along its length, except its anterior portion, where its height abruptly increases forming a symphyseal flange. This structure is less developed in *A. gracilis* than in *T. atrox* and probably *P. goini* (inferred from a portion present in the specimen from Quebrada Honda; see Material and methods, and Appendix 1, Material examined) and poorly developed in the specimen IGM 251108. The more expanded symphyseal flange, is associated in thylacosmilids with a lower canine more vertical and laterally compressed, and premolars reduced in size and number, compared to other sparassodonts (e.g., Sinclair 1906; Petter & Hoffstetter 1983; Marshall 1976; Babot *et al.* 2002, 2022; Forasiepi 2009). In the specimen IGM 251108 the first premolar (P/p1) is almost vestigial, while this tooth is absent in thylacosmilids (e.g., *A. gracilis*, *P. goini,* and *T. atrox*). In addition, P/p2-3 are relatively reduced in all these taxa, being the P/p2 smaller than the P/p3. The P2 and p2-3 are conical and single-rooted in *T. atrox*, whereas in all other thylacosmilids and specimen IGM 251108 these teeth are birradiculated and more laterally compressed.

Thylacosmilids and specimen IGM 251108 show a sigmoid (or bowed) shape in the dental row. The dentition of the thylacosmilids shows a marked carnassial morphology, with a strong reduction of the basins and well-developed crests. The protocones are strongly reduced in *A. gracilis*, more reduced in *P. goini* and vestigial in *T. atrox*, while the crests (such as the postmetacrista) are more developed in the *T. atrox*. In

the lower molars of *A. gracilis* and *P. goini*, the talonids of the m1-3 are reduced similarly, but with a basin still present, while it is extremely reduced in *T. atrox*. On the other hand, in *A. gracilis* and *P. goini*, the talonid of the m4 is extremely reduced and without basin (almost a single cusp), while it is vestigial in *T. atrox*. All these characters show a more primitive condition in the specimen IGM 251108.

Paleobiology and paleoecology

The body mass values estimated for *A. gracilis* fall within the 'large size' category (following Prevosti *et al.* 2013) of South American carnivorous mammals. Other known thylacosmilids regarded as large-sized are *P. goini* (*c.* 20-26 kg) and *T. atrox* (*c.* 41-42 kg; Table 2). The specimen IGM 251108 falls within the 'small size' category (below 7 kg). It is important to remark that *A. gracilis* and *P. goini* are similar in size and, depending on the equation used, some estimations show one larger than the other or vice versa (Table 2). Previous body mass estimations on thylacosmilids have showed a differnet values (e.g., *c.* 16 kg for *A. gracilis* and *P. goini*; and between *c.* 30 to *c.* 117 kg for *T. atrox*; Argot 2004a; Ercoli & Prevosti 2011; Prevosti *et al.* 2013).

The dietary habits estimated for *A. gracilis* using carnivory indexes (see Material and methods) indicate it was a meat-eater hypercarnivorous, like other thylacosmilids. The morphological analysis also indicates that *A. gracilis* and other thylacosmilids could have ate mainly soft tissue, because they do not show a typical "bone-breaker" morphology, having long acute crests on a gracile dentition and slender dentaries joined by ligamentous articulation (unfused). Bite force analyses indicate that *T. atrox* bite was less strong than eutherian counterparts such as *Smilodon fatalis* Leidy, 1869, and even less than *Panthera pardus* Linnaeus, 1758, which are identified as meat-eater predators (Wroe *et al.* 2013). However, the flattened upper canines of *T. atrox* may have required less force to insert than did those of *S. fatalis* (Wroe *et al.* 2013). Consequently we interpret that *T. atrox* was not be able to break bones, but its canines would facilitate killing a prey.

Typical bone breakers have robust dentaries with the symphysis fused or strongly ankylosed, and robust molars (including roots and crowns); the upper and lower molars form opposite leaves with blunt ridges that will raise the normal component of the force and therefore the cutting stress will be lower and will be accompanied by compressive forces (Zimicz 2012). That morphology allows processing bone, which is a material much harder and more brittle than vertebrate muscle (Zimicz 2012). All these features are absent in thylacosmilids. Our inferences and estimations are consistent with other analyses focused on the diet of *T. atrox*, which concluded that its dental microwear resembles that of the meat-specializing cheetah, which consumes only meat, and no bone (Phillips 1993; Janis *et al.* 2020).

Recently, Janis *et al.* (2020) concluded that *T. atrox* was probably not a predator, contrary to previous studies (e.g., Churcher 1985; Goin & Pascual 1987; Argot 2004a, 2004b; Ercoli *et al.* 2012; Prevosti *et al.* 2013; Wroe *et al.* 2013). They come to this conclusion based on a set of "unique" characters they considered untypical for a predator mammal (i.e., the reduction or absence of incisors, triangular-shaped upper canine, "large" number of postcanine teeth, blunted tip wear, and ligamentous jaw symphysis). However, most of them are generalized metatherian characters (i.e., a dental formula with more postcanine teeth – in fact, they are reduced in thylacosmilids, having only two premolars –; ligamentous jaw symphysis – with a fused or strongly ankylosed symphysis only present in a few taxa, such as *Arctodictis munizi*). Janis *et al.* (2020) supported they can "demonstrate that *T. atrox* could not have been a predator in the mode proposed for the sabre-toothed feliform carnivorans" and that "it is challenging to propose an alternative mode of life". Similarly, the analysis of the orbital morphology of *T. atrox* is not as expected as for a mammalian predator, being less convergent orbit than in any other sparassodont or marsupial and placental predator (Gaillard *et al.* 2023). However, other unique parameters of the orbital configuration of *Thylacosmilus* in combination with orbital convergence may result in a minimum of stereoscopic vision as expected for a predator (Gaillard *et al.* 2023). We agree with Janis *et al.* (2020), who concluded that "*T. atrox* may well have had no analogues in the extant or extinct fauna". However, we agree with previous hypotheses on the predatory behavior of sparassodonts, including *T. atrox* and other thylacosmilids (e.g., Churcher 1985; Goin & Pascual 1987; Argot 2004a, 2004b; Ercoli *et al.* 2012; Prevosti *et al.* 2013; Gaillard *et al.* 2023).

Based on the estimated body mass and inferred hypercarnivorous diet evaluated herein, *A. gracilis* would have a wide range of possible mammal preys (see Material and methods). Potential prey recorded in La Venta would be, for example, any smaller metatherian from this assemblage (e.g., *Hondadelphys fieldsi* Marshall, 1976, didephimorphians, paucituberculatans, or microbiotherians); rodents, such as the different species of echimyids (spiny rats), dinomyids, "*Scleromys*" Ameghino, 1887, dasyproctids such as "*Neoreomys*" *huilensis* Fields, 1957 (Fig. 18), caviids and erethizontids. Remains of "*Scleromys*" have been previously found associated to remains of *Lycopsis longirostrus* and interpreted as stomach contents (Marshall 1977). The La Venta primates fall within the body mass range of the possible prey for *A. gracilis*.

Acknowledgements

We thank A. Benites-Palomino and R. Sanchez for the discovery of the specimen VPPLT-1612, and the Colombian Geological Survey for authorizations and cooperation during and after the expedition where it was collected; A. Vanegas (VPPLT), P. Holroyd (UCMP), S. Alvarez (MACN), R. Hulbert (UF), M. Reguero (MLP), R. Kay (DU), and M. Takai (PRI), for access to collections under their care; R. Kay, R. Madden, C. Villarroel, F. Anaya, M. Sánchez, and B. Williams, for collecting the specimen B:p2-154 (MNHN-Bol; cast hosted in the MLP),

Fig. 18. — Reconstruction of *Anachlysictis gracilis* Goin, 1997 stalking some rodents ("*Neoreomys*" *huilensis* Fields, 1957) in the La Venta area during Middle Miocene. Artist: Juan Giraldo.

during the Duke University - Geobol Paleontology Expedition in 1992, in Bolivia; special thanks to R. Madden, for the field information about this specimen. We acknowledge using Mesquite© (Maddison & Maddison 2021) and the Willi Hennig Society edition of TNT in our cladistic analysis, and the vectorial maps from vemaps.com. We thank R. Engelman for providing photographs and personal observations on *E. molossus;* D. Loaiza and W. Maddison for their help to solve software issues; and François Pujos (IANIGLA) for corrections to the French abstract. C. Suarez thanks CONICET for funding her doctoral studies (part of this research); the Doris O. and Samuel P. Welles Research Fund of the UCMP, the Vertebrate Paleontology Endowment Fund at the FLMNH (International Travel Grant to study the Vertebrate Paleontology Collection), C. Jaramillo (STRI), K. Campbell (Natural History Museum of Los Angeles County), and A. Stenger, for financial support for visiting collections during her doctoral research; Smithsonian Tropical Research Institute and 'Estancia Post-doctoral 2021', Cancillería, Universidad del Rosario, for postdoctoral funding. We express special thanks to C. Castillo, the Vanegas family and residents from La Victoria and other villages in Villavieja, Huila, for their collaboration during all the stages of this research. Specimen VPPLT-1612 was prepared by F.H. Parra-Ruge and R. Vanegas. The supperficial 3D scans used in this contribution were taken by H. Larsson, A. Smith, H. Bui, A. Demers-Potvin, D. Cortés, C. Bishop, R. Bourque (Redpath Museum, McGill University). © Photographs were taken by R. Vanegas, C. Suarez and A. Forasiepi. This research was performed using infrastructure of the Adaptable Earth Observation System, funded by the Quebec government, McGill University, and Canadian Foundation of Innovation project 36146. This research was partially funded by the projects PICT 2019-2874 and SNF-SPIRIT, IZSTZ0-208545. We deeply acknowledge the reviewers S. Ladevèze and L. Chornogubsky, and our editor of Geodiversitas, for the valuable comments and suggestions that improved the quality of this manuscript.

REFERENCES

Abdala F., Flores D. A. & Giannini N. P. 2001. — Postweaning ontogeny of the skull of *Didelphis albiventris*. *Journal of Mammalogy* 82 (1): 190-200. https://doi.org/10.1644/1545-1542(2001)082<0190:POOTSO>2.0.CO;2

Álvarez D. & Tauber A. 2004. — Vertebrados de la Formación Brochero (Mioceno tardío-Plioceno) de Córdoba, Argentina, *in* Comité Editor (eds), Jornadas Argentinas de Paleontología de Vertebrados, La Plata, Argentina. *Ameghiniana* 41 (4), Abstracts Supplement: 32R-33R. https://www.ameghiniana.org.ar/index.php/ameghiniana/article/view/2705

Anderson V. J., Horton B. K., Saylor J. E., Mora A., Tesón E., Breecker D. O. & Ketcham R. A. 2016. — Andean topographic growth and basement uplift in southern Colombia: Implications for the evolution of the Magdalena, Orinoco, and Amazon river systems. *Geosphere* 12 (4): 1235-1256. https://doi.org/10.1130/GES01294.1

Argot C. 2004a. — Functional-adaptive features and palaeobiologic implications of the postcranial skeleton of the Late Miocene sabretooth borhyaenoid *Thylacosmilus atrox* (Metatheria). *Alcheringa* 28 (1): 229-266. https://doi.org/10.1080/03115510408619283

Argot C. 2004b. — Evolution of South American mammalian predators (Borhyaenoidea): anatomical and palaeobiological implications. *Zoological Journal of the Linnean Society* 140 (4): 487-521. https://doi.org/10.1111/j.1096-3642.2004.00110.x

Argot C. & Babot J. 2011. — Postcranial morphology, functional adaptations and palaeobiology of Callistoe vincei, a predaceous metatherian from the Eocene of Salta, north-western Argentina. *Palaeontology* 54 (2): 447-480. https://doi.org/10.1111/j.1475-4983.2011.01036.x

Astúa D. 2015. — Morphometrics of the largest new world marsupials, opossums of the genus *Didelphis* (Didelphimorphia, didelphidae). *Oecologia Australis* 19 (1): 117-142. https://doi.org/10.4257/oeco.2015.1901.08

Babot M. J. 2005. — *Los Borhyaenoidea (Mammalia, Metatheria) del Terciario inferior del Noroeste argentino. Aspectos filogenéticos, paleobiológicos y bioestratigráficos*. Unpublished PhD thesis, Universidad Nacional de Tucumán, Tucumán, Argentina, 454 p

Babot M. J. & Forasiepi A. M. 2016. — Mamíferos predadores nativos del Cenozoico sudamericano: evidencias filogenéticas y paleoecológicas. *Contribuciones del MACN* 6: 219-230.

Babot M. J., Powel J. E. & Muizon C. 2002. — *Callistoe vincei*, a new Proborhyaenidae (Borhyaenoidea, Metatheria, Mammalia) from the early Eocene of Argentina. *Geobios* 35 (5): 615-629. https://doi.org/10.1016/S0016-6995(02)00073-6

Babot M. J., Rougier G. W., García-López D. A., Bertelli S. B., Herrera C. M., Deraco M. V. & Giannini N. P. 2022. — New mandibular remains of *Callistoe* (Metatheria, Sparassodonta) reveal unexpected anatomical, functional, and evolutionary aspects of this carnivorous genus. *Vertebrate Zoology* 72: 469-485. https://doi.org/10.3897/vz.72.e82709

Bonaparte J. F. 1986. — Sobre *Mesungulatum houusayi* y nuevos mamíferos Cretácicos de Patagonia, Argentina, *in* Comité Editor (eds), IV Congreso Argentino de Paleontología y Biostratigrafía 2. *Ameghiniana* 24 (1-2): 48-61.

Bond M. & Pascual R. 1983. — Nuevos y elocuentes restos craneanos de *Proborhyaena gigantea* Ameghino, 1897 (Marsupialia, Borhyaenidae, Proborhyaeninae) de la Edad Deseadense. Un ejemplo de coevolución. *Ameghiniana* 20 (1-2): 47-60. https://www.ameghiniana.org.ar/index.php/ameghiniana/article/view/1791

Cabrera A. 1927. — Datos para el conocimiento de los dasiúridos fósiles argentinos. *Revista del Museo de La Plata* 30: 271-315. https://publicaciones.fcnym.unlp.edu.ar/rmlp/article/view/1409

Carneiro L. M. 2018. — A new species of *Varalphadon* (Mammalia, Metatheria, Sparassodonta) from the upper Cenomanian of southern Utah, North America: phylogenetic and biogeographic insights. *Cretaceous Research* 84: 88-96. https://doi.org/10.1016/j.cretres.2017.11.004

Churcher C. S. 1985. — Dental functional morphology in the marsupial sabre-tooth *Thylacosmilus atrox* (Thylacosmilidae) compared to that of felid sabre-tooths. *Australian Mammalogy* 8: 201-220. https://doi.org/10.1071/AM85020

Cifelli R. L. 1993a. — Early Cretaceous mammal from North America and the evolution of marsupial dental characters. *Proceedings of the National Academy of Sciences of the United States of America* 90: 9413-9416. https://doi.org/10.1073/pnas.90.20.9413

Cifelli R. L. 1993b. — Theria of metatherian-eutherian grade and the origin of marsupials, *in* Szalay F. S., Novacek M. J. & McKenna M. C. (eds), *Mammal Phylogeny*. New York, NY, Springer: 205-215. https://doi.org/10.1007/978-1-4613-9249-1_14

Cifelli R. L. & Muizon C. de 1997. — Dentition and jaw of *Kokopellia juddi*, a primitive marsupial or near-marsupial from the Medial Cretaceous of Utah. *Journal of Mammalian Evolution* 4 (4): 241-258. https://doi.org/10.1023/A:1027394430433

Cione A. L., Azpelicueta M., Bond M., Carlini A. A., Casciotta J. R., Cozzuol M. A., De la Fuente M., Gasparini Z., Goin F. J., Noriega J., Scillato Yane G., Sobelzon L., Tonni E.

P. & Verzi D. 2000. — Miocene vertebrates from Entre Ríos province, eastern Argentina, *in* Aceñolaza F. G. & Herbst R. (eds), *El Neógeno de Argentina.* Vol. 4. INSUGEO: 191-237.
Clark C. T. & Smith K. K. 1993. — Cranial osteogenesis in *Monodelphis domestica* (Didelphidae) and *Macropus eugenii* (Macropodidae). *Journal of Morphology* 215: 119-149. https://doi.org/10.1002/jmor.1052150203
Coues E. 1872. — The osteology and myology of *Didelphis virginiana*. *Memoirs of the Boston Society of Natural History* 2: 41-154. https://doi.org/10.5962/bhl.title.61012
Couto C. D. P. 1952. — Fossil mammals from the beginning of the Cenozoic in Brazil. Marsupialia: Didelphidae. *American Museum Novitates* 1567: 1-26. http://hdl.handle.net/2246/2389
Engelman R. K. & Croft D. A. 2014. — A new species of small-bodied sparassodont (Mammalia, Metatheria) from the Middle Miocene locality of Quebrada Honda, Bolivia. *Journal of Vertebrate Paleontology* 34 (3): 672-688. https://doi.org/10.1080/02724634.2013.827118
Engelman R. K., Flynn J. J., Wyss A. R. & Croft D. A. 2020. — *Eomakhaira molossus*, a new saber-toothed sparassodont (Metatheria: Thylacosmilinae) from the early Oligocene (?Tinguiririan) Cachapoal locality, Andean Main Range, Chile. *American Museum Novitates* 3957: 1-75. https://doi.org/10.1206/3957.1
Ercoli M. D. & Prevosti F. J. 2011. — Estimación de masa de las especies de Sparassodonta (Mammalia, Metatheria) de edad Santacrucense (Mioceno temprano) a partir del tamaño del centroide de los elementos apendiculares: inferencias paleoecológicas. *Ameghiniana* 48 (4): 462-479. https://www.ameghiniana.org.ar/index.php/ameghiniana/article/view/347
Ercoli M. D., Prevosti F. J. & Álvarez A. 2012. — Form and function within a phylogenetic framework: Locomotory habits of extant predators and some Miocene Sparassodonta (Metatheria). *Zoological Journal of the Linnean Society* 165 (1): 224-251. https://doi.org/10.1111/j.1096-3642.2011.00793.x
Ercoli M. D., Prevosti F. J. & Forasiepi, A. M. 2014. — The structure of the mammalian predator guild in the Santa Cruz Formation (late early Miocene). *Journal of Mammalian Evolution* 21: 369-381. https://doi.org/10.1007/s10914-013-9243-4
Flynn J. J., Guerrero J. & Swisher C. 1997. — Geochronology of the Honda group, *in* Kay R. F., Madden R. H., Cifelli R. L. & Flynn J. (eds), *Vertebrate Paleontology in the Neotropics: the Miocene Fauna of La Venta, Colombia*. Washington D.C. and London, Smithsonian Institution Press: 40-60.
Forasiepi A. 2009. — Osteology of *Arctodictis sinclairi* (Mammalia, Metatheria, Sparassodonta) and phylogeny of Cenozoic metatherian carnivores from South America. *Monografías del Museo Argentino de Ciencias Naturales, new series* 6: 1-174.
Forasiepi A. M. & Carlini A. A. 2010. — A new thylacosmilid (Mammalia, Metatheria, Sparassodonta) from the Miocene of Patagonia, Argentina. *Zootaxa* 2552: 55-68. https://doi.org/10.11646/zootaxa.2552.1.3
Forasiepi A. M. & Sánchez-Villagra M. R. 2014. — Heterochrony, dental ontogenetic diversity, and the circumvention of constraints in marsupial mammals and extinct relatives. *Paleobiology* 40 (2): 222-237. https://doi.org/10.1666/13034
Forasiepi A. M., Goin F. J. & Di Martino V. 2003. — Una nueva especie de *Lycopsis* (Metatheria, Prothylacyninae) de la Formación Arroyo Chasicó (Mioceno tardío) de la Provincia de Buenos Aires. *Ameghiniana* 40: 249-253. https://www.ameghiniana.org.ar/index.php/ameghiniana/article/view/958
Forasiepi A. M., Goin F. J. & Tauber A. A. 2004. — Las especies de Arctodictis Mercerat, 1891 (Metatheria, Borhyaenidae), grandes carnívoros del Mioceno de América del Sur. *Revista Española de Paleontología* 19 (1): 1-22. https://doi.org/10.7203/sjp.19.1.20518
Forasiepi A. M., Sánchez-Villagra M. R., Goin F. J., Takai M., Shigehara N. & Kay R. F. 2006. — A new species of Hathliacynidae (Metatheria, Sparassodonta) from the middle Miocene of Quebrada Honda, Bolivia. *Journal of Vertebrate Paleontology* 26 (3): 670-684. https://doi.org/10.1671/0272-4634(2006)26[670:ANSOHM]2.0.CO;2
Forasiepi A. M., Martinelli A. G. & Goin F. J. 2007. — Revisión taxonómica de *Parahyaenodon argentinus* Ameghino y sus implicancias en el conocimiento de los grandes mamíferos carnívoros del Mio-Plioceno de América de Sur. *Ameghiniana* 44 (1): 143-159. https://www.ameghiniana.org.ar/index.php/ameghiniana/article/view/680
Forasiepi A. M., Babot M. J. & Zimicz N. 2015. — *Australohyaena antiqua* (Mammalia, Metatheria, Sparassodonta), a large predator from the Late Oligocene of Patagonia. *Journal of Systematic Palaeontology* 13 (6): 503-525. https://doi.org/10.1080/14772019.2014.926403
Forasiepi A. M., MacPhee R. D. E. & Hernández Del Pino S. 2019. — Caudal cranium of *Thylacosmilus atrox* (Mammalia, Metatheria, Sparassodonta), a South American predaceous sabertooth. *Bulletin of the American Museum of Natural History* 433: 1-64. https://doi.org/10.1206/0003-0090.433.1.1
Fox R. C. 1979a. — Mammals from the Upper Cretaceous Oldman Formation, Alberta. II. *Pediomys* Marsh (Marsupialia). *Canadian Journal of Earth Sciences* 16: 103-113. https://doi.org/10.1139/e79-010
Fox R. C. 1979b. — Mammals from the Upper Cretaceous Oldman Formation, Alberta. I. *Alphadon* Simpson (Marsupialia). *Canadian Journal of Earth Sciences* 16: 91-102. https://doi.org/10.1139/e79-009
Fox R. C. 1983. — Notes on the North American Tertiary marsupials *Herpetotherium* and *Peradectes*. *Canadian Journal of Earth Sciences* 20: 1565-1578. https://doi.org/10.1139/e83-146
Gaillard C., MacPhee R. D. & Forasiepi A. M. 2023. — Seeing through the eyes of the sabertooth *Thylacosmilus atrox* (Metatheria, Sparassodonta). *Communications Biology* 6 (257): 1-7. https://doi.org/10.1038/s42003-023-04624-5
Giannini N. P., Abdala F. & Flores D. A. 2004. — Comparative postnatal ontogeny of the skull in *Dromiciops gliroides* (Marsupialia: Microbiotheriidae). *American Museum Novitates* 3460: 1-17. http://hdl.handle.net/2246/2770
Goin F. J. 1995. — Los marsupiales, *in* Alberdi M. A., Leone G. & Tonni E. P. (eds), *Evolución biológica y climática de la Región Pampeana durante los últimos cinco millones de años. Un ensayo de correlación con el Mediterráneo occidental*. Madrid, Museo Nacional de Ciencias Naturales, Consejo Superior de Investigaciones Científicas: 165-179.
Goin F. J. 1997. — New clues for understanding Neogene marsupial radiations, *in* Kay R. F., Madden R. H., Cifelli R. L. & Flynn J. (eds), *Vertebrate Paleontology in the Neotropics: the Miocene Fauna of La Venta, Colombia*. Washington D.C. and London, Smithsonian Institution Press: 185-204.
Goin F. J. & Candela A. M. 2004. — New Paleogene marsupials from the Amazon Basin of eastern Peru. The Paleogene Mammalian Fauna of Santa Rosa, Amazonian Peru. *Natural History Museum of Los Angeles County, Science Series* 40: 15-60.
Goin F. J. & Carlini A. A. 1993. — The most primitive South American sabretooth marsupials: their significance in the reassessment of sparassodont phylogeny, *in* Augee M. L. (ed.), *Sixth International Theriological Congress, Abstracts*. International Union of Biological Sciences, Mammalogy Section, Sydney: 113.
Goin F. J. & Pascual R. 1987. — News on the biology and taxonomy of the marsupials Thylacosmilidae (late Tertiary of Argentina). *Anales de la Academia Nacional de Ciencias Exactas, Físicas y Naturales (Argentina)* 39: 219-246.
Goin F. J., Palma R. M., Pascual R. & Powel J. E. 1986. — Persistencia de un primitivo Borhyaenidae (Mammalia, Marsupialia) en el Eoceno temprano de Salta (Fm. Lumbrera, Argentina). Aspectos geologicos y paleoambientales relacionados. *Ameghiniana* 23 (1-2): 45-56. https://www.ameghiniana.org.ar/index.php/ameghiniana/article/view/1807

GOIN F. J., MONTALVO C. I. & VISCONTI G. 2000. — Los marsupiales (Mammalia) del Mioceno Superior de la Formación Cerro Azul (Provincia de La Pampa, Argentina). *Estudios Geológicos* 56 (1-2): 101-126. https://doi.org/10.3989/egeol.00561-2158.

GOIN F. J., ABELLO A., BELLOSI E., KAY R., MADDEN R. & CARLINI A. 2007. — Los Metatheria sudamericanos de comienzos del Neógeno (Mioceno Temprano, Edad-mamífero Colhuehuapense). Parte I: Introducción, Didelphimorphia y Sparassodonta. *Ameghiniana* 44 (1): 30-33. https://www.ameghiniana.org.ar/index.php/ameghiniana/article/view/674

GOIN F. J., ABELLO M. A. & CHORNOGUBSKY L. 2010. — Middle Tertiary marsupials from central Patagonia (early Oligocene of Gran Barranca): understanding South America's Grande Coupure, *in* MADDEN R. R., CARLINI A. A., VUCETICH M. G. & KAY R. F. (eds), *The Paleontology of Gran Barranca: Evolution and Environmental Change through the Middle Cenozoic of Patagonia*. Cambridge, Cambridge University Press: 69-105.

GOIN F. J., WOODBURNE M. O., ZIMICZ A. N., MARTIN G. M. & CHORNOGUBSKY L. 2016. — *A brief history of South American metatherians. Evolutionary contexts and intercontinental dispersals*. Springer. 237 p. https://doi.org/10.1007/978-94-017-7420-8

GOLOBOFF P. A., FARRIS J. S. & NIXON K. C. 2008. — TNT, a free program for phylogenetic analysis. *Cladistics* 24 (5): 774-786. https://doi.org/10.1111/j.1096-0031.2008.00217.x

GORDON C. L. 2003. — A first look at estimating body size in dentally conservative marsupials. *Journal of Mammalian Evolution* 10 (2): 1-21. https://doi.org/10.1023/A:1025545023221

GREGORY W. K. & SIMPSON G. G. 1926. — Cretaceous mammal skulls from Mongolia. *American Museum Novitates* 225: 1-20. http://hdl.handle.net/2246/3193

GUERRERO J. 1997. — Sedimentary environments, and the Miocene uplift of the Colombian Andes, *in* KAY R.F., MADDEN R.H., CIFELLI R.L. & FLYNN J.J. (eds), *Vertebrate Paleontology in the Neotropics: the Miocene Fauna of La Venta, Colombia*. Washington and London, Smithsonian Institution Press: 14-43.

HERSHKOVITZ P. 1999. — *Dromiciops gliroides* Thomas, 1894, last of the Microbiotheria (Marsupialia), with a review of the family Microbiotheriidae. *Fieldiana, Zoology, New series* 93: 1-60. https://doi.org/10.5962/bhl.title.3259

HIATT J. L. 2020. — *Textbook of Head and Neck Anatomy*. Jones & Bartlett Learning. 412 p.

HOFFSTETTER R. & PETTER G. 1983. — *Paraborhyaena boliviana* et *Andinogale sallaensis*, deux marsupiaux (Borhyaenidae) nouveaux du Déséadien (Oligocène inférieur) de Salla (Bolivie). *Comptes rendus des séances de l'Académie des sciences, Série 2, Mécanique-physique, Chimie, Sciences de l'univers, Sciences de la Terre* 296: 205-208. https://gallica.bnf.fr/ark:/12148/bpt6k56537695/f211.item

HOROVITZ I., LADEVÈZE S., ARGOT C., MACRINI T. E., MARTIN T., HOOKER J. J., KURZ C., MUIZON C. DE & SÁNCHEZ-VILLAGRA M. R. 2008. — The anatomy of *Herpetotherium* cf. *fugax* Cope, 1873, a metatherian from the Oligocene of North America. *Palaeontographica Arbeitung A*, 284: 109-141. https://doi.org/10.1127/pala/284/2008/109

HOROVITZ I., MARTIN T., BLOCH J., LADEVÈZE S., KURZ C. & SÁNCHEZ-VILLAGRA M. R. 2009. — Cranial anatomy of the earliest marsupials and the origin of opossums. *PLoS ONE* 4 (12). https://doi.org/10.1371/journal.pone.0008278

JANIS C. M., FIGUEIRIDO B., DESANTIS L. & LAUTENSCHLAGER S. 2020. — An eye for a tooth: *Thylacosmilus* was not a marsupial "saber-tooth predator". *PeerJ* 8: e9346. https://doi.org/10.7717/peerj.9346

KAY R. F. & MADDEN R. D. 1997. — Paleogeography and paleoecology, *in* KAY R. F., MADDEN R. H., CIFELLI R. L. & FLYNN J. (eds), *Vertebrate Paleontology in the Neotropics: the Miocene Fauna of La Venta, Colombia*. Washington D.C. and London, Smithsonian Institution Press: 520-550.

KAY R. F., MADDEN R. D., CIFELLI R. L. & FLYNN J. J. 1997. — *Vertebrate Paleontology in the Neotropics: the Miocene Fauna of La Venta, Colombia*. Washington and London, Smithsonian Institution Press, 592 p.

KEALY S. & BECK R. 2017. — Total evidence phylogeny and evolutionary timescale for Australian faunivorous marsupials (Dasyuromorphia). *BMC Evolutionary Biology* 17 (1): 1-23. https://doi.org/10.1186/s12862-017-1090-0

KIELAN-JAWOROWSKA Z. 1984. — Evolution of the therian mammals in the Late Cretaceous of Asia. Part VII. Synopsis. *Palaeontologia Polonica* 46: 173-183. http://www.palaeontologia.pan.pl/Archive/1984_46_173-183.pdf

KIELAN-JAWOROWSKA Z. 1975. — Preliminary description of two new eutherian genera from the Late Cretaceous of Mongolia. *Palaeontologia Polonica* 33: 5-15. http://www.palaeontologia.pan.pl/Archive/1975-33_5-15_1-6.pdf

KRAGLIEVICH J. L. 1960. — Marsupiales tilacosmilinos de la fauna de Chapadmalal. *Publicaciones del Museo Municipal de Ciencias Naturales y Tradicional de Mar del Plata* 1: 53-72.

KRAJEWSKI C., BUCKLEY L. & WESTERMAN M. 1997. — DNA phylogeny of the marsupial wolf resolved. *Proceedings of the Royal Society of London. Series B: Biological Sciences* 264 (1383): 911-917. https://doi.org/10.1098/rspb.1997.0126

KOYABU D., MAIER W. & SÁNCHEZ-VILLAGRA M. R. 2012. — Paleontological and developmental evidence resolve the homology and dual embryonic origin of a mammalian skull bone, the interparietal. *Proceedings of the National Academy of Sciences* 109 (35): 14075-14080. https://doi.org/10.1073/pnas.120869310

LADEVÈZE S., MUIZON C. DE, BECK R. M. D., GERMAIN D. & CESPEDES-PAZ R. 2011. — Earliest evidence of mammalian social behaviour in the basal Tertiary of Bolivia. *Nature* 474 (7349): 83-86. https://doi.org/10.1038/nature09987

LILLEGRAVEN J. A. 1969. — Latest cretaceous mammals of upper part of Edmonton Formation of Alberta, Canada, and review of marsupial-placental dichotomy in mammalian evolution. *The University of Kansas Paleontology Contributions* 50 (Vertebrata 12): 1-122. http://hdl.handle.net/1808/3825

LOPATIN A. V. & AVERIANOV A. O. 2017. — The stem placental mammal *Prokennalestes* from the Early Cretaceous of Mongolia. *Paleontological Journal* 51 (12): 1293-1374. https://doi.org/10.1134/S0031030117120048

LUO Z. X., JI Q., WIBLE J. R. & YUAN C. X. 2003. — An Early Cretaceous tribosphenic mammal and metatherian evolution. *Science* 302 (5652): 1934-1940. https://doi.org/10.1126/science.1090718

MACFADDEN B. & WOLFF R. G. 1981. — Geological investigations of Late Cenozoic vertebrate bearing deposits in southern Bolivia, *in* Conselho Nacional de Desenvolvimento Cientifico e Tecnológico (ed.), *Anais II Congreso Latinoamericano de Paleontología*. Universidade Federal da Porto Alegre, Porto Alegre: 765-778.

MACKENNA M. C. & BELL S. K. 1997. — *Classification of Mammals above the Species Level*. Columbia University Press, New York, 640 p.

MACRINI T. 2005. — *Dasyurus hallucatus.* Available from http://digimorph.org/specimens/Dasyurus_hallucatus [accessed 15 June 2017].

MACRINI T. 2009. — *Sminthopsis crassicaudata*. Available from http://digimorph.org/specimens/Sminthopsis_crassicaudata [accessed 15 June 2017].

MADDEN R. H., GUERRERO J., KAY R. F., FLYNN J. J. & SWISHER C. 1997. — The Laventan Stage and Age, *in* KAY R. F., MADDEN R. H., CIFELLI R. L. & FLYNN J. (eds), *Vertebrate Paleontology in the Neotropics: the Miocene Fauna of La Venta, Colombia*. Washington D.C. and London, Smithsonian Institution Press: 409-519.

MADDISON W. P. & MADDISON D. R. 2021. — Mesquite: a modular system for evolutionary analysis. Version 3.70. http://www.mesquiteproject.org

MARSHALL L. G. 1976. — Evolution of the Thylacosmilidae, extinct saber-tooth marsupials of South America. *PaleoBios* 23: 1-30.
MARSHALL L. G. 1977. — A new species of *Lycopsis* (Borhyaenidae: Marsupialia) from the La Venta fauna (Late Miocene) of Colombia, South America. *Journal of Paleontology* 51 (3): 633-642. https://www.jstor.org/stable/1303691
MARSHALL L. G. 1978a. — *Evolution of the Borhyaenidae, Extinct South American Predaceous Marsupials*. University of California Press, Berkeley, 89 p. (University of California publications in geological sciences; 117).
MARSHALL L. G. 1978b. — *Dromiciops australis*. *American Society of Mammalogists* 99: 1-5. https://doi.org/10.2307/3504051
MARSHALL L. G. 1979. — Review of the Prothylacyninae, an extinct subfamily of South American 'dog-like' Marsupials. *Fieldiana, Geology, New Series* 3: 1-50. https://doi.org/10.5962/bhl.title.3324
MARSHALL L. G. 1981. — Review of the Hathliacyninae, an extinct subfamily of South American 'doglike' marsupials. *Fieldiana, Geology, New Series* 7: 1-120. https://doi.org/10.5962/bhl.title.3520
MARSHALL L. G. 1982. — Systematics of the South American marsupial family Microbiotheriidae. *Fieldiana, Geology, New Series* 10: 1-75. https://doi.org/10.5962/bhl.title.3420
MARSHALL L. G. & MUIZON C. DE 1995. — Part, II: The skull, *in* MUIZON C. de (ed.), *Pucadelphys andinus* (Marsupialia, Mammalia) From the early Paleocene of Bolivia. Muséum national d'Histoire naturelle, Paris: 21-90 (Mémoires du Muséum national d'Histoire naturelle; 165). https://www.biodiversitylibrary.org/page/58823242
MARSHALL L. G., CASE J. A. & WOODBURNE M. O. 1990. — Phylogenetic relationships of the families of marsupials. *Current Mammalogy* 2: 433-505.
MATTHEW W. D. 1916. — A marsupial from the Belly River Cretaceous: With critical observations upon the affinities of the Cretaceous mammals. *Bulletin American Museum of Natural History* 35: 477-500. http://hdl.handle.net/2246/1386
MONES A. & RINDERKNECHT A. 2004. — Primer registro de Thylacosmilidae en el Uruguay (Mammalia: Marsupialia: Sparassodonta). *Comunicaciones Paleontológicas del Museo Nacional de Historia Natural y Antropología* 34: 193-200.
MONTES C., SILVA C. A., BAYONA G. A., VILLAMIL R., STILES E., RODRIGUEZ-CORCHO A. F., BELTRAN-TRIVIÑO A., LAMUS F., MUÑOZ-GRANADOS M. D., PÉREZ-ANGEL L. C., HOYOS N., GOMEZ S., GALEANO J. J., ROMERO E., BAQUERO M., CARDENAS-ROZO A. L. & VON QUADT A. 2021. — A Middle to Late Miocene trans-Andean portal: Geologic record in the Tatacoa Desert. *Frontiers in Earth Science* 8: 587022. https://doi.org/10.3389/feart.2020.587022
MONTELLANO M. 1988. — *Alphadon halleyi* (Didelphidae, Marsupialia) from the two medicine formation (Late Cretaceous, Judithian) of Montana. *Journal of Vertebrate Paleontology* 8 (4): 378-382. https://doi.org/10.1080/02724634.1988.10011726
MORA-ROJAS L., CÁRDENAS A., JARAMILLO C., SILVESTRO D., BAYONA G., ZAPATA S., MORENO F., SILVA C., MORENO-BERNAL J. W., JARAMILLO J. S., VALENCIA V. & IBAÑEZ M. 2023. — Stratigraphy of a middle Miocene neotropical Lagerstätte (La Venta Site, Colombia). *Geodiversitas* 45 (6): 197-221. https://doi.org/10.5252/geodiversitas2023v45a6. http://geodiversitas.com/45/6
MUIZON C. DE 1994. — A new carnivorous marsupial from the Palaeocene of Bolivia and the problem of marsupial monophyly. *Nature* 370 (6486): 208-211. https://doi.org/10.1038/370208a0
MUIZON C. DE 1998. — *Mayulestes ferox*, a borhyaenoid (Metatheria, Mammalia) from the early Palaeocene of Bolivia. Phylogenetic and palaeobiologic implications. *Geodiversitas* 20 (1): 19-142.
MUIZON C. DE 1999. — Marsupial skulls from the Deseadan (late Oligocene) of Bolivia and phylogenetic analysis of the Borhyaenoidea (Marsupialia, Mammalia). *GeoBios* 32 (3): 483-509. https://doi.org/10.1016/S0016-6995(99)80022-9
MUIZON C. DE & LADEVÈZE S. 2020. — Cranial anatomy of *Andinodelphys cochabambensis*, a stem metatherian from the early Palaeocene of Bolivia. *Geodiversitas* 42 (30): 597-739. https://doi.org/10.5252/geodiversitas2020v42a30. http://geodiversitas.com/42/30
MUIZON C. DE, CIFELLI R. L. & PAZ R. C. 1997. — The origin of the dog-like borhyaenoid marsupials of South America. *Nature* 389 (6650): 486-489. https://doi.org/10.1038/39029
MUIZON C. DE, LADEVÈZE S., SELVA C., VIGNAUD R. & GOUSSARD F. 2018. — *Allqokirus australis* (Sparassodonta, metatheria) from the early Palaeocene of Tiupampa (Bolivia) and the rise of the metatherian carnivorous radiation in South America. *Geodiversitas* 40 (16): 363-459. https://doi.org/10.5252/geodiversitas2018v40a16. http://geodiversitas.com/40/16
MUSEUMS VICTORIA COLLECTIONS a. — *Thylacinus cynocephalus*, Specimen C 3149. Available from https://collections.museumvictoria.com.au/specimens/1838884 [accessed 15 June 2017].
MUSEUMS VICTORIA COLLECTIONS b. — *Dasyurus hallucatus*,. Available from https://collections.museumvictoria.com.au/specimens/1838884 [accessed 15 June 2017].
MYERS T. J. 2001. — Prediction of marsupial body mass. *Australian Journal of Zoology* 49 (2): 99-118. https://doi.org/10.1071/ZO01009
MYERS P., ESPINOSA R., PARR C. S., JONES T., HAMMOND G. S. Y DEWEY T. A. 2018. — *Metachirus nudicaudatus* (On-line). Available from https://animaldiversity.org/accounts/Metachirus_nudicaudatus/specimens/ [accessed 1 April 2018].
MYERS P., ESPINOSA R., PARR C. S., JONES T., HAMMOND G. S. & DEWEY T. A. 2022. — *Thylacinus cynocephalus* (On-line). Available from https://animaldiversity.org/accounts/Thylacinus_cynocephalus/specimens/ [accessed 17 August 2022].
NATURAL HISTORY MUSEUM 2014. — Collection specimens [Data set]. https://doi.org/10.5519/0002965 [accessed 15 June 2017].
O'LEARY M. A., BLOCH J. I., FLYNN J. J., GAUDIN T. J., GIALLOMBARDO A., GIANNINI N. P. *et al.* 2013. — The placental mammal ancestor and the post-K-Pg radiation of placentals. *Science* 339 (6120): 662-667. https://doi.org/10.1126/science.1229237
OLIVEIRA E. V., CARNEIRO L. M. & GOIN F. J. 2021. — A new derorhynchid (Mammalia, Metatheria) from the early Eocene Itaboraí fauna of Brazil with comments on its affinities. *Anais da Academia Brasileira de Ciências* 93 (Suppl.2): e20201554. https://doi.org/10.1590/0001-3765202120201554
PATTERSON B. & MARSHALL L. G. 1978. — The Deseadan, Early Oligocene, Marsupialia of South America. *Fieldiana, Geology* 41 (2): 37-100. https://doi.org/10.5962/bhl.title.3439
PETTER G. & HOFFSTETTER R. 1983. — Les marsupiaux du Déséadien (Oligocène inférieur) de Salla (Bolivie). *Annales de Paléontologie* 69 (3): 175-234.
PHILLIPS J. A. 1993. — Bone consumption by cheetahs at undisturbed kills: Evidence for a lack of focal-palatine erosion. *Journal of Mammalogy* 74 (2): 487-492. https://doi.org/10.2307/1382408
PREVOSTI F. & FORASIEPI A. M. 2018. — *Evolution of South American Mammalian Predators During the Cenozoic: Paleobiogeographic and Paleoenvironmental Contingencies*. Springer Cham. https://doi.org/10.1007/978-3-319-03701-1
PREVOSTI F. J., FORASIEPI A. & ZIMICZ N. 2013. — The Evolution of the Cenozoic Terrestrial Mammalian Predator Guild in South America: Competition or Replacement? *Journal of Mammalian Evolution* 20 (1): 3-21. https://doi.org/10.1007/s10914-011-9175-9
PREVOSTI F. J., TURAZZINI G. F. & CHEMUSQUY M. A. 2010. — Morfología craneana en tigres dientes de sable: alometría, función y filogenia. *Ameghiniana* 47 (2): 239-256. https://www.ameghiniana.org.ar/index.php/ameghiniana/article/view/167
RAMBAUT, A., DRUMMOND, A. J., XIE, D., BAELE, G. & SUCHARD, M. A. 2018. — Posterior summarization in Bayesian phylogenetics using Tracer 1.7. *Systematic Biology* 67 (5): 901-904. https://doi.org/10.1093/sysbio/syy032

RANGEL C. C., CARNEIRO L. M., BERGQVIST L. P., OLIVEIRA É. V., GOIN F. J. & BABOT M. J. 2019. — Diversity, affinities and adaptations of the basal sparassodont *Patene* (Mammalia, Metatheria). *Ameghiniana* 56 (4): 263-289. https://doi.org/10.5710/AMGH.06.05.2019.3222

REIG O. A. 1958. — Notas para la actualización del conocimiento de la fauna de la Formación Chapadmalal. II Amphibia, Reptilia, Aves, Mammalia (Marsupialia: Didelphidae, Borhyaenidae). *Acta Geologica Lilloana* 2: 255-283.

REIG O. A., KIRSCH J. A. W. & MARSHALL L. G. 1987. — Systematic relationships of the living neocenozoic American "opossum-like" marsupials (suborder Didelphimorphia), with comments on the classification of these and of the Cretaceous and Paleocene New World and European metatherians, *in* ARCHER M. (ed.), *Possums and Opossums: Studies in Evolution.* Vol. 1. Sidney, Australia, Surrey Beatty and Sons: 1-89.

RIGGS E. S. 1929. — New family of South American Pliocene mammals. *Bulletin of the Geological Society of America* 40: 117. https://doi.org/10.1130/GSAB-40-1

RIGGS E. S. 1933. — Preliminary description of a new marsupial saber-tooth from the Pliocene of Argentina. *Field Museum of Natural History, Geological Series* 6: 61-66. https://doi.org/10.5962/bhl.title.5427

RIGGS E. S. 1934. — A new marsupial saber-tooth from the Pliocene of Argentina and its relationships to other South American predaceous marsupials. *Transactions of the American Philosophical Society, new series* 24 (1): 1-32. https://doi.org/10.2307/3231954

RIGGS E. S. & PATTERSON B. 1939. — Stratigraphy of Late Miocene and Pliocene deposits of the Province of Catamarca (Argentina). *Physis* 14: 143-162.

RINGUELET A. B. 1966. — Marsupialia, *in* BORRELLO A. V. (ed.), *Paleontografía Bonaerense – IV Vertebrata*. Comisión de Investigaciones Científicas de la Provincia de Buenos Aires, La Plata: 46-59. https://digital.cic.gba.gob.ar/items/52d4a0b9-04b7-4e41-9426-d3bc542d36bc

RONQUIST F., TESLENKO M., VAN DER MARK P., AYRES D. L., DARLING A., HÖHNA S., LARGET B., LIU L., SUCHARD M. A. & HUELSENBECK J. P. 2012. — MrBayes 3.2: Efficient bayesian phylogenetic inference and model choice across a large model space. *Systematic Biology* 61 (3): 539-542. https://doi.org/10.1093/sysbio/sys029

ROUGIER G. W., WIBLE J. R. & NOVACEK M. J 1998. — Implications of *Deltatheridium* specimens for early marsupial history. *Nature* 396: 459-463. https://doi.org/10.1038/24856

ROUGIER G. W., WIBLE J. R. & NOVACEK M. J. 2004. — New specimen of *Deltatheroides cretacicus* (Metatheria, Deltatheroida) from the Late Cretaceous of Mongolia. *Bulletin Carnegie Museum of Natural History* 36: 245-266. https://doi.org/10.2992/0145-9058(2004)36[245:NSODCM]2.0.CO;2

ROUGIER G. W., MARTINELLI A. G. & FORASIEPI A. M. 2021. — *Mesozoic Mammals from South America and their Forerunners*. Cham, Switzerland, Springer, 388 p. https://doi.org/10.1007/978-3-030-63862-7

ROWE T. 2001. — *Vincelestes neuquenianus* (On-line), Digital Morphology. Available from http://digimorph.org/specimens/Vincelestes_neuquenianus/ [accessed 18 June 2021].

SÁNCHEZ-VILLAGRA M. R. & SMITH K. K. 1997. — Diversity and evolution of the marsupial mandibular angular process. *Journal of Mammalian Evolution* 4: 119-144. https://doi.org/10.1023/A:1027318213347

SÁNCHEZ-VILLAGRA M., LADEVÈZE S., HOROVITZ I., ARGOT C., HOOKER J. J., MACRINI T. E., MARTIN T., MOORE-FAY S., MUIZON C. DE, SCHMELZLE T. & ASHER R. J. 2007. — Exceptionally preserved North American Paleogene metatherians: Adaptations and discovery of a major gap in the opossum fossil record. *Biology Letters* 3 (3): 318-322. https://doi.org/10.1098/rsbl.2007.0090

SCHALLER O. 2007. — *Illustrated Veterinary Anatomical Nomenclature*. Stuttgart, Germany, Ferdinand Enke Verlag, 614 p.

SCHNEIDER C. A., RASBAND W. S. & ELICEIRI K. W. 2012. — NIH Image to ImageJ: 25 years of image analysis. *Nature Methods* 9: 671-675. https://doi.org/10.1038/nmeth.2089

SCOTT C. S. & FOX R. C. 2015. — Review of Stagodontidae (Mammalia, marsupialia) from the Judithian (Late Cretaceous) belly River Group of Southeastern Alberta, Canada. *Canadian Journal of Earth Sciences* 52 (8): 682-695. https://doi.org/10.1139/cjes-2014-0170

SIMPSON G. G. 1948. — The beginning of the age of mammals in South America. Part I, Introduction. Systematics: Marsupialia, Edentata, Condylarthra, Litopterna and Notioprogonia. *Bulletin of the American Museum of Natural History* 91 (1): 1-232. http://hdl.handle.net/2246/1632

SINCLAIR W. J. 1906. — Mammalia of the Santa Cruz Beds: Marsupialia. *Reports of the Princeton University, Expedition to Patagonia* 4 (3): 333-460. https://doi.org/10.5962/bhl.title.12486

SISSON S. 1965. — *Anatomía de los animales domésticos*. Barcelona, Salvat. 952 p.

SMITH R. J. 1993. — Logarithmic transformation bias in allometry. *American Journal of physical Anthropology* 90 (2): 215-228. https://doi.org/10.1002/ajpa.1330900208

SUAREZ C. 2019. — Estudios taxonómicos y paleobiológicos sobre los Metatheria (Mammalia) del Mioceno medio de La Venta, Colombia, Parts 1-2. *Universidad Nacional de La Plata*, 560 p. https://doi.org/10.35537/10915/75246

SUAREZ C., FORASIEPI A. M., GOIN F. J. & JARAMILLO C. 2016. — Insights into the Neotropics prior to the Great American Biotic Interchange: New evidence of mammalian predators from the Miocene of Northern Colombia. *Journal of Vertebrate Paleontology* 36 (1). https://doi.org/10.1080/02724634.2015.1029581

SZALAY F. S. & TROFIMOV B. A. 1996. — The Mongolian late Cretaceous *Asiatherium*, and the early phylogeny and paleobiogeography of Metatheria. *Journal of Vertebrate Paleontology* 16 (3): 474-509. https://doi.org/10.1080/02724634.1996.10011335

TURNBULL W. D. 1970. — Mammalian masticatory apparatus. *Fieldiana, Geology* 18: 149-356. https://doi.org/10.5962/bhl.title.5442

TURNBULL W. D. & SEGALL W. 1984. — The ear region of the marsupial sabertooth, Thylacosmilus: influence of the sabertooth lifestyle upon it, and convergence with placental sabertooths. *Journal of Morphology* 181: 239-270. https://doi.org/10.1002/jmor.1051810302

VAN DER HAMMEN T. 1958. — Estratigrafía del Terciario y Maastrichtiano continentales y tectogénesis de los Andes colombianos. *Boletin Geologico* 6 (1-3): 60-116. https://doi.org/10.32685/0120-1425/bolgeol6.1-3.1958.309

VAN VALKENBURGH B. 1991. — Iterative evolution of hypercarnivory in canids (Mammalia: Carnivore): evolutionary interactions among sympatric predators. *Paleobiology* 17 (4): 340-362. https://doi.org/10.1017/S0094837300010691

VAN VALKENBURGH B. & KOEPFLI K. P. 1993. — Cranial and dental adaptation to predation in canids. *Symposia of the Zoological Society of London* 65: 15-37.

VILLARROEL C. & MARSHALL L. G. 1982. — Geology of the Deseadan (early Oligocene) Age Estratos Salla in the Salla-Luribay basin, Bolivia, with description of new Marsupialia. *Geobios, mémoire spécial* 6: 201-211. https://doi.org/10.1016/S0016-6995(82)80114-9

VOSS R. S. & JANSA S. A. 2009. — Phylogenetic relationships and classification of didelphid marsupials, an extant radiation of New World metatherian mammals. *Bulletin of the American Museum of Natural History* (322): 1-177. https://doi.org/10.1206/322.1

WERDELIN L. 1987. — Jaw geometry and molar morphology in marsupial carnivores: analysis of a constraint and its macroevolutionary consequences. *Paleobiology* 13 (3): 342-350. https://doi.org/10.1017/S0094837300008915

WESTERMAN M., KRAJEWSKI C., KEAR B. P., MEEHAN L., MEREDITH R. W., EMERLING C. A. & SPRINGER M. S. 2016. — Phylogenetic

relationships of dasyuromorphian marsupials revisited. *Zoological Journal of the Linnean Society* 176 (3): 686-701. https://doi.org/10.1111/zoj.12323

WIBLE J. R. 2003. — On the cranial osteology of the short-tailed opossum *Monodelphis brevicaudata* (Didelphidae, Marsupialia). *Annals of Carnegie Museum* 72 (3): 137-202. https://doi.org/10.5962/p.316087

WIBLE J. R., ROUGIER G. W., NOVACEK M. J. & ASHER R. J. 2009. — The Eutherian Mammal *Maelestes gobiensis* from the Late Cretaceous of Mongolia and the phylogeny of Cretaceous Eutheria. *Bulletin of the American Museum of Natural History* 2009 (327): 1. https://doi.org/10.1206/623.1

WROE S., CHAMOLI U., PARR W. C. H., CLAUSEN P., RIDGELY R. & WITMER L. 2013. — Comparative biomechanical modeling of metatherian and placental saber-tooths: a different kind of bite for an extreme pouched predator. *PLoS ONE* 8 (6): e66888. https://doi.org/10.1371/journal.pone.0066888

WILSON G. P., EKDALE E. G., HOGANSON J. W., CALEDE J. J. & VANDER LINDEN A. 2016. — A large carnivorous mammal from the Late Cretaceous and the North American origin of marsupials. *Nature Communications* 7. https://doi.org/10.1038/ncomms13734

ZIMICZ A. N. 2012. — Ecomorfología de los marsupiales paleógenos de América del Sur La Plata, *Universidad Nacional de La Plata*. 1-454 p. https://doi.org/10.35537/10915/29337

Submitted on 18 October 2022;
accepted on 11 May 2023;
published on 12 October 2023.

APPENDICES

APPENDIX 1. — Supplementary information on comparisons and analyses.

SUPPLEMENTARY FIGURES

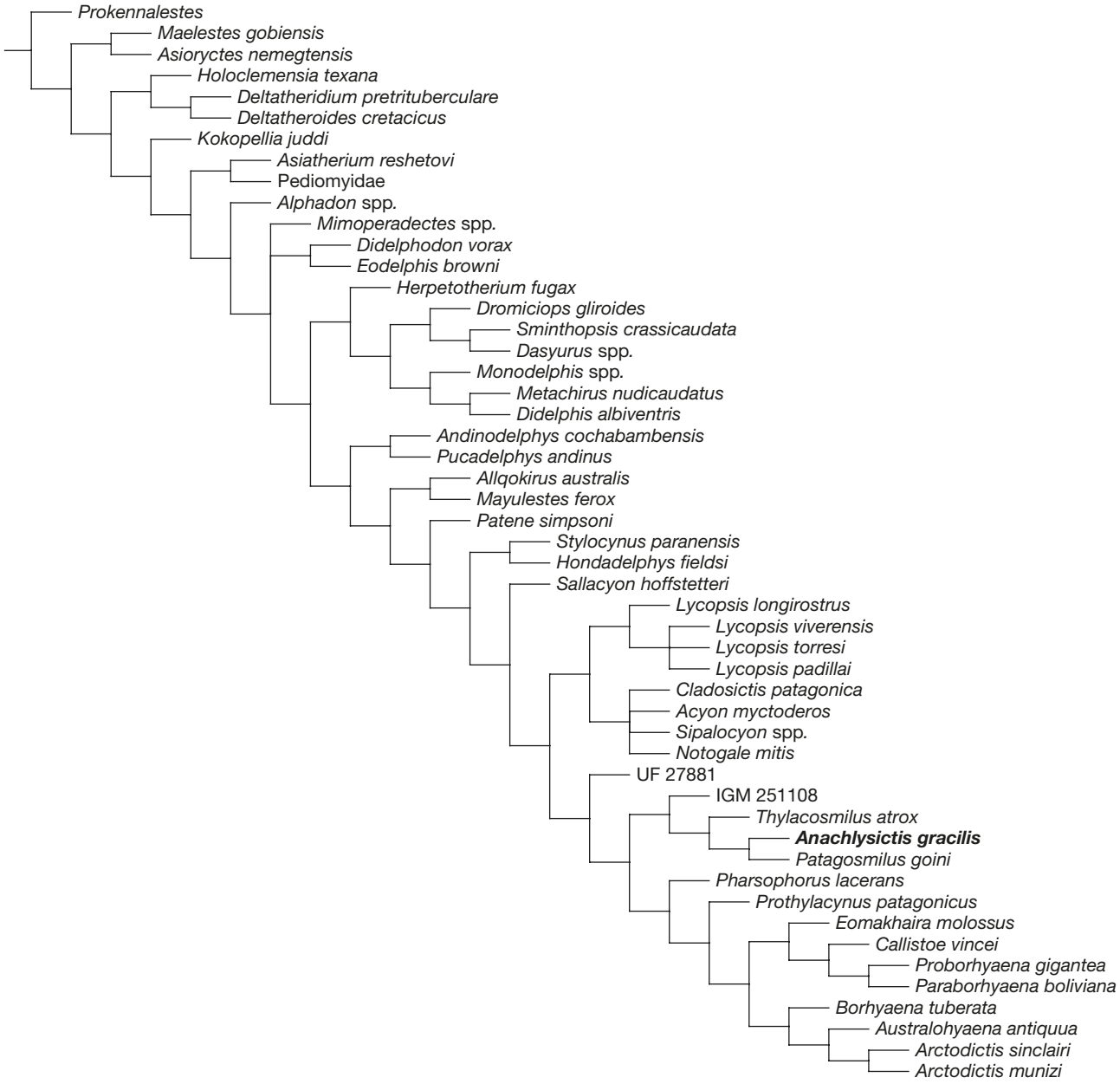

FIG. A1. — Consensus tree resulted from the alternative phylogenetic analysis under equal weights, excluding *Thylacinus cynocephalus* (Harris, 1808), made to test differences in topology.

Appendix 1. — Continuation.

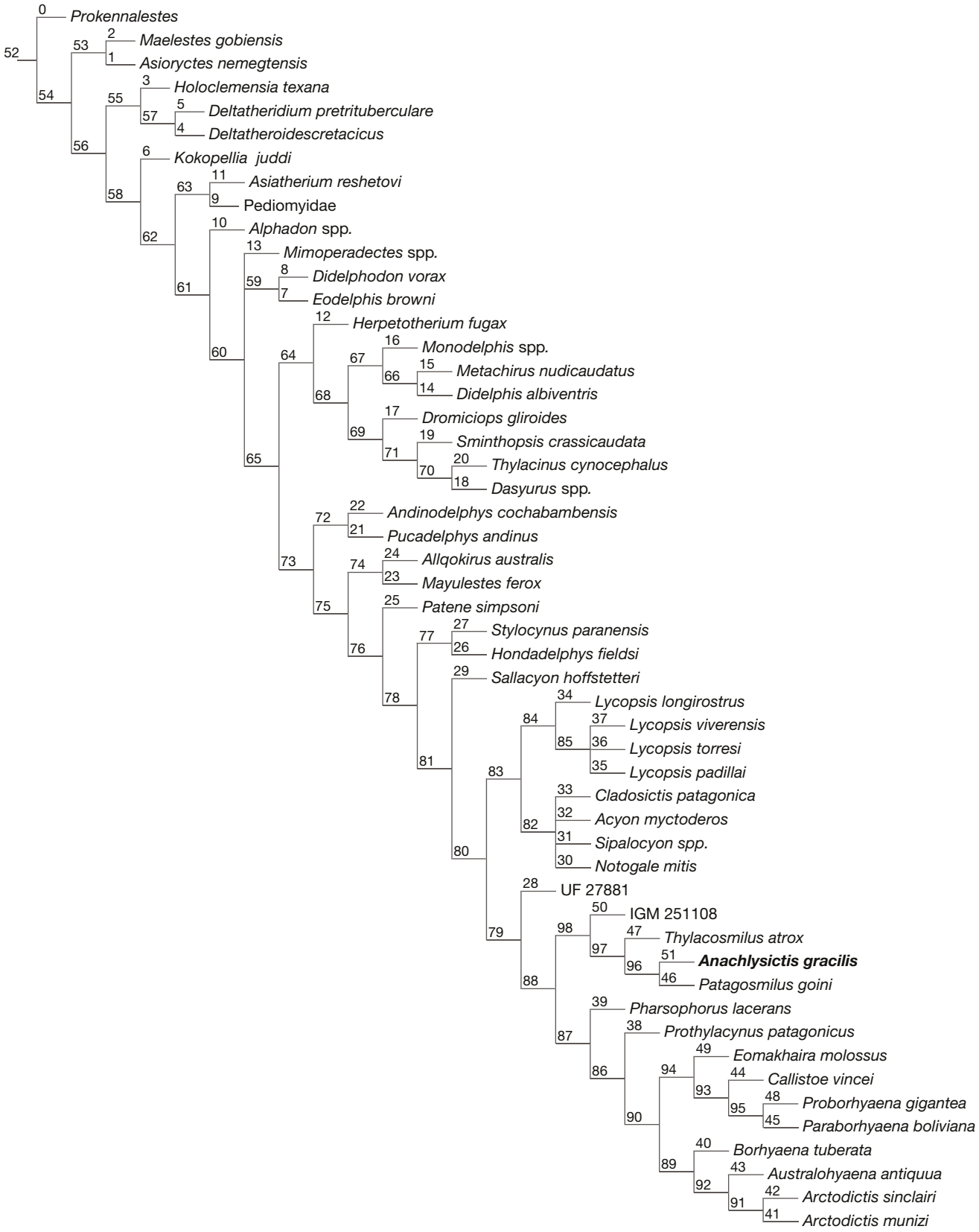

Fig. A2. — Strict consensus of six most parsimonious trees obtained from the parsimony phylogenetic analysis under equal weights, including *Thylacinus cynocephalus* (Harris, 1808) and constraining the Dasyuromorphian clade. Numbers indicate the number of nodes. For additional information, see Synapomorphies below.

Appendix 1. — Continuation.

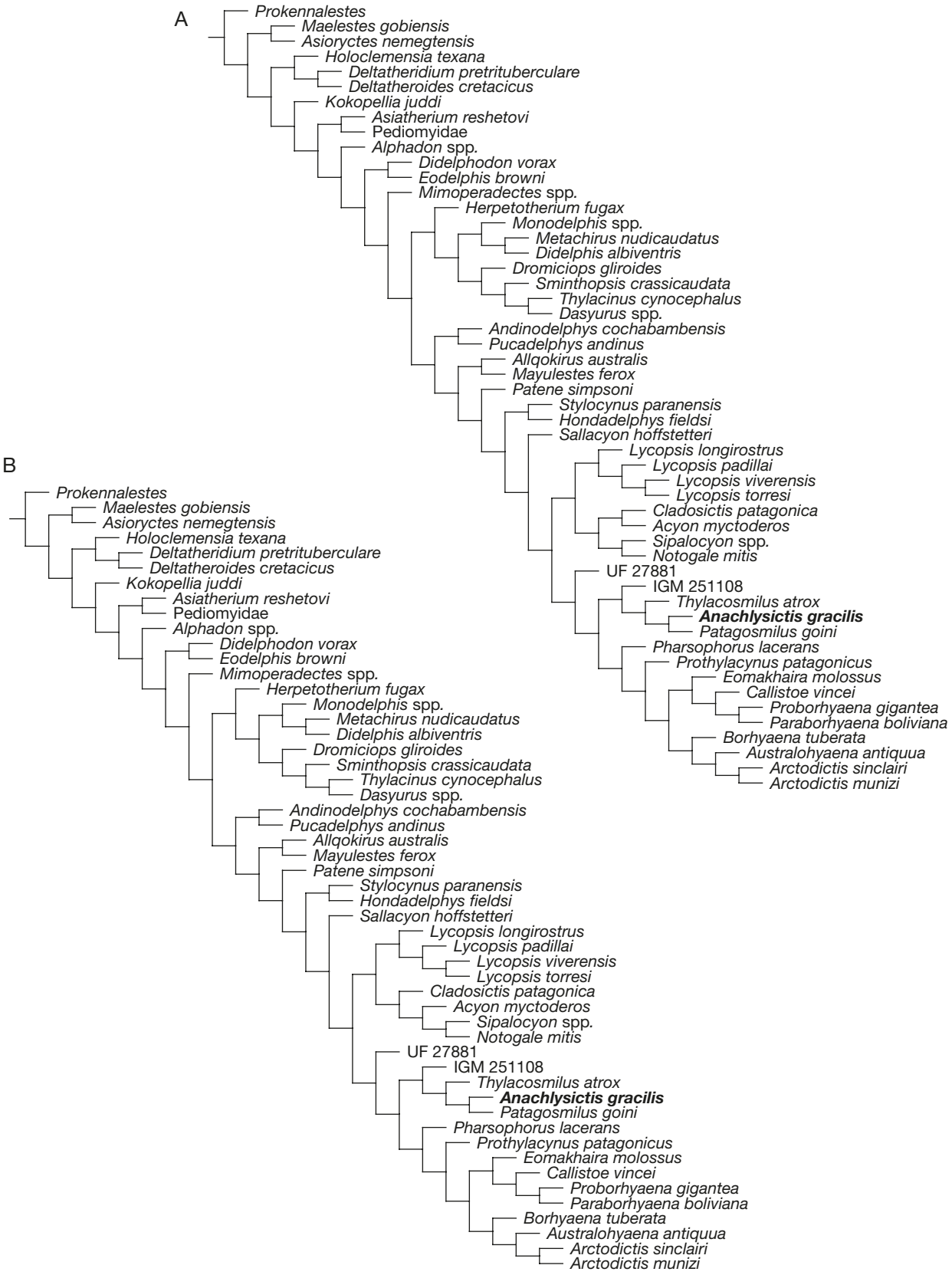

FIG. A3A, B. — Six most parsimonious trees (**A**-**F**) obtained from the parsimony phylogenetic analysis under equal weights, with the Dasyuromorphia node constrained.

Appendix 1. — Continuation.

Fig. A3C, D. — Six most parsimonious trees (**A**-**F**) obtained from the parsimony phylogenetic analysis under equal weights, with the Dasyuromorphia node constrained.

Appendix 1. — Continuation.

Fig. A3E, F. — Six most parsimonious trees (**A**-**F**) obtained from the parsimony phylogenetic analysis under equal weights, with the Dasyuromorphia node constrained.

Appendix 1. — Continuation.

Fig. A4. — Result of parsimony phylogenetic analysis under implied weights, with concavity constant k = 3, showing the single recovered most parsimonious tree. Numbers represent bootstrap values. Support values not given for Dasyuromorphia, as this node was constrained a priori (see text).

Appendix 1. — Continuation.

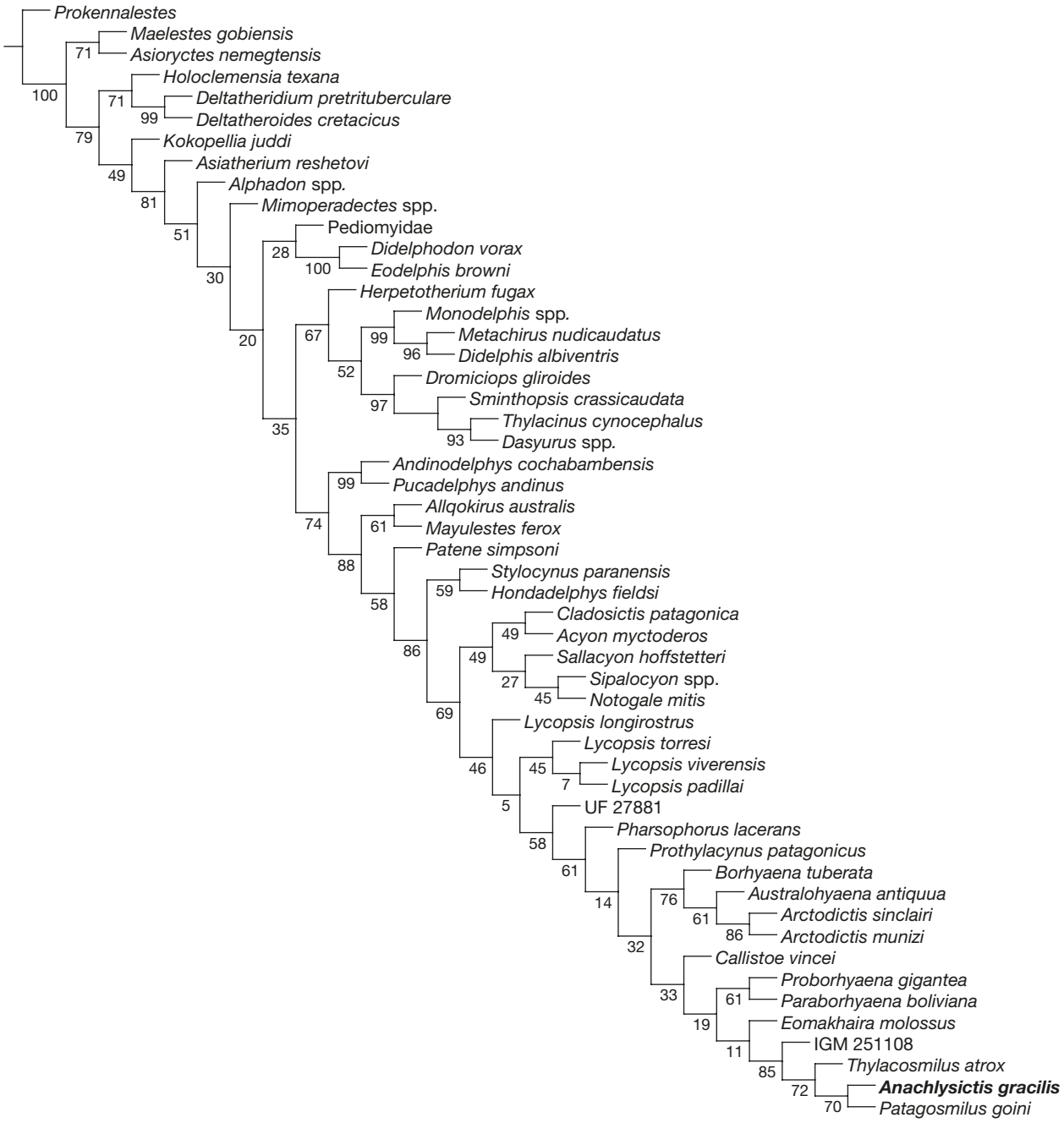

FIG. A5. — Result of parsimony phylogenetic analysis under implied weights, with concavity constant k = 12, showing the single recovered most parsimonious tree. Numbers represent bootstrap values. Support values not given for Dasyuromorphia, as this node was constrained a priori (see text).

Appendix 1. — Continuation.

INSTITUTIONAL ABBREVIATIONS

AMNH	American Museum of Natural History, New York, United States;
DTC	Donald Thomson Collection, Museums Victoria, Australia;
FMNH	Field Museum of Natural History, Chicago, United States;
IBIGEO-P	Colección de Paleontología del Instituto de Bio y Geociencias del Noroeste Argentino, Salta, Argentina;
IGM	collections from the Servicio Geológico Colombiano (former Ingeominas), Bogota, Colombia, and Duke University, Durham, United States;
MACN	Museo Argentino de Ciencias Naturales "Bernardino Rivadavia", Buenos Aires, Argentina (MACN-A = Ameghino Collection);
MLP	Museo de La Plata, La Plata, Argentina;
MMH	Museo Municipal de Ciencias Naturales "Vicente Di Martino", Monte Hermoso, Argentina;
MMP	Museo Municipal de Ciencias Naturales "Lorenzo Scaglia", Mar del Plata, Argentina;
MNHN-Bol	Museo Nacional de Historia Natural, La Paz, Bolivia;
NHMUK	Natural History Museum, London, England;
PVL	Paleontología de Vertebrados Lillo, Tucumán, Argentina;
TMM	Texas Memorial Museum, Austin, United States;
UCMP	University of California Museum of Paleontology, Berkeley, United States;
UF	Florida Museum of Natural History, Gainesville, United States.

MATERIAL EXAMINED

The following is the list of specimens examined for comparisons, scoring of new characters for the phylogenetic analysis and modifications with respect to the previous version of the matrix used (Engelman *et al.* 2020). Only the studied material from each specimen is listed. The revision was made using original material, casts and/or photographs, and additional information from the literature. Some species were coded only from literature when any other resource was not available.

Vincelestes neuquenianus Bonaparte, 1986
Bonaparte (1986), Rowe (2001).

Deltatheridium pretrituberculare Gregory & Simpson, 1926
Gregory & Simpson (1926); Rougier *et al.* (1998).

Deltatheroides cretacicus Gregory & Simpson, 1926
Gregory & Simpson (1926); Rougier *et al.* (2004).

Prokennalestes Kielan-Jaworowska & Dashzeveg, 1989
Lopatin & Averianov (2017).

Maelestes gobiensis Wible, Rougier, Novacek & Asher, 2007
Wible *et al.* (2009).

Asioryctes nemegtensis Kielan-Jaworowska, 1975
Kielan-Jaworowska (1975, 1984).

Kokopellia juddi Cifelli, 1993
Cifelli (1993a, b); Cifelli & Muizon (1997).

Asiatherium reshetovi Trofimov & Szalay, 1994
Szalay & Trofimov (1996).

PEDIOMYIDAE
Lillegraven (1969); Fox (1979a).

Alphadon Simpson, 1927
Lillegraven (1969); Fox (1979b); Montellano (1988).

Mimoperadectes houdei Horovitz, Martin, Bloch, Ladevèze, Kurz & Sánchez-Villagra, 2009
Horovitz *et al.* (2009).

STAGODONTIDAE
Didelphodon vorax (Marsh, 1889)
Wilson *et al.* (2016).

Eodelphis cutleri (Woodward, 1916)
Matthew (1916); Scott & Fox (2015).

Herpetotherium fugax
Fox (1983); Sánchez-Villagra *et al.* (2007); Horovitz *et al.* (2008, 2009).

DIDELPHIDAE
Monodelphis spp.

Monodelphis dimidiata (Wagner, 1847)
MLP 1-I-90-2, skull and associated dentaries (Sierra de La Ventana locality); MLP 1-I-90-8, skull and associated dentaries (Miramar locality); MLP 1-I-90-3, skull and left dentary (Sierra de La Ventana locality); MLP 1-I-90-74, skull (Sierra de La Ventana locality). All the specimens are extant individuals and come from Buenos Aires Province, Argentina.
Additional information: Reig *et al.* (1987); Wible (2003).

Metachirus nudicaudatus (É.Geoffroy Saint-Hilaire, 1803)
Photographs available in Myers *et al.* (2018).

Didelphis albiventris Lund, 1840
Coues (1872); Reig *et al.* (1987); Abdala *et al.* (2001); Voss & Jansa (2009); Astúa (2015).

AUSTRALIDELPHIA
Dromiciops gliroides Thomas, 1894
NHMUK 92.5.9.3 (holotype), complete skull with mandible (Huite, northeastern Chiloé Island, Chile). Photographs available online: Natural History Museum (2014).

Appendix 1. — Continuation.

Additional information: Marshall (1978b, 1982); Reig *et al.* (1987); Hershkovitz (1999); Giannini *et al.* (2004).

Sminthopsis crassicaudata (Gould, 1844)
NHMUK 2.9.8.7 (*Sminthopsis crassicaudata centralis* – holotype), complete skull with mandible (Killalpanima, East of Lake Eyre, Southern Australia); AMNH 196686, complete skull (Northampton, Western Australia). Photographs available online: NHMUK specimen, Natural History Museum (2014); AMNH specimen, Macrini (2009).

Thylacinus cynocephalus (Harris, 1808)
C 3149, complete skull with mandible; USNM 155407, complete skull with mandible. Photographs available online: C specimen, Museums Victoria Collections (a); USNM specimen, (Myers *et al.* 2022). Both recent specimens from Tasmania, Australia.

Dasyurus hallucatus Gould, 1842
TMM M-6921, complete skull with mandible (Batchelor, Northern Territory, Australia); DTC 302-1, complete skull (Trial Bay, Northern Territory, Australia); NHMUK 9.4.23.8 (*Dasyurus hallucatus exilis* – holotype), complete skull with mandible (Parry's Creek, near Wyndham, NE Kimberley, Northern Australia); NHMUK 15.3.5.77 (*Dasyurus hallucatus predator* – holotype), complete skull (Utingu, Queensland, Australia); NHMUK 26.3.11.125 (*Dasyurus hallucatus nesaeus* – holotype), complete skull with mandible ('Groote Eylandt', western part of the Gulf of Carpentaria, Northern Territory, Australia). Photographs available online: TMM specimen, Macrini (2005); DTC specimen, Museums Victoria Collections (b); NHMUK specimens, Natural History Museum (2014).

Pucadelphidae
Andinodelphys cochabambensis Marshall & Muizon, 1988
Muizon *et al.* (1997).

Pucadelphys andinus Marshall & Muizon, 1988
Marshall & Muizon (1995); Ladevèze *et al.* (2011).

Mayulestidae
Allqokirus australis Marshall & Muizon, 1988
Muizon *et al.* (2018).

Mayulestes ferox Muizon, 1994
Muizon (1994, 1998).

SPARASSODONTA
Patene simpsoni Paula Couto, 1952
Marshall (1981); Goin *et al.* (1986); Babot & Forasiepi (2016).

Stylocynus paranensis Mercerat, 1917
MLP 11-94 (holotype), left mandibular ramus; MLP 41-XII-13-1112, anterior fragment of right mandibular ramus. Both specimens come from Paraná, Entre Ríos Province, Argentina; Entre Ríos Formation, Huayquerian Stage/Age, late Miocene.
Additional information: Cabrera (1927); Marshall (1979).

Hondadelphys fieldsi Marshall, 1976
UCMP 37960, fragmentary skull, right mandibular ramus with dentition; IGM 253049, partial left mandibular ramus with dentition (La Venta, Colombia; Honda Group, Laventan SALMA, middle Miocene).

Hathliacynidae
Sallacyon hoffstetteri
Petter & Hoffstetter (1983).

Cladosictis patagonica Ameghino, 1887
MLP 11-19 (holotype), anterior portion of skull and partial mandible (Monte León locality); MLP 11-4, left mandibular ramus with dentition (Monte León locality?); MACN-A 2079, partial skull; MACN-A 5927-5928, nearly complete skull and right mandibular ramus with dentition (Corriguen Kaik locality); MACN 5950, anterior portion of skull (Corriguen Kaik locality); MACN-A 6288, right and left mandibular rami with dentition. All the specimens come from Santa Cruz Province, Argentina; Santa Cruz Formation, Santacrucian SALMA, early Miocene.
Additional information: Sinclair (1906); Cabrera (1927); Marshall (1981).

Acyon myctoderos Forasiepi, Sánchez-Villagra, Goin, Takai, Shigehara & Kay, 2006
MNHN-Bol-V-003668 (holotype; casts in MLP), skull and associated mandibular rami (Quebrada Honda, Bolivia; Laventan SALMA, middle Miocene).
Additional information: Forasiepi *et al.* (2006).

Sipalocyon gracilis Ameghino, 1887
MACN 647 (holotype; cast in MLP), fragment of right mandibular ramus with dentition (Monte Observación locality); MACN 691-692 (casts in MLP), left mandibular ramus and right fragment of maxilla with dentition; MACN 5952-5953, fragmentary skull and broken left mandibular ramus; MACN-A 5958, left maxillary fragment with dentition; MLP 11-2, fragment of left mandibular ramus. All the specimens come from Santa Cruz Province, Argentina; Santa Cruz Formation, Santacrucian SALMA, early Miocene.
Additional information: Sinclair (1906); Cabrera (1927); Marshall (1981).

Notogale mitis (Ameghino, 1897)
Marshall (1981); Villarroel & Marshall (1982).

Appendix 1. — Continuation.

Borhyaenoidea
Lycopsis longirostrus Marshall, 1977
UCMP 38061 (holotype), right half of the skull and right mandibular ramus with dentition (La Venta, Colombia; Honda Group, Laventan SALMA, middle Miocene).

Lycopsis viverensis Forasiepi, Goin & Di Martino, 2003
MMH 87-6-1 (holotype; cast in MLP), a fragment of left maxilla with dentition; MMH 95-6-1, right mandibular ramus with dentition (cast in MLP). Both specimens from Arroyo Chasicó, Villarino Department, Buenos Aires Province, Argentina; Arroyo Chasicó Formation, Chasicoan Stage/Age, late Miocene.
Additional information: Forasiepi *et al.* (2003).

Lycopsis torresi Cabrera, 1927
MLP11-113 (holotype), fragmentary mandible and maxilla with dentition (Santa Cruz River, Santa Cruz Province, Argentina; Santa Cruz Formation, Santacrucian SALMA, early Miocene).

Lycopsis padillai Suarez, Forasiepi, Goin & Jaramillo, 2015
MUN-STRI 34113, partial left maxilla with M1-M4, partial lacrimal and jugal (Makaraipao locality, La Guajira Department, Colombia; Castilletes Formation, middle Miocene, Langian).
UF 27881 (un-nominated species), fragmentary skull (Quebrada Honda, Bolivia; Laventan SALMA, middle Miocene).
Additional information: Engelman & Croft (2014).

Pharsophorus lacerans Ameghino, 1897
MACN-A 52-391 (holotype; cast in MLP), left mandibular ramus; MLP 11-114, incomplete left mandibular ramus (north of Lake Colhue Huapi). Both specimens from Chubut Province, Argentina; Deseadan SALMA, middle-late Oligocene.
Additional information: Cabrera (1927); Marshall (1978a); Patterson & Marshall 1978).

Prothylacynus patagonicus Ameghino, 1891
MACN-A 706 (holotype), left mandibular ramus and the anterior portion of the right ramus fused; MACN 5931, nearly complete skull. Both specimens come from Santa Cruz Province, Argentina; Santa Cruz Formation, Santacrucian SALMA, early Miocene.
Additional information: Sinclair (1906); Cabrera (1927); Marshall (1979).

Borhyaenidae
Borhyaena tuberata Ameghino, 1887
MACN-A 5922, fragmentary skull; MACN-A 9344, nearly complete skull (Yegua Quemada locality); MACN-A 9341-9342, left and right maxillae and mandibular rami (Corriguen-Kaik). MLP 11-5, fragment of right dentary. All the specimens come from Santa Cruz Province, Argentina; Santa Cruz Formation, Santacrucian SALMA, early Miocene.
Additional information: Sinclair (1906); Cabrera (1927); Marshall (1978a).

Australohyaena antiquua Forasiepi, Babot & Zimicz, 2015
Forasiepi *et al.* (2015).

Arctodictis sinclairi
MLP 87-VII-3-1, a nearly complete skeleton (Gran Barranca, Chubut Province, Argentina; Sarmiento Formation, Colhuehuapian SALMA, early Miocene).
Additional information: Marshall (1978a); Forasiepi (2009).

Arctodictis munizi Mercerat, 1891
MLP 11-85 (holotype), left mandibular ramus and the anterior portion of the right, fused at the simphysis (Monte León locality); MLP 11-65, skull and mandible badly preserved. Both specimens come from Santa Cruz Province, Argentina; Santa Cruz Formation, Santacrucian SALMA, early Miocene.
Additional information: Forasiepi *et al.* (2004).

Eomakhaira molossus Engelman, Flynn, Wyss & Croft, 2020
Photographs of the holotype (SGOPV 3490) shared by Engelman.
Additional information: Engelman *et al.* (2020).

Proborhyaenidae
Callistoe vincei Babot, Powel & Muizon, 2002
PVL 4187 (holotype), complete skull and dentary and almost complete postcranium; IBIGEO P-110, fragment of right mandible with partial intra alveolar and complete extra alveolar portion of the canine, p1 with complete crown and distal root, roots of the p3, and complete m1 to m4.
Additional information: Babot *et al.* (2002, 2022).

Paraborhyaena boliviana Hoffstetter & Petter, 1983
Hoffstetter & Petter (1983); Petter & Hoffstetter (1983).

Proborhyaena gigantea Ameghino, 1897
MACN 52-382 (holotype), right mandibular ramus with partial dentition (Cabeza Blanca locality, Chubut Province; Sarmiento Formation); MLP 79-XI1-18-1 (cf. *Proborhyaena*), left maxilla fragment with partial dentition and a portion of the left mandibular ramus with partial dentition (Quebrada Fiera, Mendoza Province; "Lower Tertiary volcano-sedimentary complex"). Both specimens from Argentina, Deseadan SALMA, early Oligocene.
Additional information: Patterson & Marshall (1978); Bond & Pascual (1983).

Thylacosmilidae
IGM 251108 (un-nominated species), partial left horizontal ramus without dentition, right horizontal ramus with dentition, right maxillary fragment with a proximal portion of

Appendix 1. — Continuation.

the canine, and incomplete postcranial elements (La Venta, Colombia; Honda Group, Laventan SALMA, middle Miocene).

Additional information: Goin (1997)

Comment: This species is being described in a work in progress from Suarez *et al.*

Thylacosmilus atrox Riggs, 1933
FMNH P14531 (holotype), nearly complete skull (Chiquimil locality, Catamarca Province, Argentina; Corral Quemado Formation, Chapadmalalan Stage/Age, late Pliocene; FMNH P143344 (paratype): left mandibular ramus with dentition (Chiquimil locality, Catamarca Province, Argentina; Andagala Formation, Huayquerian Stage/Age, late Miocene); MLP 65-VII-29-41, partial skull, partial right mandibular ramus with dentition and a fragment of the right upper canine isolated (Salinas Grandes de Hidalgo, La Pampa Province, Argentina; Cerro Azul Formation, Huayquerian Stage/Age, late Miocene).

Additional information: Riggs (1934); Goin & Pascual (1987); Forasiepi *et al.* (2019).

Comment: The FMNH specimens were revised in photographs provided by A. Forasiepi.

Anachlysictis gracilis Goin, 1997
IGM 184247, almost complete right mandibular ramus with dentition, fragment of left mandibular ramus with dentition, fragment of left symphyseal process, skull fragment from the postorbital region, postcraneal elements; UCMP 39705, a posterior fragment of the right mandibular ramus, preserving the condyle and angular process; VPPLT 1612, a nearly complete skull. All specimens from La Venta, Colombia; Honda Group, Laventan SALMA, middle Miocene.

Additional information: Goin (1997).

Patagosmilus goini Forasiepi & Carlini, 2010
MLP 07-VII-1-1 (holotype), most of the left side of the skull with upper dentition, right magnum, and proximal portion of ungual phalanx (Río Negro Province, Argentina; Collón Curá Formation, Colloncuran SALMA, middle Miocene); B:p2-154 (MNHN-Bol: cast hosted in the MLP and observations from F. Goin), posterior portion of a skull, a fragment of left maxilla with the proximal portion of the canine, fragments of left and right maxillae with dentition, incomplete left and right mandibular rami with dentition ("Bone wash" locality, Río Rosario, Tarija Department, Bolivia; un-named formation, Honda Group, Bolivia [not homologous to the Honda Group from Colombia (MacFadden & Wolff 1981)], Laventan SALMA, middle Miocene).

Additional information: MacFadden & Wolff (1981); Goin & Carlini (1993); Forasiepi & Carlini (2010).

Comment: *P. goini* is currently known for the holotype and the only published specimen. However, another still-undescribed specimen from Quebrada Honda, Bolivia (middle Miocene) has been mentioned by Goin & Carlini (1993) as belonging to the same, or closely related species than the future holotypes of *A. gracilis* (named a few years later by Goin 1997) and *P. goini* (named some years later by Forasiepi & Carlini 2010). The specimen is identified with the field number "B: p2-154 (July 1992)" and was collected during the Duke University/Geobol Paleontology Expedition in 1992 (collectors: Richard Kay, Richard Madden, Carlos Villarroel, Federico Anaya, Marcelo Sánchez, Blythe Williams). The fossil stayed in the La Plata Museum (MLP) for study by Dr Francisco Goin's team. Still, that research could not be finished because the specimen was requested by the Natural History of Bolivia (MNHN-Bol), which was designed as its official repository until now. During the development of this research, we did not have access to the original material of this specimen, trying to establish communication with that museum several times over several years without success. We hope this communication is finally possible soon, so the study of this specimen can be finally completed. However, we had access to a cast hosted in the MLP and the notes of observations made by Dr Goin while he was studying the fossil. We used that material and information for comparisons and to complete some scorings in the matrix for *P. goini*, as we agree with the hypothesis of this specimen belonging to *P. goini*.

MODIFICATIONS IN DATA MATRIX

The matrix used for the phylogenetic analysis is a modification of the matrix from Engelman *et al.* (2020), which is based on Muizon *et al.* (2018) and previous matrices (Forasiepi 2009; Engelman & Croft 2014; Forasiepi *et al.* 2015; Suarez *et al.* 2016). The matrix was modified for this work, including adding new taxa, changes in some characters and scorings, and excluding redundant characters. We list these changes below:

New taxa
Anachlysictis gracilis and specimen IGM 251108.

New characters
Characters 45 (posterior extent of lacrimal), 140 (shape of dentary in occlusal view); 144 (symphyseal flange), 147 (anterior-most mental foramen location), 172 (asymmetry in mesiodistal length of the canines), 173 (lateral compression of lower canine), 178 (shape of the labial face of the upper canine), and 179 (lower canine implantation), are proposed in this work and coded for all the taxa included in the analysis.

Modifications of characters
The following are modifications to the previous version of the matrix (Engelman *et al.* 2020). The number of character correspond to that in the present work matrix.

– The characters 35, 170, 171, and 175 of Engelman *et al.* (2020) where not included in this matrix, as they were considered redundant (see next items for more details).

Appendix 1. — Continuation.

Character 33 (char. 33 of Engelman *et al.* 2020): modified with the wording similar to Forasiepi (2009: char. 26), as character 35 of Engelman *et al.* (2020) was not included in the matrix because it evaluates structures not necessarily related. Although the presence of the palatine spine is in general related to a posterior edge double-arched, there are exceptions, as in *Dasyurus* and *Eomakhaira*, where the spine is present, but there is not a double arch. The margin is straight. The double arch is, in general, related with the presence of a spine, but the presence of a spine not always implies a double-arched margin. For this reason, character 35 was removed, and the wording of the character 33 (also 33 in this work) was modified, similar to Forasiepi (2009: char. 26). The character 34 (char. 34 of Engelman *et al.* 2020) was maintained instead of merging the information in one character with the 33 (similar to Forasiepi 2009: char. 26), as the presence of a postpalatine torus in the taxa evaluated is not always related with a straight posterior end of the palate.

Character 59 (char. 59 of Engelman *et al.* 2020): reverted to the original version (Forasiepi 2009: wording, states and parsimony model), maintaining the scorings from Muizon *et al.* (2018: char. 177) because Engelman *et al.* (2020) re-definition was considered unnecessary. The sample is not large enough to consider a new, more detailed state only present in one specimen. The states of the previous version include this condition.

Character 139 (char. 139 of Engelman *et al.* 2020): character and states reverted to previous versions (char. 97 in Forasiepi 2009 and Suarez *et al.* 2016; Muizon *et al.* 2018: char. 103) because the re-definition of Engelman *et al.* (2020) uses a dental measurement (m1-4 length) to evaluate a dentary measurement. This is not congruent because the dental measurements are not always dependent on the dentary measurements. For example, depending on the ontogenetical stage or the taxon, the specimen could have a deep or shallow dentary and have the same m1-4 length because it has small or large teeth, respectively. So, following this argument, we reverted the scorings to previous versions for *Didelphis albiventris*, Mayulestes ferox, *Allqokirus australis*, *Lycopsis torresi*, *Lycopsis viverensis*, *Pharsophorus lacerans*, *Paraborhyaena boliviana*, *Thylacosmilus atrox*; and changed the scoring in *Stylocynus paranensis*, *Proborhyaena gigantea* and *Eomakhaira molossus* to "?".

Character 142 (char. 142 of Engelman *et al.* 2020): wording and states were modified to include more complex information, being replaced by definition and states from character 311 from Suarez (2019). Scorings were modified for all taxa. As it was impossible to access a *Paraborhyaena boliviana* preserving this portion of the jaw, the scoring was left empty (?).

Character 143 (char. 141 of Engelman *et al.* 2020): the states were modified using the wording of Forasiepi (2009) because they are more suitable for this analysis. For example, the wording of state 1 of Engelman *et al.* (2020) evaluates a fused symphysis. However, most taxa coded with this state do not have a fused symphysis but are strongly ankylosed. The only taxon in the matrix with the symphysis completely fused is *Arctodictis*.

Character 151 (char. 148 of Engelman *et al.* 2020): Due to a strong relationship with character 309 from Suarez (2019), we opted to combine them instead of adding that character to the matrix, resulting in the following modifications: the character description was modified to "Masseteric fossa area" because the states involve not only the masseteric fossa but also the structures around it; and the state 2 was added (masseteric fossa and coronoid process extremely reduced).

Character 158 (char. 155 of Engelman *et al.* 2020): Reverted to a previous version (Muizon *et al.* 2018), as Engelman does not explain the reason for creating a new state, and we don't consider it necessary. They also changed the polarity and made the character ordered, but there was no explanation for choosing that order.

Character 171 is a fusion of characters 168 and 170 of Engelman *et al.* (2020). This character has states and, consequently, scorings, similar to the previous version (Muizon *et al.* 2018: char. 14). Engelman *et al.* (2020) separated into two different characters the information contained in one (Forasiepi 2009: char. 115; Muizon *et al.* 2018: char. 14). This separation is unnecessary and duplicates information evaluable in only one character.

Character 175 is a fusion of characters 171 and 172 of Engelman *et al.* (2020). It was reverted to the previous version (Muizon *et al.* 2018: char. 15; modified from Forasiepi 2009: char. 116), and scorings were changed accordingly. Engelman *et al.* (2020) divided this character in two, and this causes duplication in information because it is possible to evaluate the same information in one character.

Character 177 is a fusion of characters 174 and 175 of Engelman *et al.* (2020). The information can be evaluated in only one character with more states.

Character 179 (char. 176 of Engelman *et al.* 2020): This character was added by Muizon *et al.* (2018: char. 13) and maintained in Engelman *et al.* (2020). However, none of the authors explains a measurement to differentiate a procumbent lower canine from a non-procumbent. For this reason, we considered it adequate to replace this character with the version of Suarez (2019; char. 316) because it is more informative and easier to determine. And consequently, we codified all the taxa using the new states.

Character 203 (char. 200 of Engelman *et al.* 2020): the wording of state 0 was changed to "Straight or nearly straight".

Character 245 (char. 242 of Engelman *et al.* 2020): the wording of states 1 and 2 was corrected, changing the word "smaller" to "shorter" and "larger" to "longer", as this character is evaluating length, not size.

Character 247 (char. 244 of Engelman *et al.* 2020): Scoring was changed for *Sallacyon hoffstetteri*, *Notogale mitis*, *Sipalocyon* spp., *Acyon myctoderos*, *Cladosictis patagonica*, *Lycopsis longirostrus*, *Lycopsis torresi*, *Lycopsis viverensis*, and *Prothylacynus patagonicus*, following the argument from Forasiepi (2009)

Appendix 1. — Continuation.

and Muizon *et al.* (2018) that this character is inapplicable to those taxa with incomplete trigonid (lacking metaconid). It is important to annotate that Muizon *et al.* (2018) posted this argument in the comments of this character (Muizon *et al.* 2018: 441, appendix 1, char. 70, comment) but did not apply it in the matrix, as several taxa lacking metaconid were not coded as inapplicable.

Character 254 (char. 251 of Engelman *et al.* 2020): Wording in state 0 was changed, as there was probably a mistake in Engelman *et al.* (2020) because there are no metatherians with the protoconid in a lingual position, so probably they referred to a "labial" position, as in all the taxa coded with this state.

Modifications in scoring

Several modifications in scoring were made based on observations on materials listed in the Material examined. The number of character correspond to the current version (this work).

Maelestes gobiensis

Character 57 was coded 1 (glenoid process narrower than glenoid cavity).

Hondadelphys fieldsi

Character 23 was changed from 1 to 0 (flaring of maxillary cheeks present)

Character 27 was changed from 0 to "?". This condition is not clearly evaluable because the holotype does not have a complete palate, just two parts separated.

Character 231 was changed from 2 to 1 (stylar cusp B small or forming an ectocingulum), as observed on the holotype.

Character 232 changed from 0 to 1 (present) because the StC is observed in the holotype, being part of the ectocingulum but distinguishable.

Lycopsis longirostrus

Character 93: reverted to 1, because the medial keel is present in the holotype.

Lycopsis viverensis

Character 181: the scoring was changed from 1 to 0 (P/p1 parallel to tooth row – less than 19 degrees) because the angle is oblique but less than 19º

Patagosmilus goini

Character 51 was changed from 1 to 0 (interparietal present) based on observations on the Quebrada Honda specimen (see Material examined), where the suture between parietal and interparietal is partially visible. This taxon was probably scored 1 by mistake because this portion of the skull is not preserved in the holotype, and there are no more specimens different to these two.

Character 176: changed from 0 to "?", because the lower canine is unknown.

Character 212: changed from 0 to 1, because the protocone is not vestigial but very small.

Character 214: changed from 1 to 0, because the protocone has a small basin.

Character 219: changed from "–" to 0.

The next characters were coded based on specimen from Quebrada Honda, Bolivia (see Material examined): 49, 54, 56, 57, 58, 59, 61, 66, 83, 84, 85, 87, 88, 89, 91, 93, 95, 98, 99, 100, 101, 103, 146, 148, 151, 152, 155, 182, 183, 190, 191, 233, 234, 239, 240, 241, 242,243, 244, 245, 246, 247, 249, 250, 251, 252, 253, 254, 257, 258, 259, 260, 261, 262, 263, 264, 265, 266,267, 268, 270, 271, 272, 273, 274, 275, and 276.

Thylacosmilus atrox

Character 19: changed from 2 to inapplicable (–) because despite a fronto-maxillary contact is present, this condition is secondary, not homologous to that present in other taxa codified with state 2 (e.g., marsupials). In this species, this contact is caused by the posterior expansion of the maxilla on the skull roof, interrupting the naso-lacrimal contact present in Sparassodonts, including more plesiomorphic thylacosmilids (e.g., *A. gracilis* and *P. goini*).

Character 24: changed from polymorphic to 1 (fossa for levator labii muscle mainly on maxilla (following Forasiepi *et al.* 2019).

Characters 61, 134 and 135 were changed following Forasiepi *et al.* (2019) and observations examined material. Character 61 was changed from 0 to inapplicable (–), because *Thylacosmilus atrox* lacks a suprameatal foramen (Riggs 1934; Forasiepi *et al.* 2019). However, it has two couple of openings on the squamosal (two on each side), which correspond to the foramina for temporal rami (Forasiepi *et al.* 2019). Consequently, character 134 was changed from 1 to 0 (Foramina for temporal ramus with well-developed internal branch of stapedial artery present), and character 135 from inapplicable (–) to 1 (foramina for temporal rami located on squamosal). The functional role of the suprameatal foramen would presumably have been taken up by one of the canals for rami temporales (Forasiepi *et al.* 2019).

Character 52: changed from 1 to 0 (shape of fronto-parietal suture formed by a posterior wedge of frontals), according to observations on the material observed (see Material examined) and figures in Forasiepi *et al.* (2019), where the suture is not completely straight but with a small posterior wedge of frontals entering between parietals, though more reduced than in *Anachlysictis*.

Character 83: coded 2 (primary foramen ovale on alisphenoid), following Forasiepi *et al.* (2019).

Character 84: coded 1 (foramen ovale located on the ventral surface of the skull), following Forasiepi *et al.* (2019) and observations on the material examined.

Character 145: coded 1 (three or more mental foramina).

APPENDIX 1. — Continuation.

Character 146: coded inapplicable (–). The anterior-most mental foramen in *Thylacosmilus* does not correspond topographically to the same enlarged anterior foramen as in non-thylacosmilid sparassodonts because the symphyseal flange has additional foramina anterior to it. For this reason, we coded it as inapplicable, and homologies of these foramina should be tested in the future.

Character 151: changed from 1 to 2, following the changes in this character, including the addition of state 2.

Character 159: changed from 3 to "?", following Churcher (1985) and Goin & Pascual (1987). The presence of at least two upper incisors is an inference based on the position of the lower incisors preserved and the wear facets and space between upper canines. However, no evidence has ever been collected with a clearly complete incisor series. Evidence of "at least two", not exactly two, does not allow scoring the taxon with state 3 (i.e., two or fewer incisors) because the possibility of a third incisor has not been discarded.

Character 177: coded 3 (prominent median sulci present on labial and lingual faces of the lower canine only), according to the modification in states.

Character 193: changed from "?" to 0 (p2 smaller than p3).

Character 194: changed from "?" to "–". With an incomplete premolar series, this character (change in the height of lower premolars) cannot be evaluated for *Thylacosmilus*.

Character 89 changed from 0 to 1 following Forasiepi *et al.* 2019.

Character 224: changed from "?" to 1 (carnassial notch in postmetacrista present) following Goin *et al.* (2007) and observations on examined material.

Character 238: coded 1 (talonid of m4 reduced and narrower than m3).

Characters 248, 262, 263, 268, and 269 were changed to "?" due to uncertainties and changes in the interpretation of homologies of the talonid cusps. Goin & Pascual (1987) describe the talonid of *Thylacosmilus* as composed of one main cusp. This cusp is well differentiable in the m1-3 and vestigial in the m4. Goin & Pascual (1987) identify the vestigial cusp in the m4 as an extremely reduced talonid, apparently without cusps. However, they do not mention a homology hypothesis for the main structure in the m1-3, which is evidently a cusp. Forasiepi (2009) codifies the absence of a hypoconid, presence of a hypoconulid and a vestigial entoconid. These scorings suggest that the main cusp in the talonid would be the hypoconulid.

In our revision, it was observed that the main cusp has, in fact, a posterior position and has a crest running to the base of the trigonid, which probably corresponds to the *cristid obliqua*. Additionally, there is an extremely reduced, almost vestigial cusp in lingual position. Due to this topographical location, this last cusp could be the entoconid, as codified by Forasiepi (2009). This condition is different in *A. gracilis* and *P. goini*, with the entoconid being the dominant cusp of the talonid, almost completely fused to the hypoconulid (the tips are still visible). On the other hand, the main cusp in *Thylacosmilus* could be either a hypoconulid (as coded by Forasiepi 2009), a hypoconid displaced posteriorly, or the fusion of these two. Goin *et al.* (2007) analyzed the homologies of the talonid in some borhyaenoids, grouped at that moment in two subfamilies within the family Borhyaenidae: "Borhyaeninae" and "Prothylacyninae" (currently invalid classification). These sparassodonts have a strong reduction in the talonid as part of a typical morphology related to carnivory, which, in more specialized groups, preserves basically one posterior cusp.

After observing and analyzing plesiomorphic and derived morphologies, Goin *et al.* (2007) concluded that the main cusp in "prothylacynids" is homologous to the hypoconid, while in the "borhyaenids" it would be the entoconid, or the entoconid fused to the metaconid. We do not pretend to establish a relationship of Thylacosmilus with any of these groups but to show the variability spectrum of these structures within other carnivore morphologies. Assuming that the vestigial cusp in the lingual margin of the talonid of *Thylacosmilus* is a reduced entoconid and, considering that the *cristid obliqua* connects with the main cusp, the more probable hypothesis is that this main cusp is the hypoconid displaced posteriorly and that the hypoconulid disappeared or fused with one of these two cusps. In fact, a fusion of the hypoconulid with the hypoconid would explain that posterior position, as it occurs with the block entoconid + hypoconulid in the other thylacosmilids, which is displaced to a more posterior position (posterolingual).

Character 264: changed from 0 to 1, because there is a vestigial entoconid, but it is still observable and clearly identifiable as an entoconid, as explained before (see explanation of the change in the scoring of characters 248, 262, 263, 268, and 269).

Eomakhaira molossus

Character 33: coded 2 (posterior end of palate straight posteriorly), following descriptions of Engelman *et al.* (2020) and figures, the posterior border is clearly straight.

Character 171: coded 1 (large canines). The upper canines are large, robust and not sabre-like.

Character 176: changed from 0 to "?". The preservation does not allow to affirm that the exposed surfaces (labial) of the canines are smooth or with small grooves and ridges. The lingual surfaces are not exposed because the jaw is occluded. They are only visible in the CT scans shown by Engelman *et al.* (2020). However, the images do not allow to identity clearly if the lingual surface is smooth or not, although it is possible to identify the prominent sulci. Observing the photographs of the labial face of the canine and the CT images (Engelman *et al.* 2020: fig. 10), there are distinct rugosities visible close to the alveolar border in both, lingual and labial faces, and on the lingual face at the level of the tooth row. However, due to the preservation condition, we cannot define whether these rugosities correspond to the "longitudinal small grooves and ridges" present in sparassodonts or are caused by external factors.

Appendix 1. — Continuation.

Character 177: changed to 2 (prominent median sulci present only on lingual faces of the canines) following descriptions and figures in Engelman *et al.* (2020), as this structure is absent in labial faces, except for a shallow sulcus observable only in the CT scans, but it is not prominent.

Character 194: changed from 1 to 0 (lower premolars increase gradually in height), because there is not an abrupt change in size, it is gradual.

Character 199: coded 1 (marked posterior increase in size of molars).

LIST OF CHARACTERS

This matrix is a modification of the matrix from Engelman *et al.* (2020), which is based on the matrices of Forasiepi (2009), with posterior modifications (Engelman & Croft 2014; Forasiepi *et al.* 2015; Suarez *et al.* 2016), and Muizon *et al.* (2018), which is partially based on the first. Ordered characters are indicated with an asterisk (*).

1. Length of the skull
   0 Short (less than twice width at level of zygomatic arch);
   1 Long (greater than twice width at level of zygomatic arch).

2. Length of rostrum
   0 Less than 1/3 total length of skull;
   1 Between 1/3 and 1/2 total length of skull;
   2 More than 1/2 total length of skull.

3. Expanded apex of rostrum
   0 Absent;
   1 Present.

4. Width of braincase versus maximum postorbital width
   0 Braincase wider than maximum postorbital width;
   1 Braincase narrower than maximum postorbital width.

5. Dimensions of braincase
   0 As wide as long, or slightly wider than long;
   1 Much longer than wide.

6. Level of the palate relative to the basicranium
   0 Palate lower than basicranium;
   1 Palate and basicranium at the same level.

7. Paracanine fossa
   0 Formed by premaxilla and maxilla;
   1 Formed by premaxilla only.

8. Dimensions of paracanina fossa
   0 Longer than high;
   1 Higher than long.

9. Precanine notch
   0 Absent;
   1 Present.

10. Lateral palatal process of premaxilla
   0 Anterior to or just reaches anterior border of canine alveolus;
   1 Posterior to anterior border of canine alveolus.

11. Posterior border of incisive foramen
   0 Anterior to or just reaches anterior border of canine alveolus;
   1 Posterior to anterior border of canine alveolus.

12. Position of medial palatal process of premaxilla
   0 Horizontal;
   1 With posterior end more dorsal, forming an incisive fossa.

13. Tubercle or internarial process on anterodorsomedial surface of premaxilla
   0 Absent;
   1 Present.

14. Posteriormost point of premaxilla-nasal contact
   0 Anterior or at the level of the canine;
   1 Posterior to the canine;
   2 Posterior to p2.

15. Anterior extent of nasals
   0 Protrude anteriorly, obscuring the nasal opening in dorsal view;
   1 Retracted posteriorly, exposing the narial opening in dorsal view.

16. Shape of naso-frontal suture
   0 Open W-shape or posteriorly convex;
   1 Acute W or V-shaped.

17. Median process of frontals wedged between nasals
   0 Absent;
   1 Present.

APPENDIX 1. — Continuation.

18. Postorbital processes
0 Absent or indistinct;
1 Well-developed.

19. Fronto-maxillary or naso-lacrimal contact
0 Naso-lacrimal contact;
1 Fronto-maxillary contact.

20. Angle of maxillo-jugal contact
0 More than 140 degrees;
1 Between 95 and 140 degrees.

21. Postorbital process of jugal
0 Absent;
1 Present.

22. Location of the infraorbital foramen
0 Anterior or dorsal to the anterior root of P3;
1 Dorsal to the midpoint or posterior root of P3;
2 Dorsal to M1;
3 Posterior to M1.

23. Flaring of maxillary "cheeks" behind infraorbital foramen
0 Present;
1 Absent.

24. Fossa for levator labii muscle
0 Mainly on jugal;
1 Mainly on maxilla.

25. Large foramen at anteroventral end of maxilla medial to canines
0 Absent;
1 Present.

26. Palatal length/width ratio
0 Lesser than or equal to 1.5;
1 Greater than 1.5.

27. Shape of the palate
0 Rectangular (molar rows near parallel);
1 Triangular (wider posteriorly).

28. Number of palatal pits
0 Absent;
1 One (between M3-M4);
2 Two (between M2-M3 and M3-M4);
3 Three (one between each pair of molars).

29. Maxillopalatine fenestrae
0 Absent;
1 Present.

30. Major palatine foramen
0 One pair opening in maxilla, palatine, or maxillo-palatine suture;
1 Many small foramina on the surface of the maxilla.

31. Minor palatine foramen
0 Complete;
1 Incomplete or absent.

32. Posterior extent of palatines
0 Extend to the level of the last molar;
1 Extend beyond the level of the last molar.

33. Shape of posterior end of palate
0 Concave posteriorly (single-arched);
1 Concave posteriorly (double-arched);
2 Straight posteriorly.

34. Postpalatine torus
0 Present and well-developed;
1 Absent or only a slight thickening around choanae.

35. Palatine contributes to infraorbital canal
0 Present;
1 Absent.

36. Postpalatine torus foramen
0 Small (less than half size of minor palatine foramen);
1 Large (more than half size of minor palatine foramen).

37. Morphology of postpalatine torus foramen
0 Closed;
1 Open;
2 Absent.

38. Posterolateral corners of the palate inflected ventrally forming prominent lateral corners
0 Absent;
1 Present.

39. Position of sphenorbital foramen relative to lacrimal
0 Posterior to the level of the posterior border of lacrimal;
1 Anterior or at the level of the posterior border of lacrimal.

40. Position of sphenorbital foramen relative to molars
0 Anterior or dorsal to M3;
1 Posterior to or dorsal to M4.

Appendix 1. — Continuation.

41. Development of pterygoids
- 0 Well-developed and expanded on medial side, with midline contact;
- 1 Well developed and expanded on medial side, but no midline contact;
- 2 Reduced, not expanded on medial side.

42. Posterior process of pterygoids covering alisphenoid-basisphenoid suture
- 0 Absent;
- 1 Present.

43. Anterior extent of lacrimal (width of facial process relative to lacrimal dorsoventral height
- 0 Restricted to orbit (less than half height);
- 1 Extending onto rostrum (more than half height).

44. Shape of facial process of lacrimal
- 0 Rounded;
- 1 Triangular with anterodorsal projection.

45. Posterior extent of lacrimal
- 0 Anterior to the level of the postorbital process /bar;
- 1 Extends posteriorly, reaching the level of the postorbital process /bar.

Comments: this character is applicable to those taxa with postorbital processes present, even if these processes are extremely reduced. Taxa with absent post-orbital processes are coded as inapplicable. This character is evaluated in dorsal view.

46. Lacrimal tubercle
- 0 Present;
- 1 Absent.

47. Position of lacrimal foramina
- 0 Within orbit;
- 1 Exposed on face.

48. Number of lacrimal foramina
- 0 Two;
- 1 One.

49. Glenoid process of jugal
- 0 With articular facet;
- 1 Without articular facet.

50. Orbital crest
- 0 Absent;
- 1 Present.

51. Interparietal
- 0 Present;
- 1 Absent (or fused with parietal).

52. Shape of fronto-parietal suture
- 0 Formed by posterior wedge of frontals;
- 1 Straight;
- 2 Formed by anterior wedge of parietals.

53. Parietal-alisphenoid or fronto-squamosal contact
- 0 Parietal-alisphenoid;
- 1 Fronto-squamosal.

54. Width of glenoid cavity
- 0 Less than twice anteroposterior length;
- 1 More than twice anteroposterior length.

55. Distinct preglenoid process of squamosal
- 0 Absent;
- 1 Present.

56. Morphology of postglenoid process
- 0 Wider than high (half as tall as wide or less);
- 1 Wide and low;
- 2 Height subequal to or greater than width.

57. Proportions of postglenoid process
- 0 As wide as glenoid cavity;
- 1 Narrower than glenoid cavity.

58. Postglenoid foramen
- 0 Absent;
- 1 Present.

59. Location of postglenoid foramen
- 0 Posterior to postglenoid process;
- 1 Medial to postglenoid process.

60. Anteroposterior position of postglenoid foramen relative to postglenoid process
- 0 Close and in contact or nearly so;
- 1 Well-separated.

61. Suprameatal foramen (Muizon *et al.* (2018), character 178)
- 0 Above suprameatal crest;
- 1 Below suprameatal crest.

62. Squamosal at external acoustic meatus
- 0 Not thickened at meatus;
- 1 Thickened at meatus with mediolateral width shorter than anteroposterior width;
- 2 Thickened at meatus with mediolateral width longer than anteroposterior width.

63. Paracondylar process of occipital
- 0 Low tubercle or absent;
- 1 Long process with diameter at apex smaller than proximodistal length.

APPENDIX 1. — Continuation.

64. Paracondylar process of exoccipital and post-tympanic process of squamosal
0 Paracondylar process larger;
1 Both processes similar in length.

65. Orientation of the post-tympanic and/or paracondylar processes
0 Ventrally projecting;
1 Anteroventrally projecting.

66. Alisphenoid glenoid process
0 Absent;
1 Present.

67. Optic foramen and sphenorbital fissure
0 Separate;
1 Joined.

68. Transverse foramen
0 Absent;
1 Present.

69. Tympanic process of alisphenoid
0 Absent;
1 Present.

70. Hypotympanic sinus
0 Absent;
1 Present.

71. Petrosal contribution to hypotympanic sinus
0 Absent;
1 Present.

72. Squamosal contribution to hypotympanic sinus
0 Absent;
1 Present.

73. Medial process of the squamosal
0 Absent;
1 Present.

74. Concave process of alisphenoid contributing to antero-dorsal portion of hypotympanic sinus
0 Present;
1 Absent.

75. Squamosal epitympanic sinus excavated in the roof of the external auditory meatus
0 Absent;
1 Present.

76. Intratympanic sinus excavated in the exoccipital
0 Absent;
1 Present.

77. Intratympanic sinus in the pars mastoidea
0 Absent;
1 Present.

78. Dorsal epitympanic expansion of hypotympanic sinus above glenoid fossa
0 Absent;
1 Present.

79. Anterior expansion of middle ear sinus within the lateral wall of the braincase
0 Absent;
1 Present.

80. Pneumatization of squamosal
0 Absent;
1 Present.

81. Tensor tympani fossa
0 Smooth and shallow area;
1 Distinct circular pit or elongated fossa;
2 Long and narrow groove bordering anterior edge of promontorium.

82. Eustachian foramen
0 No impression;
1 Notch on the alisphenoid;
2 Foramen on petrosal.

83. Composition of primary foramen ovale
0 On petrosal;
1 Between petrosal and alisphenoid;
2 On alisphenoid.

84. Location of foramen ovale
0 On lateral wall of braincase;
1 On ventral surface of skull.

85. Secondary foramen ovale completely enclosed in alisphenoid
0 Absent;
1 Present.

86. Foramen for the greater petrosal nerve
0 Distinct notch or foramen;
1 Without distinct notch or foramen.

87. Position of carotid foramen
0 Anterior to the basisphenoid-basoccipital suture;
1 At the level of the basisphenoid-basoccipital suture.

Appendix 1. — Continuation.

88. Hypoglossal foramina
0 Two or more;
1 One.

89. Groove between hypoglossal foramina and foramen for inferior petrosal sinus
0 Shallow or absent;
1 Well-defined with prominent lateral border.

90. Size of jugular foramen relative to fenestra vestibuli
0 Subequal;
1 Larger.

91. Jugular fossa
0 Absent;
1 Present.

92. Jugular foramen and foramen for inferior petrosal sinus
0 Separate;
1 Confluent.

93. Median keel in basioccipital
0 Absent;
1 Present.

94. Median rod or crest of basisphenoid/presphenoid (sphenoid crest)
0 Absent;
1 Present.

95. Dorsal margin of the foramen magnum
0 Formed only by exoccipitals;
1 Formed by both exoccipitals and supraoccipital.

96. Ascending canal
0 Present;
1 Absent.

97. Contribution of squamosal to occiput
0 Absent or small;
1 Large.

98. Mastoid foramen or other emissary foramina in the occiput
0 Present;
1 Absent.

99. Connection between condylar articular facets in ventral view
0 Absent;
1 Present.

100. Inclination of the major axis of the condyle in posterior view
0 Inclined (less than 55 degrees);
1 Vertical to subvertical (between 90 and 55 degrees).

101. Supraoccipital in posterior view
0 Concave;
1 Convex or flat.

102. Sagittal crest
0 Prominently developed (extending to frontals);
1 Weakly developed (not extending to frontals);
2 Absent.

103. Position of nuchal crest
0 At or posterior to the level of the condyles;
1 Anterior to the condyles.

104. Morphology of the stapes
0 Columelliform (not perforated by stapedial foramen);
1 Bicrurate (perforated by stapedial foramen).

105. Ectotympanic shape
0 Ring-shaped;
1 Expanded.

106. Ectotympanic attachment to skull
0 Ligamentous;
1 Tight articulation with marked ridges and grooves;
2 Fused to rostral tympanic process.

107. Position of petrosal
0 At the level of the ventral margin of the braincase;
1 Dorsal to the ventral level of the braincase.

108. Orientation of the pars cochlearis of the petrosal (plane defined by the apex of the promontorium-fenestra vestibuli-fenestra cochleae)
0 Subhorizontal or slightly oblique;
1 Subvertical.

109. Orientation of the major axis of the petrosal (as defined by subarcuate fossa-internal acoustic meatus)
0 Subhorizontal to slightly oblique;
1 Oblique to subvertical;
2 Vertical.

110. Mastoid portion of the petrosal
0 Contributes to the occipital shield;
1 Excluded from the occipital shield.

111. Petrosal-squamosal fusion
0 Absent;
1 Present.

112. Cavum epiptericum
0 Floored by petrosal;
1 Floored by petrosal and alisphenoid;
2 Floored primarily or exclusively by alisphenoid.

APPENDIX 1. — Continuation.

113. Internal acoustic meatus
0 Deep with thick prefacial commissure;
1 Shallow with thin prefacial commissure.

114. Subarcuate fossa
0 Deep;
1 Shallow.

115. Medial expansion of the crista petrosa that forms a thin and straight lamina covering the anterolateral part of the subarcuate fossa
0 Absent;
1 Present.

116. Deep sulcus for carotid artery on anterior end of promontorium
0 Absent;
1 Present.

117. Epitympanic wing of petrosal
0 Present;
1 Absent.

118. Prootic canal
0 Present;
1 Absent.

119. Prootic canal morphology
0 Large with endocranial opening;
1 Reduced with intramural opening.

120. Rostral tympanic process of petrosal
0 Absent;
1 Low crest;
2 Raised process.

121. Anterior extent of rostral tympanic process of petrosal
0 Restricted to posterior half;
1 Extends anteriorly and contacts alisphenoid.

122. Caudal tympanic process completely floors postpromontorial sinus
0 Absent;
1 Present.

123. Petrosal plate
0 Absent;
1 Present.

124. Paroccipital process of petrosal
0 Distinct process;
1 Indistinct or absent.

125. Position of hiatus fallopii
0 On dorsal (cerebellar) face of petrosal;
1 Intermediate;
2 On ventral (tympanic) face of petrosal.

126. Stylomastoid foramen
0 Absent;
1 Present.

127. Floor of cavum supracochleare
0 Absent;
1 Present.

128. Stapedial ratio
0 Rounded, less than 1.8;
1 Elliptical, more than 1.8.

129. Contribution of squamosal to epitympanic recess
0 Squamosal contribution much smaller than petrosal;
1 Squmosal contribution roughly as large as petrosa;
2 Squamosal contribution much larger than petrosa.

130. Fossa incudis
0 Continuous with epitympanic recess;
1 Separated from the epitympanic recess.

131. Tympanic petrosal crest
0 Present;
1 Absent.

132. Tuberculum tympani
0 Weakly developed;
1 Large.

133. Stapedial fossa
0 Twice the size of fenestra vestibuli;
1 Small and shallow.

134. Foramina for temporal ramus with well-developed internal branch of stapedial artery
0 Present;
1 Absent.

135. Location of foramina for temporal rami
0 On petrosal;
1 On parietal or squamosal.

136. Foramina for veinous drainage of the temporal cavity on parietal or squama of squamosal
0 Present;
1 Absent.

Appendix 1. — Continuation.

137. Post-temporal canal or notch
0 Present;
1 Absent.

138. Post-temporal sulcus on squamosal surface of petrosal
0 Present;
1 Absent.

139. Shape of dentary (depth below m3/m4 embrasure/total length of dentary)
0 Shallow (less than 0.15);
1 Intermediate (between 0.15 and 0.2);
2 Deep (greater than 0.2).

140. Shape of dentary in occlusal view
0 Stright or slightly curved;
1 Sigmoid (laterally concave at the canine-premolar series and laterally convex at the molar series).
Comments: this character should be evaluated on the dentary; the curvature of the upper teeth row is not applicable. As observed in the specimens examined, apparently these two features are independent: some taxa with a marked sigmoid curvature in the upper teeth row show a straight or slightly curved dentary (e.g., *Arctodictis sinclairi*), while other taxa show a marked sigmoid curvature in both (e.g., *Thylacosmilus atrox*). In this character we are evaluating specifically the curvature of the dentary.

141. Ventral margin of dentary posterior to last molar in lateral view
0 Straight;
1 Curved.

142. Shape of the anterior portion of dentary
0 Tapering forward, with ventral border continuous or bending upwards in an angle < 40?;
1 Increasing in height forward, with ventral border bending upwards in an angle > or = 40?;
2 Increasing in height forward, with ventral border bending upwards in an angle > or = 40? and forming an antero-labial crest.
Comments: the angle evaluated corresponds to the symphyseal angle. It was measured with respect to the horizontal line, which generally coincides with the alveolar line. When the alveolar line was vertically curve (as seen lateral and medial views), the horizontal line was taken as a straight line connecting the anterior end of the anterior alveolus of the p1, with the posterior end of the posterior alveolus of the m4.

143. Mandibular symphysis
0 Dentaries articulated at symphysis (unfused);
1 Dentaries strongly ankylosed or fused at symphysis.

144. Symphyseal flange
0 Absent;
1 Poorly developed (slightly projected below the level of the ventral margin of the horizontal ramus);
2 Well developed (height of dentary below m2/height at the level of the flange < 0.65).

145. Number of mental foramina
0 One to two;
1 Three or more.

146. Enlarged anterior mental foramen
0 Absent;
1 Present.

147. Anterior-most mental foramen location
0 Approximately at the same level as the other mental foramina;
1 Clearly ventral to the level of the other mental foramina;
Comments: the foramen is clearly ventral when it does not overlap or partially overlap vertically with the other foramina.

148. Posteriormost mental foramen
0 Below p3;
1 At p3/m1 embrasure;
2 Below m1;
3 Posterior to m1.

149. Retromolar space
0 Absent;
1 Present.

150. Labial mandibular foramen inside masseteric fossa
0 Absent;
1 Present.

151. Masseteric fossa area
0 Restricted dorsally by crest reaching condyle;
1 Extends ventrally to lower margin of dentary;
2 Masseteric fossa and coronoid process extremely reduced.

152. Posterior shelf of masseteric fossa
0 Absent;
1 Present.

153. Medially inflected angular process
0 Absent;
1 Present.

154. Shape of the angular process
0 Shelf-like (ASL/AL > 0.81);
1 Intermediate (0.72 < ASL/AL < 0.81);
2 Rod-like (ASL/AL < 0.72).

APPENDIX 1. — Continuation.

155. Angle between anterior border of coronoid process and tooth row
0 Between 95 and 105 degrees;
1 Between 106 and 125 degrees;
2 Greater than 126 degrees.

156. Position of the mandibular foramen
0 Posterior to the mid-point of the coronoid process;
1 At the mid-point of the coronoid process;
2 Anterior to the mid-point of the coronoid process.

157. Morphology of mandibular condyle
0 Subspherical;
1 Cylindrical.

158. Position of mandibular condyle relative to tooth row
0 Approximately at the same level or slightly below;
1 Above.

159. Number of upper incisors
0 Five;
1 Four;
2 Three;
3 Two or fewer.

160. Height of first upper incisor (serially homologous I1)
0 Taller than other incisors;
1 Subequal to or smaller than remaining incisors.

161. Roots of I1 in anterior view
0 Parallel;
1 Diverging dorsally.

162. Diastema between I1-2
0 Present;
1 Absent.

163. Size of I3 versus I2
0 I3 smaller;
1 I3 subequal to I2;
2 I3 larger.

164. Size of I4 versus I3
0 I4 subequal to I3;
1 I4 larger.

165. Size of I5 versus I4
0 I5 subequal to I4;
1 I5 smaller than I4.

166. Shape of upper incisors (I2-5)
0 Peg-shaped;
1 Spatulate.

167. Shape of upper incisor arcade
0 Parabolic;
1 Slightly anteriorly convex;
2 Transverse.

168. Number of lower incisors
0 Four;
1 Three;
2 Two or less.

169. Staggered lower incisor (serially homologous i3)
0 Absent;
1 Present.

170. Procumbent lower incisors
0 Procumbent;
1 Not procumbent.

171. Size of canines
0 Small (same height or lower than protoconids);
1 Large (higher than protoconids);
2 Large, with upper canines hyper-developed and saber-like.

172. Asymmetry in mesio-distal length of the canines (taken at the alveolar level)
0 Upper canine less than 50% longer than lower canine;
1 Upper canine between 50 to 70% longer than lower canine;
2 Upper canine more than 70% longer than lower canine;
Comments: length taken at the level of the alveolus.

173. Lateral compression of lower canine
0 Without compression or slightly compressed (length/width < 1.60);
1 Very compressed (length/width > or = 1.60);
Comments: this character was coded as inapplicable for taxa with more than a single canine.

174. Number of roots on upper canine
0 Two;
1 One.

175. Pulp cavity of canines
0 Closed in adults;
1 Open in upper canines only;
2 Open in upper and lower canines.

176. Surface of the roots of the canines
0 Smooth;
1 With small grooves and ridges.

Appendix 1. — Continuation.

177. Prominent median sulci on labial and lingual faces of canines
0 Absent;
1 Present;
2 Present only on lingual faces;
3 Present only in lower canine (both faces);
4 Present only on lingual face of lower canine.

178. Shape of the labial face of the upper canine
0 Continuous;
1 Divided into two flat surfaces (antero-labial and postero-labial);
Comments: taxa with labial sulcus are coded as continuous. The character only evaluates the presence of two facets on the labial surface of the upper canine.

179. Lower canine implantation
0 Oblique, inclined forward;
1 Sub-vertical (root inclination > 60 degrees respect to the horizontal plane);
2 Vertical;
Comments: this character refers to the implantation of the intra-alveolar portion of the canine into the alveolus, different from the verticalization of the extra-alveolar portion. Some taxa (e.g., *Acyon myctoderos*) show a verticalization in the extra-alveolar portion but with an oblique (inclined forward) implantation. Those species are coded as "0".

180. Number of premolars
0 Four or more;
1 Three;
2 Two or less.

181. Orientation of P/p1 relative to tooth row
0 Parallel to tooth row (less than 19 degrees);
1 Obliquely oriented to tooth row (20 degrees or more);
2 Transversely oriented to tooth row.

182. Orientation of P/p2 relative to tooth row
0 Parallel to tooth row;
1 Oblique.

183. Diastema between C-P1
0 Absent (alveolar margins in contact);
1 Small (less than one tooth root in length);
2 Long (greater than one tooth root in length).

184. Diastema between P1-2
0 Absent (alveolar margins in contact);
1 Small (less than one tooth root in length);
2 Long (greater than one tooth root in length).

185. Diastema between c-p1
0 Absent (alveolar margins in contact);
1 Small (less than one tooth root in length);
2 Long (greater than one tooth root in length).

186. Diastema between p1-2
0 Absent (alveolar margins in contact);
1 Small (less than one tooth root in length);
2 Long (greater than one tooth root in length).

187. Shape of premolars
0 Uninflated;
1 Inflated, with apical wear strongly developed.

188. Shape and position of main cusp of P1
0 Asymmetrical and aligned with anterior root;
1 Posterior to anterior root.

189. Shape and position of main cusp of p1
0 Anteroposteriorly aligned with or anterior to anterior root;
1 Posterior to anterior root.

190. Cusp on the posterior heel of P3
0 Absent or vestigial;
1 Well-developed.

191. Posterolingual cingulum on P3
0 Absent;
1 Small cingulum;
2 With a small posterolingual cusp.

192. Posterolabial cingulum on P3
0 Present;
1 Absent.

193. Size of p2
0 Smaller than p3;
1 Larger than p3.

194. Change in height of lower premolars
0 Increase gradually in height;
1 Abrupt change in size between p1 and p2-3;
2 Abrupt change in size between p1-2 and p3.

195. Roots of lower premolars
0 Flat (as wide as crown);
1 Bulbous on only one premolar;
2 Bulbous on all premolars and some molars.

196. Precingulid or cingulid cusp on p2
0 Absent;
1 Present.

APPENDIX 1. — Continuation.

197. Symmetry of main cusp on p3
0 Anterior edge of cusp more convex than posterior edge;
1 Both edges similar in curvature.

198. Replacement of dP3
0 dP3 is replaced;
1 dP3 is not replaced.

199. Timing of eruption between dP/p3 and M/m3-4
0 p3 erupts before m3;
1 p3 and m3 erupt almost simultaneously;
2 p3 erupts almost simultaneously with or after m4.

200. Timing of eruption between M3-4 and m4
0 M3 and m4 erupt simultaneously;
1 M/m4 erupt simultaneously.

201. Morphology of dp3
0 With trigonid and talonid;
1 With a main cusp and smaller accessory cusps.

202. Size of molars increasing posteriorly
0 Moderate posterior increase in size;
1 Marked posterior increase in size.

203. Shape of upper molar row
0 Straight or nearly straight;
1 Bowed.

204. Width of M4 relative to M3
0 Narrower than M3;
1 Subequal to wider than M3.

205. Size of metacone relative to paracone (based on M2 when possible)
0 Paracone slightly larger or subqeual to metacone;
1 Paracone slightly smaller (*c.* 10%) than metacone;
2 Paracone distinctly smaller (*c.* 30%) than metacone;
3 Paracone much smaller (*c.* 50%) than metacone.

206. Position of the metacone relative to paracone (based on M2 when possible)
0 Approximately at the same level;
1 Lingual.

207. Shape of paracone and metacone
0 Conical;
1 Subtriangular with a flat labial face.

208. Bases of paracone and metacone
0 Separate;
1 Partially adjoined;
2 Almost completely connate (only tips separate).

209. Centrocrista
0 Straight;
1 V-shaped.

210. Metacone on M4
0 Distinct cusp;
1 Present but adjoined to paracone or poorly distinct from crista;
2 Absent.

211. Number of roots on M4
0 Three;
1 Two or less.

212. Size of protocone
0 Vestigial or absent;
1 Small (narrower than bases of paracone and metacone);
2 Somewhat expanded anteroposteriorly (as wide as bases of paracone and metacone);
3 Greatly expanded anteroposteriorly (wider than bases of paracone and metacone).

213. Eccentric/procumbent protocone
0 Absent;
1 Present.

214. Trigon basin
0 Present;
1 Absent.

215. Height of protocone
0 Less than 60% of para/metacone height;
1 Between 60 to 80% para/metacone height;
2 Greater than or equal to 80% of para/metacone height.

216. Paraconule and metaconule
0 Present;
1 Absent.

217. Wing-like cristae associated with para- and metaconules
0 Absent;
1 Present.

218. Relative position of para- and metaconule (based on M2 when possible)
0 At or lingual to the midpoint between protocone and para/metacone;
1 Closer to the paracone or metacone.

219. Extent of postprotocrista
0 Ends lingual to apex of metacone;
1 Extends labially beyond apex of metacone.

APPENDIX 1. — Continuation.

220. Orientation of the preparacrista (based on M2 when possible)
0 Nearly perpendicular to long axis of tooth;
1 Oriented anterobucally to long axis of tooth;
2 Absent.

221. Lengths of preparacrista on M3 and M4
0 M4 preparacrista shorter;
1 M4 preparacrista subequal or longer than M3 preparacrista.

222. Postmetacrista (based on M3 if possible)
0 Strongly developed (longer than preparacrista);
1 Weakly developed (shorter than preparacrista).

223. Orientation of postmetacrista (based on M3 if possible)
0 Nearly perpendicular to tooth row;
1 Oblique to tooth row.

224. Carnassial notch in postmetacrista
0 Absent;
1 Present.

225. Anterolabial cingulum (based on M3 if possible)
0 Long (continuous between stylar margin and talon);
1 Short (not continuous between stylar margin and talon);
2 Vestigial to Absent.

226. Postcingulum
0 Absent or weakly developed;
1 Present.

227. Width of parastylar lobe relative to metastylar lobe (on M3)
0 Metastylar lobe narrower;
1 Parastylar and metastylar lobes uniform in width;
2 Parastylar lobe slightly narrower;
3 Parastylar lobe significantly narrower (stylar shelf small or absent on M2-3).

228. Width of stylar shelf (widest lobe on M3)
0 More than 50% total width;
1 Less than 50% total width;
2 Vestigial or absent.

229. Deep ectoflexus (>10% tooth width) on upper molars
0 On M2 and M3;
1 On M3 only;
2 Strongly reduced or absent.

230. Stylar cusp A
0 Absent;
1 Smaller than StB;
2 Large, subequal to StB.

231. Stylar cusp B
0 Large;
1 Small or forming an ectocingulum;
2 Vestigial or absent.

232. Stylar cusp C
0 Absent;
1 Present.

233. Stylar cusp D
0 Absent;
1 Present, smaller than stylar cusp B;
2 Present, larger than stylar cusp B.

234. Stylar cusp E
0 Present and distinct;
1 Indistinct or absent.

235. Size of m4
0 m4 subequal or smaller than m3;
1 m4 larger than m3.

236. Posterior lobe of the crown lower than anterior lobe
0 Absent;
1 Present only on m1-2 and slightly developed;
2 Present on m1-3 and strongly developed.

237. Roots of lower molars (based on m3 when possible)
0 Anterior root much larger than posterior root;
1 Both roots similar in size.

238. Talonid of m4 relative to m3
0 Talonid of m4 reduced and narrower than m3;
1 Talonid of m4 similar to m3.

239. Alignment of the main cusps of m1
0 Reverse triangle acute;
1 Single longitudinal row.

240. Trigonid configuration posterior to m1
0 Open, with paraconid anterolingual;
1 Acute, with paraconid more posteriorly placed;
2 Anteroposteriorly compressed.

241. Relative positions of paraconid and metaconid (considered based on the apices of both cusps)
0 Paraconid and metaconid aligned labiolingually;
1 Metaconid located more lingual.

242. Orientation of postprotocristid/metacristid
0 Transverse to lower jaw;
1 Parallel or oblique to lower jaw.

Appendix 1. — Continuation.

243. Relative lengths of paracristid and metacristid
0 Paracristid longer;
1 Paracristid and metacristid subequal;
2 Metacristid longer.

244. Morphology of talonid
0 Small basinless heel;
1 Multicuspidate and basined.

245. Trigonid versus talonid length (m1-m3)
0 Trigonid shorter than talonid;
1 Trigonid subequal to talonid;
2 Trigonid longer than talonid.

246. Dimensions of trigonid
0 Longer than wide;
1 Subequal;
2 Wider than long.

247. Width of talonid relative to trigonid (m1-3)
0 Narrower than trigonid;
1 Subequal to trigonid;
2 Wider than trigonid.

248. Hypoconid versus protoconid height (based on m2-3)
0 hypoconid/protoconid height radio less than 20%;
1 hypoconid/protoconid height radio between 25-35%;
2 hypoconid/protoconid height radio between 40-60%.

249. Metaconid on m1
0 Present;
1 Vestigial or absent;
Comments: *Anachlysictis* was coded as 1, because although there is a small cuspule probably corresponding to the metaconid, it would be vestigial.

250. Metaconid on m2-4
0 Present on m2-4;
1 Absent on m4;
2 Absent on m2-4.

251. Paraconid height relative to metaconid (m2-4)
0 Taller;
1 Subequal;
2 Lowe.

252. Volume of metaconid relative to paraconid
0 Larger;
1 Subequal;
2 Smaller.

253. Height of protoconid
0 Tallest cusp of the trigonid;
1 Subequal to metconid or paraconid.

254. Location of protoconid relative to midline of tooth (on m2-4)
0 Slightly labial to midline of tooth;
1 Protoconid at midline of tooth.

255. Labial extension of protoconid
0 Protoconid subequal or narrower at mid-height than base;
1 Protoconid wider at mid-height than base.

256. Protoconid height/length of m3 or m4
0 less than 0.9;
1 0.9 or greater.

257. Anterior keel at anterolingual angle of paraconid with hypoconulid notch
0 Rounded;
1 Forming a keel.

258. Paraconid elongated with anteroventral projection of the paraconid keel
0 Absent;
1 Present.

259. Anterolabial cingulid
0 Well-developed, extending from the protoconid to paraconid basins;
1 Reduced, extended only on the base of the paraconid;
2 Absent.

260. Paraconid of m1
0 Distinct;
1 Low and confluent with cingulum.

261. Length versus width of talonid basin (based on m2 when possible)
0 Longer than wide;
1 Subequal;
2 Wider than long.

262. Presence of hypoconid (on m2-4)
0 Present;
1 Absent.

263. Location of hypoconid (on m2-4)
0 Appoximately at the middle of the buccal margin of the talonid;
1 At the posterobuccal corner of the tooth.

264. Presence of the entoconid
0 Present;
1 Vestigial or absent.

APPENDIX 1. — Continuation.

265. Shape of the entoconid
0 Conical;
1 Labio-lingually compressed.

266. Height of entoconid
0 Smaller than the hypoconid;
1 Subequal to larger than the hypoconid.

267. Location of entoconid
0 At the posterolingual corner of the tooth;
1 Between the metaconid and posterior tooth margin.

268. Position of hypoconulid
0 In posteromedial position;
1 Lingually placed and twinned with entoconid.

269. Hypoconulid of m4
0 Taller than other talonid cusps;
1 Subequal to other talonid cusps;
2 Absent.

270. Pre-entocristid
0 Present;
1 Absent.

271. Direction of the pre-entocristid
0 To the base of the trigonid;
1 Lingual to the trigonid.

272. Cristid obliqua
0 Lingual to the carnassial notch;
1 To the carnassial notch;
2 Labial to the carnassial notch.

273. Posthypocristid
0 Oblique to long axis of tooth;
1 Transverse to long axis of tooth.

274. Lower molar hypoflexid
0 Deep (40-50% of talonid width);
1 Shallow or absent.

275. Carnassial notch in cristid obliqua
0 Absent;
1 Present.

276. Labial postcingulid on m1-3
0 Absent;
1 Present.

277. Labial postcingulid on m4
0 Absent;
1 Present.

278. Atlas intervertebral foramen
0 Absent;
1 Present.

279. Atlas transverse foramen
0 Absent;
1 Present.

280. Ventral foramen on transverse process of axis
0 Absent;
1 Present.

281. Posterior extent of transverse processes of atlas
0 Anterior or just reaches caudal facets for axis;
1 Extend caudally just beyond level of caudal facets for axis;
2 Extend caudally far beyond caudal facets for axis and processes much longer than wide.

282. Anterior extent of transverse processes of atlas
0 Does not reach level of atlantal foramen or groove;
1 Extends anterior beyond atlantal foramen or groove.

283. Shape of cranial facets
0 Only concave;
1 Dorsal edge curved.

284. Atlas and intercentrum
0 Unfused;
1 Fused.

285. Axis transverse foramen
0 Absent, represented by a notch;
1 Present, enclosed.

286. Axis posterior spinous process extension
0 Extends beyond the level of the postzygapophyses;
1 Extends to the level of the postzygapophyses.

287. Ventral sagittal crest of axis
0 Roughly straight;
1 Distinctly concave because of the development of a prominent ventral process posteriorly.

288. C3-C4 ventral sagittal process
0 Absent;
1 Present.

289. C5 transverse process heads overlap transversally
0 present;
1 absent.

APPENDIX 1. — Continuation.

290. C5 and T1 body length
0 C5 subequal or longer than T1;
1 C5 shorter than T1.

291. C6 spinous process
0 Protuberance;
1 Lamina.

292. C7 transverse foramen
0 Absent;
1 Represented by a notch;
2 Complete foramen.

293. Shape of anterior face of C7 centrum
0 Circular to ovoid;
1 Rectangular to trapezoidal.

294. Position of tallest spinous process of thoracic vertebrae
0 On T1;
1 On T2;
2 On T3.

295. Anticlinal vertebra
0 On lumbar;
1 On thoracic;
2 No anticlinal vertebra.

296. Foramen on dorsal arch of last lumbar vertebra
0 Present;
1 Absent.

297. Metapophyses in third lumbar vertebra anterior to last
0 Absent or weak;
1 Present.

298. Ventral median keel on lumbar vertebra
0 Absent;
1 Present.

299. Auricular process of sacrum
0 Developed on two sacral vertebrae;
1 Developed on one sacral vertebra.

300. Size of sacral spinous process
0 Shorter than last lumbar;
1 Taller than last lumbar.

301. Length of the tail
0 Shorter than twice the length of the precaudal vertebral column;
1 Greater than twice the length of the precaudal vertebral column.

302. Angle between scapular spine and dorsal border of scapula
0 Acute or almost straight (between 80 and 95 degrees);
1 Obtuse (between 100 and 110 degrees).

303. Coracoid process
0 Large (extends beyond medial border of glenoid cavity);
1 Small (just reaches medial border of glenoid cavity).

304. Ventral extension of acromion process
0 Extends ventrally below glenoid cavity;
1 Does not extend ventrally below glenoid cavity.

305. Anterior extension of acromion process
0 Posterior to anterior edge of glenoid cavity;
1 Anterior to or just lateral to anterior edge of glenoid cavity.

306. Width of infraspinous fossa
0 Less than 1/4 its length;
1 More than 1/4 its length.

307. Width of the acromion process at the level of the neck
0 Wider than infraspinous fossa;
1 Subequal;
2 Narrower than infraspinous fossa.

308. Infraspinous/supraspinous fossa width at the level of the neck
0 Supraspinous fossa subequal or wider;
1 Supraspinous fossa narrower.

309. Scapular notch
0 More than 130 degrees;
1 Between 90 and 130 degrees.

310. Clavicle
0 Present;
1 Absent.

311. Medial process for teres major
0 Absent;
1 Present.

312. Tricipital line of humerus
0 Absent;
1 Ridge or crest;
2 Massive crest continuous with deltopectoral crest.

313. Capitulum for radius on humerus
0 Spherical;
1 Cylindrical.

APPENDIX 1. — Continuation.

314. Entepicondylar foramen
0 Present;
1 Absent.

315. Olecranon fossa or foramen
0 Large fossa;
1 Foramen.

316. Laminar supinator crest/ectepicondylar crest
0 Large;
1 Intermediate;
2 Absent.

317. Greater tuberosity height relative to humeral head height
0 Greater tuberosity subequal or lower in height to humeral head;
1 Greater tuberosity is higher.

318. Development of greater tuberosity in proximal view
0 Small (less than half the anteroposterior length of head);
1 Large (greater than or equal to half the anteroposterior length of head).

319. Extension of the deltoid crest
0 Restricted to proximal half of humerus;
1 Reaches distal half of humerus.

320. End of deltoid crest
0 Merging with diaphysis;
1 Forming a distinct angle or process.

321. Relative heights of trochlea and capitulum in anterior view
0 Longer proximal extension of capitulum;
1 Subequal;
2 Longer proximal extension of trochlea.

322. Humerus medial epicondyle size
0 Large;
1 Small.

323. Humerus distal end size
0 Large;
1 Small.

324. Lateral extension of capitulum
0 Rounded;
1 Straight.

325. Depth of intercondylar notch in posterior view
0 Wide and relatively shallow concave;
1 Narrower and concave posteriorly.

326. Curvature of the posterior border of the humeral shaft
0 Curved;
1 Straight.

327. Medial development of the ulnar anconeal process
0 Does not protrude beyond medial border of olecranon process;
1 Medially protruding.

328. Medial curvature of the ulna
0 Present;
1 Absent.

329. Posterior border of the ulna
0 Convex;
1 Straight or concave.

330. Shape of articular facet for humerus
0 Anteroposteriorly compressed;
1 Circular.

331. Distal shaft of radius
0 Oval (wider than long);
1 Rounded (almost as wide as long).

332. Prepollex
0 Absent;
1 Present.

333. Distolateral process of scaphoid
0 Absent;
1 Present, does not separate lunate from magnum;
2 Present, separates lunate from magnum.

334. Number of plantar tubercles (distal heads) on trapezium
0 Two;
1 One.

335. Angle between transverse axis of proximal and distal epiphyses of metacarpal I
0 Absent;
1 Present.

336. Orientation of ilium relative to ischium
0 Prominent dorsally;
1 Aligned with ischium.

337. Tuberosity for rectus femoris muscle
0 Absent;
1 Protuberance;
2 Depression.

Appendix 1. — Continuation.

338. Length of iliac neck
0 Longer than 15% total pelvis length;
1 Between 6 and 15% total pelvis length;
2 Less than 6% total pelvis length.

339. Greater sciatic notch
0 Greater than 120 degrees;
1 Between 90 and 115 degrees.

340. Iliac and gluteous fossa
0 No fossa;
1 Two fossa subequal in size;
2 Gluteous fossa larger.

341. Epipubic bones
0 Present;
1 Absent.

342. Proximal size of epipubic bones
0 Short;
1 Long.

343. Torsion between proximal and distal epiphyses of femur
0 Present;
1 Absent.

344. Relative heights of greater trochanter and femoral head
0 Greater trochanter lower or equal in height to femoral head;
1 Greater trochanter higher than femoral head.

345. Lesser trochanter of femur
0 Present;
1 Vestigial or absent.

346. Femoral condyles
0 Lateral condyle wider than medial condyle;
1 Subequal;
2 Medial condyle wider than lateral condyle.

347. Ossified patella
0 Absent;
1 Present.

348. Parafibula
0 Present;
1 Absent.

349. Femoro-fibular articulation
0 Present;
1 Absent.

350. Tibia length relative to femur length
0 Tibia subequal to or longer than femur;
1 Tibia shorter than femur.

351. Proximal dimensions of tibia
0 Larger mediolaterally than anteroposteriorly;
1 Subequal;
2 Larger anteroposteriorly than mediolaterally.

352. Tibia shape
0 Sigmoid;
1 Straight.

353. Torsion between proximal and distal epiphyses of tibia
0 Present;
1 Absent.

354. Type of distal articulation of tibia
0 Spiral;
1 Sagittal.

355. Posterior shelf of tibia
0 Present but does not extend posteriorly beyond the medial astragalotibial facet;
1 Present and extends posteriorly beyond the medial astragalotibial facet.

356. Orientation of the lateral edge of the astragalus-tibia articular facet
0 Parallel to epiphyseal suture of tibia;
1 Oblique to epiphyseal suture of tibia.

357. Anteroposterior length of medial malleolus relative to distal epiphysis
0 Subequal;
1 Medial malleolus much shorter.

358. Distal malleolus of tibia
0 Indistinct or absent;
1 Distinct.

359. Angle between medial and lateral astragalotibial facets
0 90 degrees;
1 Intermediate;
2 180 degrees.

360. Astragalonavicular facet extends onto ventromedial side of head
0 Absent;
1 Present.

361. Width and height of navicular facet in distal view
0 Transversely wider;
1 Dorsoventrally wider.

Appendix 1. — Continuation.

362. Visibility of medial plantar tuberosity in dorsal view
0 Not visible;
1 Visible.

363. Angle between lateral tibial and fibular facets
0 No angle;
1 With angle.

364. Medial extent of sustentacular facet
0 Does not reach the medial edge of neck;
1 Reaches the medial edge of neck.

365. Astragalar canal
0 Present;
1 Absent.

366. Width of astragalar neck
0 Neck wider than head;
1 Neck narrower or as wide as head.

367. Major orientation of posterior astragalocalcaneal facet
0 Anteromedial-posterolateral;
1 Posteromedial-anterolateral.

368. Malleolar shelf of astragalus
0 Absent;
1 Present.

369. Astragalo-distal tuber
0 Absent;
1 Present.

370. Astragalo-cuboid facet on astragalar head
0 Absent;
1 Present.

371. Connection between astragalonavicular facet and sustentacular facet
0 Present;
1 Absent.

372. Longest dimension of sustentacular facet
0 Anteromedial-posterolateral;
1 Sagittally longer;
2 Transversely longer.

373. Orientation of the calcaneoastragalar facet
0 Medial;
1 Intermediate;
2 Dorsal.

374. Calcaneal peroneal tubercle
0 Protuberance;
1 Crest-like;
2 Poorly developed or absent.

375. Position of peroneal tubercle
0 Anterior, non-protruding;
1 At a distance from the anterior end of the calcaneus.

376. Calcaneal peroneal groove for the peroneous longus
0 Indistinct or weakly developed;
1 Distinct, deep separation.

377. Position of sustentaculum
0 Reaches anterior end of calcaneus;
1 Subterminal.

378. Outline of sustentacular process
0 Triangular or rounded;
1 Rectangular.

379. Mesiolateral orientation of sustentacular facet
0 Medial;
1 Dorsal.

380. Anteroposterior orientation of sustentacular facet
0 Dorsal;
1 45 degrees dorsoanteriorly.

381. Sustentacular facet morphology
0 Slightly concave or flat;
1 Posteriorly convex.

382. Secondary distal calcaneoastragalar facet
0 Absent;
1 Present.

383. Sustentacular and posterior calcaneoastragalar facets
0 Separate;
1 Merged.

384. Calcaneal facet for fibula
0 Present;
1 Absent.

385. Orientation of calcaneal facet for fibula
0 Dorsal;
1 Lateral.

386. Length of the tuber calci
0 Longer than the body;
1 Shorter than the body.

APPENDIX 1. — Continuation.

387. Medial curvature of the tuber calci
0 Present;
1 Absent.

388. Ventral curvature of the tuber calci
0 Present;
1 Absent.

389. Proximal calcaneocuboid facet
0 Absent;
1 Present.

390. Angle between proximal and distal areas of calcaneocuboid facet
0 No angle;
1 Oblique calcaneocuboid facet.

391. Spatial relationship between navicular and entocuneiform
0 Entocuneiform anterior to navicular;
1 Entocuneiform extends proximally medial to the distal area of the navicular.

392. Angle between navicular and distal metatarsal facets of ectocuneiform
0 Oblique;
1 Parallel to the distal facet.

393. Prehallux
0 Absent;
1 Present.

394. Mt I length relative to Mt III
0 Greater than or equal to than 50% the length of Mt III;
1 Less than 50% the length of Mt III or Mt I absent.

395. Metatarsal V proximal process
0 Does not extend ventral to cuboid;
1 Extends ventral to cuboid.

396. Proximal ends of metatarsal II and III
0 Subequal in length;
1 Mt II extends more proximally than Mt III.

397. Ridge on proximal articular facet of metatarsal I
0 Absent;
1 Present.

398. Mt III thickness relative to that of Mt IV
0 Mt III thicker or subequal to Mt IV;
1 Mt III thinner.

399. Mt III thickness relative to that of Mt I
0 Mt I thicker than Mt III;
1 Mt III thicker than Mt I.

400. Median keel on palmar/plantar surface of metapodials
0 Sharp;
1 Blunt.

401. Foot ungual phalanx of digit IV in proximal view
0 Larger dorsoventrally than mediolaterally;
1 Larger mediolaterally than dorsoventrally.

402. Groove on dorsal surface of tip of ungual phalanges
0 Absent;
1 Present.

403. Dorsal border of ungual phalanges
0 Forming a crest-like border;
1 Rounded;

Appendix 1. — Continuation.

LIST OF SYNAPOMORPHIES

Node numbers refer to nodes in consensus.

PROKENNALESTES
All trees:
No autapomorphies.

Asioryctes nemegtensis
All trees:
Char. 24: 0 → 1
Char. 31: 0 → 1
Char. 93: 1 → 0
Char. 118: 0 → 1
Char. 125: 1 → 2
Char. 130: 0 → 1
Char. 137: 0 → 1
Char. 227: 1 → 0

Maelestes gobiensis
All trees:
Char. 2: 0 → 1
Char. 20: 0 → 1
Char. 40: 1 → 0
Char. 47: 1 → 0
Char. 168: 0 → 1
Char. 224: 1 → 0
Char. 225: 0 → 1
Char. 226: 0 → 1
Char. 233: 1 → 0
Char. 234: 0 → 1
Char. 247: 0 → 1
Char. 253: 0 → 1
Char. 261: 0 → 1
Char. 271: 0 → 1
Char. 272: 0 → 1
Char. 277: 1 → 0

Holoclemensia texana
All trees:
Char. 229: 1 → 2
Char. 231: 0 → 2
Char. 232: 0 → 1
Char. 253: 0 → 1

Deltatheroides cretacicus
All trees:
Char. 233: 1 → 2

Deltatheridium pretrituberculare
All trees:
Char. 22: 1 → 0
Char. 211: 0 → 1
Char. 233: 1 → 0

Kokopellia juddi
All trees:
Char. 181: 0 → 1
Char. 233: 1 → 0
Char. 234: 0 → 1
Char. 251: 2 → 1
Char. 266: 0 → 1

Eodelphis browni
All trees:
Char. 136: 1 → 0
Char. 156: 1 → 2
Char. 233: 1 → 0
Char. 234: 0 → 1
Char. 362: 0 → 1
Some trees:
Char. 272: 2 → 01

Didelphodon vorax
All trees:
Char. 22: 1 → 2
Char. 54: 0 → 1
Char. 139: 0 → 1
Char. 170: 0 → 1
Char. 182: 0 → 1
Char. 192: 0 → 1

PEDIOMYIDAE
All trees:
Char. 155: 1 → 0
Char. 183: 1 → 2
Char. 184: 1 → 2
Char. 191: 1 → 2
Char. 194: 0 → 2
Char. 206: 0 → 1
Char. 212: 2 → 3
Char. 222: 1 → 0
Char. 227: 1 → 3
Char. 233: 1 → 2
Char. 273: 0 → 1
Char. 274: 0 → 1

Alphadon spp.
All trees:
Char. 273: 0 → 1
Some trees:
Char. 229: 1 → 0

Asiatherium reshetovi
All trees:
Char. 120: 1 → 2
Char. 156: 1 → 2
Char. 186: 1 → 0
Char. 210: 0 → 1
Char. 223: 0 → 1
Char. 235: 0 → 1
Char. 251: 2 → 1
Char. 265: 1 → 0
Char. 266: 0 → 1

Some trees:
Char. 121: 0 → 1

Herpetotherium fugax
All trees:
Char. 1: 0 → 1
Char. 44: 0 → 1
Char. 47: 1 → 0
Char. 48: 0 → 1
Char. 51: 0 → 1
Char. 55: 0 → 1
Char. 59: 0 → 1
Char. 155: 1 → 2
Char. 169: 1 → 0
Char. 183: 0 → 1
Char. 184: 1 → 2
Char. 185: 0 → 1
Char. 186: 01 → 2
Char. 215: 2 → 1
Char. 313: 0 → 1
Char. 326: 0 → 1
Char. 327: 0 → 1
Char. 394: 0 → 1

Mimoperadectes spp.
All trees:
Char. 1: 0 → 1
Char. 22: 1 → 0
Char. 28: 0 → 1
Char. 46: 0 → 1
Char. 52: 0 → 2
Char. 120: 1 → 2
Char. 125: 1 → 2
Char. 136: 1 → 0
Char. 245: 1 → 2

Some trees:
Char. 121: 0 → 1
Char. 188: 1 → 0
Char. 261: 1 → 2

Didelphis albiventris
All trees:
Char. 4: 0 → 1
Char. 22: 1 → 0
Char. 102: 1 → 0
Char. 185: 1 → 2
Char. 186: 1 → 2
Char. 281: 0 → 1
Char. 300: 0 → 1
Char. 307: 0 → 1
Char. 313: 0 → 1
Char. 330: 1 → 0
Char. 359: 1 → 2

Metachirus nudicaudatus
All trees:
Char. 18: 1 → 0
Char. 53: 0 → 1
Char. 90: 1 → 0
Char. 93: 0 → 1
Char. 94: 1 → 0
Char. 164: 0 → 1
Char. 297: 0 → 1
Char. 303: 1 → 0
Char. 304: 0 → 1
Char. 309: 0 → 1
Char. 327: 0 → 1
Char. 336: 1 → 0
Char. 344: 0 → 1
Char. 354: 0 → 1
Char. 362: 0 → 1
Char. 363: 0 → 1

Monodelphis spp.
All trees:
Char. 10: 0 → 1
Char. 40: 1 → 0
Char. 100: 1 → 0
Char. 128: 0 → 1
Char. 184: 1 → 0
Char. 195: 0 → 1
Char. 212: 2 → 1
Char. 215: 2 → 1
Char. 266: 1 → 0
Char. 390: 1 → 0

Dromiciops gliroides
All trees:
Char. 11: 1 → 0
Char. 26: 1 → 0
Char. 28: 1 → 2
Char. 83: 1 → 2

Appendix 1. — Continuation.

Char. 90: 1 → 0
Char. 92: 0 → 1
Char. 93: 0 → 1
Char. 103: 0 → 1
Char. 106: 0 → 2
Char. 128: 0 → 1
Char. 155: 1 → 2
Char. 169: 1 → 0
Char. 183: 0 → 1
Char. 205: 2 → 1
Char. 209: 1 → 0
Char. 211: 0 → 1
Char. 212: 2 → 3
Char. 220: 0 → 1
Char. 221: 1 → 0
Char. 222: 0 → 1
Char. 227: 2 → 1
Char. 228: 1 → 2
Char. 230: 1 → 2
Char. 233: 1 → 0
Char. 241: 0 → 1
Char. 245: 1 → 0
Char. 259: 0 → 1
Char. 300: 0 → 1
Char. 301: 0 → 1
Char. 302: 0 → 1
Char. 326: 0 → 1
Char. 336: 1 → 0
Char. 371: 0 → 1
Char. 373: 01 → 2
Char. 375: 0 → 1
Char. 380: 1 → 0
Char. 398: 0 → 1

Dasyurus spp.
All trees:
Char. 11: 1 → 0
Char. 26: 1 → 0
Char. 53: 1 → 0
Char. 155: 1 → 0
Char. 180: 1 → 2
Char. 216: 1 → 0
Char. 256: 0 → 1
Char. 279: 0 → 1
Char. 300: 0 → 1
Char. 302: 0 → 1
Char. 312: 2 → 0
Char. 313: 0 → 1
Char. 314: 0 → 1
Char. 320: 0 → 1
Char. 365: 1 → 0
Char. 385: 0 → 1

Sminthopsis crassicaudata
All trees:
Char. 8: 0 → 1
Char. 48: 0 → 1
Char. 130: 0 → 1
Char. 162: 1 → 0
Char. 184: 1 → 0
Char. 196: 0 → 1
Char. 236: 0 → 1
Char. 246: 1 → 2
Char. 269: 1 → 0
Char. 294: 0 → 2
Char. 307: 0 → 2
Char. 315: 0 → 1
Char. 328: 0 → 1
Char. 330: 1 → 0
Char. 344: 0 → 1
Char. 346: 01 → 2
Char. 353: 1 → 0
Char. 356: 1 → 0
Char. 357: 1 → 0
Char. 376: 0 → 1
Char. 390: 1 → 0

Thylacinus cynocephalus
All trees:
Char. 1: 0 → 1
Char. 2: 0 → 2
Char. 3: 0 → 1
Char. 4: 0 → 1
Char. 7: 0 → 1
Char. 10: 0 → 1
Char. 17: 0 → 1
Char. 20: 1 → 0
Char. 22: 2 → 3
Char. 34: 0 → 1
Char. 37: 1 → 2
Char. 41: 2 → 1
Char. 42: 0 → 1
Char. 49: 0 → 1
Char. 56: 2 → 1
Char. 57: 1 → 0
Char. 59: 0 → 1
Char. 66: 1 → 0
Char. 71: 0 → 1
Char. 81: 0 → 1
Char. 82: 2 → 0
Char. 83: 1 → 2
Char. 95: 1 → 0
Char. 102: 1 → 0
Char. 108: 0 → 1
Char. 113: 1 → 0
Char. 122: 1 → 0
Char. 123: 1 → 0
Char. 125: 1 → 2
Char. 126: 1 → 0
Char. 128: 0 → 1
Char. 154: 2 → 1
Char. 155: 1 → 2
Char. 158: 1 → 0
Char. 163: 1 → 2
Char. 164: 0 → 1
Char. 183: 0 → 1
Char. 184: 1 → 2
Char. 186: 1 → 2
Char. 202: 0 → 1
Char. 206: 1 → 0
Char. 208: 0 → 1
Char. 212: 2 → 1
Char. 215: 2 → 0
Char. 220: 0 → 1
Char. 228: 1 → 2
Char. 229: 0 → 1
Char. 239: 0 → 1
Char. 246: 1 → 0
Char. 248: 2 → 1
Char. 249: 0 → 1
Char. 250: 0 → 2
Char. 251: 2 → 0
Char. 254: 0 → 1
Char. 258: 0 → 1
Char. 259: 0 → 1
Char. 263: 1 → 0
Char. 264: 0 → 1
Char. 266: 1 → 0
Char. 269: 1 → 2
Char. 270: 0 → 1
Char. 284: 1 → 0
Char. 288: 0 → 1
Char. 297: 0 → 1
Char. 316: 1 → 2
Char. 318: 0 → 1
Char. 331: 0 → 1
Char. 336: 1 → 0
Char. 339: 0 → 1
Char. 341: 0 → 1
Char. 349: 0 → 1
Char. 351: 01 → 2
Char. 352: 0 → 1
Char. 359: 2 → 1
Char. 371: 0 → 1
Char. 372: 0 → 2
Char. 373: 1 → 2
Char. 379: 1 → 0
Char. 401: 0 → 1

Pucadelphys andinus
All trees:
Char. 47: 1 → 0
Char. 50: 1 → 0
Char. 52: 0 → 1
Char. 57: 0 → 1
Char. 212: 2 → 3
Char. 230: 1 → 2
Char. 266: 0 → 1

Some trees:
Char. 241: 0 → 1

Andinodelphys cochabambensis
All trees:
Char. 1: 0 → 1
Char. 13: 0 → 1
Char. 17: 1 → 0
Char. 43: 1 → 0
Char. 162: 1 → 0
Char. 275: 0 → 1
Char. 297: 1 → 0
Char. 301: 0 → 1
Char. 385: 0 → 1

Mayulestes ferox
All trees:
Char. 54: 0 → 1
Char. 132: 1 → 0
Char. 136: 1 → 0
Char. 184: 1 → 0
Char. 210: 0 → 1
Char. 229: 1 → 0
Char. 269: 1 → 0

Allqokirus australis
All trees:
Char. 22: 1 → 0
Char. 43: 1 → 0
Char. 46: 0 → 1
Char. 56: 1 → 2
Char. 173: 0 → 1
Char. 177: 0 → 1
Char. 271: 0 → 1
Char. 272: 2 → 1

Patene simpsoni
All trees:
Char. 148: 2 → 0
Char. 191: 1 → 0
Char. 266: 0 → 1
Char. 272: 2 → 1

Appendix 1. — Continuation.

Hondadelphys fieldsi
All trees:
Char. 184: 1 → 2
Char. 194: 1 → 0
Char. 207: 0 → 1
Char. 236: 0 → 1
Char. 238: 0 → 1
Char. 245: 2 → 1
Char. 248: 1 → 2
Char. 266: 0 → 1
Char. 267: 1 → 0
Char. 271: 0 → 1

Stylocynus paranensis
All trees:
Char. 23: 0 → 1
Char. 197: 0 → 1
Char. 231: 1 → 2

UF 27881
All trees:
Char. 18: 1 → 0
Char. 28: 2 → 3
Char. 102: 0 → 12
Char. 202: 1 → 0
Char. 213: 1 → 0
Sallacyon hoffstetteri
All trees:
Char. 28: 1 → 0
Char. 35: 0 → 1
Char. 80: 0 → 1
Char. 229: 1 → 0
Char. 235: 1 → 0

Some trees:
Char. 230: 1 → 0

Notogale mitis
All trees:
Char. 88: 1 → 0
Char. 216: 0 → 1
Char. 276: 0 → 1

Sipalocyon spp.
All trees:
Char. 138: 1 → 0
Char. 148: 3 → 2
Char. 227: 3 → 2

Some trees:
Char. 1: 1 → 0
Char. 4: 1 → 0
Char. 98: 0 → 1
Char. 156: 1 → 0
Char. 158: 0 → 1
Char. 221: 1 → 0
Char. 284: 1 → 0
Char. 308: 1 → 0
Char. 375: 0 → 1
Char. 388: 0 → 1

Acyon myctoderos
Some trees:
Char. 9: 0 → 1
Char. 59: 1 → 0
Char. 68: 1 → 0
Char. 154: 0 → 1
Char. 167: 1 → 2
Char. 293: 0 → 1

Cladosictis patagonica
All trees:
Char. 211: 0 → 1

Some trees:
Char. 12: 0 → 1
Char. 52: 0 → 2
Char. 86: 0 → 1
Char. 94: 0 → 1
Char. 167: 1 → 2
Char. 365: 0 → 1
Char. 376: 1 → 0
Char. 386: 1 → 0

Lycopsis longirostrus
All trees:
Char. 275: 0 → 1

Lycopsis padillai
All trees:
No autapomorphies

Lycopsis torresi
Some trees:
Char. 23: 1 → 0

Lycopsis viverensis
All trees:
Char. 205: 3 → 2

Prothylacynus patagonicus
All trees:
Char. 21: 1 → 0
Char. 68: 0 → 1
Char. 88: 0 → 1
Char. 177: 2 → 0
Char. 191: 1 → 0
Char. 210: 2 → 1
Char. 220: 1 → 2
Char. 231: 1 → 0
Char. 276: 1 → 0
Char. 293: 0 → 1
Char. 298: 1 → 0
Char. 318: 1 → 0
Char. 321: 1 → 0
Char. 322: 1 → 0
Char. 324: 1 → 0
Char. 326: 0 → 1
Char. 392: 0 → 1

Pharsophorus lacerans
All trees:
Char. 43: 1 → 0
Char. 125: 1 → 2
Char. 190: 0 → 1
Char. 250: 2 → 0
Char. 277: 0 → 1

Borhyaena tuberata
All trees:
Char. 14: 1 → 0
Char. 32: 1 → 0
Char. 118: 1 → 0
Char. 141: 0 → 1
Char. 177: 2 → 0
Char. 196: 1 → 0
Char. 325: 0 → 1
Char. 384: 0 → 1

Arctodictis munizi
All trees:
Char. 14: 1 → 0
Char. 177: 2 → 1
Char. 312: 1 → 0

Arctodictis sinclairi
All trees:
Char. 31: 0 → 1
Char. 93: 1 → 0
Char. 204: 0 → 1

Australohyaena antiquua
All trees:
Char. 43: 1 → 0
Char. 55: 0 → 1
Char. 98: 1 → 0
Char. 155: 1 → 2
Char. 194: 0 → 2
Char. 210: 2 → 1
Char. 211: 1 → 0
Char. 237: 0 → 1
Char. 250: 1 → 0
Char. 277: 0 → 1

Callistoe vincei
All trees:
Char. 16: 0 → 1
Char. 18: 0 → 1
Char. 61: 0 → 1
Char. 88: 0 → 1
Char. 97: 1 → 0
Char. 141: 0 → 1
Char. 167: 1 → 0
Char. 229: 1 → 0
Char. 237: 0 → 1

Paraborhyaena boliviana
All trees:
No autapomorphies

Patagosmilus goini
All trees:
Char. 39: 0 → 1
Char. 43: 1 → 0
Char. 52: 0 → 1
Char. 54: 0 → 1

Thylacosmilus atrox
All trees:
Char. 56: 1 → 0
Char. 89: 0 → 1
Char. 103: 0 → 1
Char. 134: 1 → 0
Char. 151: 1 → 2
Char. 154: 0 → 1
Char. 176: 1 → 0
Char. 177: 2 → 3
Char. 179: 1 → 2
Char. 187: 0 → 1
Char. 195: 0 → 12
Char. 207: 0 → 1
Char. 212: 1 → 0
Char. 228: 1 → 2
Char. 231: 1 → 2
Char. 244: 1 → 0
Char. 259: 1 → 2
Char. 264: 0 → 1
Char. 270: 0 → 1

Proborhyaena gigantea
All trees:
No autapomorphies

Eomakhaira molossus
All trees:
Char. 32: 1 → 0
Char. 33: 1 → 2
Char. 34: 1 → 0
Char. 143: 1 → 0

Appendix 1. — Continuation.

Char. 204: 0 → 1
Char. 211: 1 → 0

IGM 251108
All trees:
Char. 148: 3 → 0
Char. 177: 2 → 4
Char. 259: 1 → 0

Anachlysictis gracilis
All trees:
Char. 1: 0 → 1
Char. 33: 1 → 0

Node 53
All trees:
Char. 128: 0 → 1
Char. 220: 0 → 1
Char. 223: 0 → 1
Char. 230: 1 → 2
Char. 240: 1 → 2

Node 54
All trees:
No synapomorphies

Node 55
All trees:
Char. 212: 2 → 1
Char. 219: 1 → 0
Char. 227: 1 → 0
Char. 228: 1 → 0
Char. 248: 2 → 0
Char. 276: 1 → 0

Node 56
All trees:
Char. 96: 0 → 1
Char. 134: 0 → 1
Char. 148: 0 → 2
Char. 151: 0 → 1
Char. 153: 0 → 1
Char. 180: 0 → 1

Some trees:
Char. 113: 1 → 0

Node 57
All trees:
Char. 202: 0 → 1
Char. 204: 1 → 0
Char. 221: 1 → 0
Char. 222: 1 → 0
Char. 223: 0 → 1
Char. 229: 1 → 0
Char. 240: 1 → 0
Char. 241: 1 → 0
Char. 243: 2 → 0
Char. 251: 2 → 0
Char. 252: 0 → 2

Node 58
All trees:
Char. 215: 1 → 2
Char. 217: 0 → 1
Char. 247: 0 → 1
Char. 265: 0 → 1
Char. 272: 0 → 1

Node 59
All trees:
Char. 55: 0 → 1
Char. 111: 0 → 1
Char. 155: 1 → 0
Char. 167: 0 → 1
Char. 168: 0 → 1
Char. 181: 0 → 1
Char. 184: 1 → 0
Char. 187: 0 → 1
Char. 190: 0 → 1
Char. 191: 1 → 2
Char. 195: 0 → 1
Char. 224: 0 → 1
Char. 238: 0 → 1
Char. 240: 1 → 2
Char. 247: 1 → 2
Char. 251: 2 → 0
Char. 252: 1 → 2
Char. 253: 0 → 1

Some trees:
Char. 186: 1 → 0
Char. 229: 1 → 0
Char. 263: 1 → 0

Node 60
All trees:
Char. 171: 0 → 1
Char. 219: 1 → 0
Char. 274: 0 → 1

Some trees:
Char. 235: 0 → 1

Node 61
All trees:
Char. 252: 0 → 1
Char. 269: 0 → 1

Node 62
All trees:
Char. 224: 1 → 0
Char. 243: 2 → 1
Char. 245: 0 → 1
Char. 261: 0 → 1
Char. 268: 0 → 1

Some trees:
Char. 263: 0 → 1

Node 63
All trees:
Char. 183: 0 → 1
Char. 220: 0 → 1
Char. 226: 0 → 1
Char. 230: 1 → 2
Char. 231: 0 → 2

Node 64
All trees:
Char. 60: 0 → 1
Char. 93: 1 → 0
Char. 98: 0 → 1
Char. 124: 0 → 1
Char. 154: 0 → 1
Char. 171: 1 → 0
Char. 266: 0 → 1
Char. 273: 0 → 1
Char. 360: 0 → 1
Char. 376: 1 → 0
Char. 387: 0 → 1

Some trees:
Char. 11: 0 → 1

Node 65
All trees:
Char. 2: 0 → 1
Char. 137: 0 → 1
Char. 138: 0 → 1

Some trees:
Char. 66: 0 → 1
Char. 90: 0 → 1
Char. 131: 1 → 0
Char. 161: 0 → 1

Node 66
All trees:
Char. 1: 0 → 1
Char. 59: 0 → 1
Char. 60: 1 → 0
Char. 85: 0 → 1
Char. 95: 1 → 0
Char. 171: 0 → 1
Char. 184: 1 → 2
Char. 185: 0 → 1
Char. 247: 1 → 2
Char. 291: 0 → 1
Char. 324: 0 → 1
Char. 375: 0 → 1
Char. 398: 0 → 1

Node 67
All trees:
Char. 38: 0 → 1
Char. 81: 0 → 2
Char. 101: 1 → 0
Char. 138: 1 → 0
Char. 155: 1 → 0
Char. 162: 1 → 0
Char. 225: 0 → 1
Char. 267: 0 → 1
Char. 274: 1 → 0
Char. 319: 0 → 1
Char. 325: 0 → 1
Char. 331: 0 → 1
Char. 332: 0 → 1
Char. 348: 0 → 1
Char. 353: 1 → 0
Char. 389: 0 → 1
Char. 393: 0 → 1
Char. 397: 0 → 1

Node 68
All trees:
Char. 21: 0 → 1
Char. 46: 0 → 1
Char. 56: 1 → 2
Char. 57: 0 → 1
Char. 120: 1 → 2
Char. 166: 0 → 1
Char. 356: 0 → 1
Char. 379: 0 → 1
Char. 384: 0 → 1

Node 69
All trees:
Char. 2: 1 → 0
Char. 17: 1 → 0
Char. 20: 0 → 1
Char. 22: 1 → 2
Char. 28: 0 → 1
Char. 52: 0 → 1
Char. 53: 0 → 1
Char. 75: 0 → 1
Char. 82: 01 → 2
Char. 115: 0 → 1

Appendix 1. — Continuation.

Char. 121: 0 → 1
Char. 123: 0 → 1
Char. 126: 0 → 1
Char. 163: 2 → 1
Char. 204: 1 → 0
Char. 210: 0 → 1
Char. 231: 0 → 2
Char. 232: 1 → 0
Char. 294: 1 → 0
Char. 312: 1 → 2
Char. 316: 0 → 1
Char. 333: 1 → 2
Char. 334: 0 → 1
Char. 359: 1 → 2
Char. 374: 01 → 2
Char. 383: 0 → 1

Node 70
All trees:
Char. 39: 0 → 1
Char. 60: 1 → 0
Char. 87: 0 → 1
Char. 101: 1 → 0
Char. 167: 0 → 1
Char. 171: 0 → 1
Char. 199: 2 → 0
Char. 225: 0 → 1
Char. 242: 0 → 1
Char. 245: 1 → 2
Char. 273: 1 → 0
Char. 296: 1 → 0
Char. 309: 0 → 1
Char. 317: 0 → 1
Char. 324: 0 → 1
Char. 325: 0 → 1
Char. 327: 0 → 1
Char. 329: 0 → 1
Char. 384: 1 → 0

Node 71
All trees:
Char. 6: 0 → 1
Char. 12: 0 → 1
Char. 15: 0 → 1
Char. 27: 0 → 1
Char. 104: 1 → 0
Char. 105: 0 → 1
Char. 129: 1 → 0
Char. 159: 0 → 1
Char. 168: 0 → 1
Char. 205: 2 → 3
Char. 213: 1 → 0
Char. 233: 1 → 2
Char. 299: 0 → 1
Char. 323: 0 → 1
Char. 361: 0 → 1
Char. 362: 0 → 1
Char. 381: 0 → 1
Char. 382: 0 → 1
Char. 391: 1 → 0
Char. 394: 0 → 1
Char. 396: 0 → 1
Char. 399: 0 → 1
Char. 400: 1 → 0

Some trees:
Char. 14: 0 → 12
Node 72
All trees:
Char. 22: 1 → 0
Char. 56: 1 → 2
Char. 132: 1 → 0
Char. 136: 1 → 0
Char. 252: 1 → 0
Char. 253: 0 → 1
Char. 265: 1 → 0
Char. 269: 1 → 0
Char. 299: 0 → 1
Char. 348: 0 → 1
Char. 351: 0 → 1
Char. 362: 0 → 1
Char. 394: 0 → 1
Char. 401: 0 → 1
Char. 402: 0 → 1

Some trees:
Char. 205: 2 → 1
Char. 222: 0 → 1
Char. 246: 1 → 2
Char. 277: 0 → 1

Node 73
All trees:
Char. 23: 1 → 0
Char. 24: 0 → 1
Char. 29: 1 → 0
Char. 33: 2 → 1
Char. 72: 0 → 1
Char. 73: 0 → 1
Char. 81: 0 → 1
Char. 101: 1 → 0
Char. 116: 0 → 1
Char. 120: 1 → 0
Char. 247: 1 → 0
Char. 319: 0 → 1
Char. 324: 0 → 1
Char. 368: 0 → 1
Char. 369: 0 → 1
Char. 372: 0 → 1
Char. 391: 1 → 0
Char. 399: 0 → 1

Some trees:
Char. 86: 1 → 0
Node 74
All trees:
Char. 18: 1 → 0
Char. 33: 1 → 0
Char. 112: 2 → 1
Char. 181: 0 → 1
Char. 232: 1 → 0
Char. 275: 0 → 1

Some trees:
Char. 9: 0 → 1
Char. 241: 0 → 1

Node 75
All trees:
Char. 3: 0 → 1
Char. 8: 0 → 1
Char. 15: 0 → 1
Char. 19: 1 → 0
Char. 28: 0 → 1
Char. 36: 0 → 1
Char. 40: 1 → 0
Char. 44: 0 → 1
Char. 59: 0 → 1
Char. 100: 1 → 0
Char. 102: 1 → 0
Char. 170: 0 → 1
Char. 208: 0 → 1
Char. 212: 2 → 1
Char. 215: 2 → 1
Char. 245: 1 → 2
Char. 246: 12 → 0
Char. 251: 2 → 1
Char. 252: 1 → 2
Char. 255: 0 → 1
Char. 256: 0 → 1
Char. 258: 0 → 1
Char. 267: 0 → 1
Char. 287: 0 → 1
Char. 309: 0 → 1
Char. 338: 0 → 1
Char. 341: 0 → 1
Char. 357: 1 → 0

Some trees:
Char. 207: 1 → 0

Node 76
All trees:
Char. 220: 0 → 1
Char. 233: 1 → 0
Char. 234: 0 → 1
Char. 242: 0 → 1
Char. 248: 2 → 1

Node 77
All trees:
Char. 208: 1 → 0
Char. 212: 1 → 2
Char. 247: 0 → 2
Char. 256: 1 → 0
Char. 273: 0 → 1
Char. 276: 1 → 0
Node 78
All trees:
Char. 145: 0 → 1
Char. 148: 2 → 3
Char. 218: 0 → 1
Char. 227: 2 → 3
Char. 231: 0 → 1
Char. 239: 0 → 1
Char. 240: 1 → 0
Char. 251: 1 → 0
Char. 259: 0 → 1
Char. 260: 0 → 1

Node 79
All trees:
Char. 184: 1 → 0
Char. 214: 0 → 1
Char. 216: 0 → 1

Node 80
All trees:
Char. 28: 1 → 2
Char. 210: 1 → 2

Some trees:
Char. 118: 0 → 1
Node 81
All trees:
Char. 125: 0 → 1
Char. 202: 0 → 1
Char. 204: 1 → 0
Char. 210: 0 → 1
Char. 215: 1 → 0
Char. 232: 1 → 0
Char. 250: 0 → 2

Appendix 1. — Continuation.

Node 82
All trees:
Char. 69: 0 → 1
Char. 80: 0 → 1
Char. 82: 0 → 1
Char. 89: 0 → 1
Char. 117: 1 → 0
Char. 184: 1 → 2
Char. 185: 0 → 2
Char. 197: 0 → 1
Char. 380: 1 → 0

Some trees:
Char. 93: 1 → 0
Char. 125: 1 → 2

Node 83
All trees:
Char. 5: 0 → 1
Char. 88: 0 → 1
Char. 191: 1 → 0
Char. 194: 1 → 0
Char. 276: 1 → 0
Char. 320: 1 → 0
Char. 321: 1 → 2
Char. 370: 1 → 0
Char. 392: 0 → 1

Some trees:
Char. 1: 0 → 1
Char. 68: 0 → 1

Node 84
All trees:
Char. 22: 1 → 0
Char. 268: 1 → 0
Char. 269: 1 → 2

Node 85
All trees:
Char. 204: 0 → 1
Char. 210: 2 → 1
Char. 225: 1 → 2
Char. 261: 1 → 2

Some trees:
Char. 230: 1 → 0

Node 86
All trees:
Char. 18: 1 → 0
Char. 52: 0 → 2
Char. 125: 1 → 0
Char. 143: 0 → 1
Char. 197: 0 → 1
Char. 244: 1 → 0

Node 87
All trees:
Char. 12: 0 → 1
Char. 51: 0 → 1
Char. 54: 0 → 1
Char. 181: 0 → 1
Char. 264: 0 → 1
Char. 268: 1 → 0
Char. 269: 1 → 2

Some trees:
Char. 167: 01 → 2

Node 88
All trees:
Char. 17: 1 → 0
Char. 183: 1 → 0

Node 89
All trees:
Char. 44: 1 → 0
Char. 76: 0 → 1
Char. 131: 0 → 1
Char. 159: 1 → 2
Char. 191: 1 → 2
Char. 229: 1 → 2
Char. 250: 2 → 1
Char. 314: 0 → 1
Char. 400: 1 → 0
Char. 402: 0 → 1

Node 90
All trees:
Char. 56: 1 → 0
Char. 194: 1 → 0
Char. 195: 0 → 1
Char. 212: 1 → 0
Char. 228: 1 → 2
Char. 237: 1 → 0
Char. 278: 1 → 0
Char. 284: 1 → 0
Char. 308: 1 → 0
Char. 321: 1 → 2
Char. 329: 0 → 1
Char. 364: 0 → 1

Node 91
All trees:
Char. 22: 1 → 2
Char. 28: 2 → 1
Char. 142: 0 → 1
Char. 181: 1 → 2
Char. 182: 0 → 1

Node 92
All trees:
Char. 26: 1 → 0
Char. 179: 0 → 1
Char. 236: 1 → 2

Node 93
All trees:
Char. 177: 2 → 1
Char. 194: 0 → 2
Char. 195: 1 → 2

Node 94
All trees:
Char. 23: 0 → 1
Char. 188: 1 → 0
Char. 225: 1 → 2
Char. 258: 1 → 0

Node 95
All trees:
Char. 182: 0 → 1
Char. 259: 1 → 2

Node 96
All trees:
Char. 28: 2 → 3
Char. 32: 1 → 0
Char. 93: 1 → 0
Char. 214: 1 → 0
Char. 267: 1 → 0

Some trees:
Char. 230: 1 → 0

Node 97
All trees:
Char. 144: 1 → 2
Char. 171: 1 → 2
Char. 172: 1 → 2
Char. 180: 1 → 2

Node 98
All trees:
Char. 140: 0 → 1
Char. 142: 0 → 2
Char. 144: 0 → 1
Char. 147: 0 → 1
Char. 168: 1 → 2
Char. 172: 0 → 1
Char. 173: 0 → 1
Char. 179: 0 → 1
Char. 260: 1 → 0

Appendix 1. — Continuation.

AUTHORSHIPS OF CITED TAXA IN FIGURES

Acyon myctoderos Forasiepi, Sánchez-Villagra, Goin, Takai, Shigehara & Kay, 2006
Allqokirus australis Marshall & Muizon, 1988
Anachlysictis gracilis Goin, 1997
Andinodelphys cochabambensis Marshall & Muizon, 1988
Arctodictis munizi Mercerat, 1891
Arctodictis sinclairi Marshall, 1978
Asiatherium reshetovi Trofimov & Szalay, 1994
Asioryctes nemegtensis Kielan-Jaworowska, 1975
Australohyaena antiquua (Ameghino, 1894)
Borhyaena tuberata Ameghino, 1887
Callistoe vincei Babot, Powel & Muizon, 2002
Cladosictis patagonica Ameghino, 1887
Deltatheridium pretrituberculare Gregory & Simpson, 1926
Deltatheroides cretacicus Gregory & Simpson, 1926
Didelphis albiventris Lund, 1840
Didelphodon vorax (Marsh, 1889)
Dromiciops gliroides Thomas, 1894
Eodelphis browni Matthew, 1916
Eomakhaira molossus Engelman, Flynn, Wyss & Croft, 2020
Herpetotherium fugax (Cope, 1873)
Holoclemensia texana (Slaughter, 1968)
Hondadelphys fieldsi Marshall, 1976
Kokopellia juddi Cifelli, 1993
Lycopsis longirostrus Marshall, 1977
Lycopsis padillai Suarez, Forasiepi, Goin & Jaramillo, 2015
Lycopsis torresi Cabrera, 1927
Lycopsis viverensis Forasiepi, Goin & Di Martino, 2003
Maelestes gobiensis Wible, Rougier, Novacek & Asher, 2007
Mayulestes ferox Muizon, 1994
Metachirus nudicaudatus (É.Geoffroy Saint-Hilaire, 1803)
Notogale mitis (Ameghino, 1897)
Paraborhyaena boliviana Hoffstetter & Petter, 1983
Patagosmilus goini Forasiepi & Carlini, 2010
Patene simpsoni Paula Couto, 1952
Pharsophorus lacerans Ameghino, 1897
Proborhyaena gigantea Ameghino, 1897
Prothylacynus patagonicus Ameghino, 1891
Pucadelphys andinus Marshall & Muizon, 1988
Sallacyon hoffstetteri Villarroel & Marshall, 1982
Sminthopsis crassicaudata (Gould, 1844)
Stylocynus paranensis Mercerat, 1917
Thylacinus cynocephalus (Harris, 1808)
Thylacosmilus atrox Riggs, 1933

Appendix 2. — Phylogenetic matrix modified from Engelman *et al.* 2020 to test phylogenetic affinities of *Anachlysictis gracilis* Goin, 1997: https://doi.org/10.5852/geodiversitas2023v45a18_s2 (MorphoBank Project 4893: http://morphobank.org/permalink/?P4893).

Appendix 3. — 3D scan of the skull of *Anachlysictis gracilis* Goin, 1997, specimen VPPLT-1612: https://doi.org/10.5852/geodiversitas2023v45a18_s3

Appendix 4. — 3D scan of the right mandibular ramus of *Anachlysictis gracilis* Goin, 1997, specimen VPPLT-1612: https://doi.org/10.5852/geodiversitas2023v45a18_s4

Appendix 5. — 3D scan of the left mandibular ramus of *Anachlysictis gracilis* Goin, 1997, specimen VPPLT-1612: https://doi.org/10.5852/geodiversitas2023v45a18_s5